Redesign and optimization of UHPC sluice gates

MSc Thesis

Emil Kapron

TU Delft Delft University of Technology

F D N

Redesign and optimization of UHPC sluice gates

MSc Thesis

by

Emil Kapron

Student number:	5628393
University:	Delft University of Technology
Faculty:	Civil Engineering and Geosciences
Masters track:	Structural Engineering
Specialization:	Structural Mechanics

Master's Thesis Committee:

Prof. dr. ir. Max A.N. Hendriks	Chair of the committee	Delft University of Technology
Prof. dr. ir Jan G. Rots	Committee member	Delft University of Technology
Ir. Dil Tirimanna MBA	Company supervisor	FDN – Functional Design Netherlands

July 2025

TU Delft Delft University of Technology

F D N

Abstract

Steel has typically been used in the sluice gate design for well over a century. However, the development of ultra-high performance fibre reinforced concrete (UHPFRC) in the recent decades has presented an interesting alternative to traditional steel sluice gates. The appeal of UHPFRC is based on its extraordinary durability and resistance to most forms of corrosion. Gates produced with the material could function without the need for replacement or maintenance works for extremely long periods of time. Due to higher material strength parameters, UHPFRC elements are also significantly more slender and therefore lighter than their standard concrete counterparts. That makes UHPFRC a potential alternative to traditionally used steel.

A UHPFRC mitre gate had already been designed as a replacement for one of the gates in the Robbengatsluis complex. However, due to the novelty of the solution, there were concerns about whether the design choices and solutions used in the process may have resulted in an overly conservative design. The goal of the project was to redesign the UHPFRC gate, verifying if a more optimal design was possible and which of the available methods of analysis were most suitable in the context of UHPFRC sluice gate design.

The gate's design was focused around the concept of a plate gate strengthened on its inner side by beam segments running along the edges of the structure and through its most significantly loaded areas. In the project, two main approaches were considered. The first focused on reviewing the analytical design procedure used for the original design. The applied standards and assumptions were reassessed, leading to modifications such as the adoption of alternative analytical formulas, the inclusion of fibre contribution in relevant limit states, and the adjustment of the fibre orientation factor for thin plate segments. Relevant ultimate limit state (ULS) and serviceability limit state (SLS) verifications were conducted. This approach was supported by linear finite element analysis as a conservative estimation of the structure's behaviour.

The second approach aimed at incorporating nonlinear finite element analysis (NLFEA) to verify the accuracy of the utilized analytical design methods. Additionally, the application of NLFEA allowed for consideration of load redistribution effects, which are of significance in the case of UHPFRC structures. Material tests (compression tests, 3-point bending tests, etc.) had been conducted to prepare the NLFE model of the considered UHPFRC mix and to evaluate material parameters utilized in the analytical design verifications. The nonlinear approach was based on a total strain-based rotating crack model. Two nonlinear numerical solution strategies were developed, one based on plane stress elements and the other based on shell elements. The solution strategies were validated within the framework presented in Model Code 2020. The plane stress element solution strategy was validated by comparing numerical simulation results with literature-based results from 4-point bending tests of reinforced UHPFRC beams. The shell element-based strategy was validated by comparing numerical simulation results with experimental data from one-way plate bending tests conducted by FDN Engineering. It was evaluated that both solution strategies closely predicted the experimental results. The modelling uncertainty of the plane stress element strategy regarding prediction of beam bending capacity was quantified through the application of Global Factor Method. The strategy was then used to evaluate the bending capacity of all beam segments within the structure. The shell-based solution strategy was used to take into consideration load redistribution effects in the critical plate segment.

The numerical results confirmed the accuracy of the applied analytical verifications. Numerical capacities differed from analytical ones by -5.7% to +4.4%, they gave more conservative predictions for low reinforcement ratios and less conservative ones for high reinforcement ratios. Due to the lack of experimental benchmark data for UHPFRC plate segments, nonlinear numerical analysis could not be used to comprehensively evaluate the load redistribution effects for the structure at large, as the modelling uncertainty of the solution strategy could not be estimated. A new design for the UHPFRC mitre gate was prepared based on the revised analytical approach. Among other changes, the new design included altered aspect ratios of beam segments and reductions in segments' reinforcement. The original design and the new design were compared in terms of the amount of concrete and reinforcement used. The new gate variant required slightly less UHPFRC and significantly lower shear and longitudinal reinforcement ratios, with the total decrease in the amount of reinforcing steel reaching 56.2%.

Reinforcement design was strongly influenced by crack width SLS verifications, which required significantly higher reinforcement ratios than ULS requirements. The dominance of crack width SLS was high enough to nullify any potential benefits from less conservative ULS verification approaches. A review of available information suggested that the applied MC2020 SFRC crack width SLS verification could be improved upon to provide less conservative estimations by either utilizing a UHPFRC-specific code-based analytical verification or applying NLFEA in the process.

The concluding results can be used as a reference point for future attempts at designing UHPFRC mitre gates. Currently available UHPFRC and SFRC design standards provide a good framework for the design of those elements, with significantly reduced material use compared to the previous design. With superior durability, UHPFRC offers a feasible alternative to the use of steel. The proposed plate and beam segment structure is a viable solution for UHPFRC mitre gates of similar dimensions. Efficient design requires a series of material tests to properly quantify the necessary input parameters and the benefits of the utilized material on a case-by-case basis. The new design simplifies manufacturing and improves efficiency without compromising performance.

Table of Contents

LIST OF FIGURES

LIST OF TABLES

1 Introduction

1.1 Background

One of the pathways of advancement in the field of cementitious materials has always been the drive to produce the material with ever increasing strength parameters. This process led to the development of ultra-high performance concrete in the late 20th century. The materials' strength parameters significantly exceed those of the standard strength concretes, due to which UHPC can facilitate the construction of substantially more slender structures. These benefits are offset by the significantly higher price of UHPC. However, the main reason behind the steady increase in the application of the material, ever since it entered the market at the turn of the 90s and 2000s, has been the property that due to its very dense microstructure, it proves to be extremely durably and resistant to all forms of corrosion. As the result, structural elements made out of UHPC require virtually no maintenance, which makes them more attractive. This is especially true in the case of infrastructural projects, when the potential future maintenance activities could lead to significant hurdles, particularly in highly developed geographical areas, where they can result in substantial economic loses.

Excluding some special applications, such as industrial floor surfaces etc., UHPC mixes usually contain steel fibres to enhance the tensile behaviour of the material. The material is then referred to as ultra-high performance fibre-reinforced concrete (UHPFRC) and can be classified as a fibre reinforced concrete (FRC). However, same as when compared with standard concretes, it is characterised by much higher compressive strength than typical FRC.

Within the last decade, several standards dealing with the design of structures in UHPFRC have been introduced, such as AFGC-SETRA's Ultra High Performance Fibre-Reinforced Concretes – Recommendations [1], [2], SIA 2052 UHPFRC: Materials, Design and Application [3], or new French standards on UHPFRC [4]. Simultaneously, many developments have been made regarding guidelines and standards dealing with SFRC, such as Model Code 2020 [5]. These documents, based on a significant amount of scientific research and commercial projects conducted in the preceding years, create a good basis for engineers intending to utilize UHPFRC in their projects. However, in many cases, the typical analytical design approach is not enough to provide an efficient design of a UHPFRC structure. The standards themselves advise the user, on multiple occasions, to perform tests on either the material or already cast structural elements when the use of highly suboptimal material parameters is to be avoided. This state of things is linked to the fact that properties of UHPFRC depend on many more factors than those of more traditional cementitious materials, such as the content, type, and orientation of fibres in the concrete. The result is that efficient design of a UHPFRC structure often requires more than just the use of one of the aforementioned standards. Often, activities such as various strength tests, numerical modelling, or combinations of both need to be conducted.

FDN Engineering was tasked with replacing the sluice gates of the Ebdeuren Robbengatsluis in Lauwersoog. The old gates were constructed using wood and steel. FDN, as a company, has a large amount of experience in both the design and construction of UHPFRC structures. UHPFRC, as a material, is suitable for the task that had been considered, as its high durability reduces the need for maintenance of the new sluice gates, which is especially beneficial considering the role that the sluice fulfils in the infrastructural system. Additionally, due to the high impact resistance of the material, the risk of potential damage to the gate is also reduced.

The gate was designed through the application of AFGC-SETRA's Ultra High Performance Fibre-Reinforced Concretes – Recommendations, in combination with Dutch versions of Eurocodes and their respective national annexes. However, the direct application of the requirements of the

aforementioned standards, together with several highly conservative assumptions made within the design process, resulted in a structure that consequently overperformed in all conducted tests. The apparent overdesign also introduced several hurdles in the process of manufacturing of the considered element.

UHPFRC, as a material, presents an interesting alternative to the currently widespread use of steel in this area. As such, the goal of this project was to increase the attractiveness of this solution through the revision of the design process, developing a more optimal solution that would also be less problematic in manufacturing, as well as verifying how best to utilize the advantages that UHPFRC provides as a material.

1.2 Research question, aims and objectives

In this section, the problem that had been considered was described. The main research question is presented, and primary objectives of the project were outlined.

FDN completed the design process of the considered sluice gate, producing a structure that proved to be heavily overdesigned. This state of things has been asserted based on the structure's overperformance in several tests. As an example, in the impact test that the gate underwent, it withstood impact energies few times larger than the required safety levels. Additionally, the manufacturing of the element proved to be troublesome, hinting at issues such as over reinforcement of the design. Based on those concerns, the main research question was formulated as defined below:

"How to approach the design of UHPFRC sluice gate in order to acquire more optimal and easily manufacturable product, while maintaining standing safety and serviceability standards?"

This research question was answered through achieving the main project objective of providing a new design alternative to the original design of the sluice gate. On the pathway to this overarching objective, several intermediate sub-goals had to be fulfilled. Their aim was to ensure that the final results covered by this project had been thoroughly vetted, and not only provided a more optimal design, but fulfilled the bounds set by the above-formulated question, of the alternative fully satisfying standing safety and serviceability requirements. The most important of these sub-goals were formulated as:

- Conducting the literature study aiming at: acquiring knowledge regarding the most suitable and efficient ways of modelling adequate UHPFRC problems, reviewing available and most applicable design standards, and studying and understanding the material behaviour of UHPFRC.
- Revision of the conservative assumptions taken in the prior design process regarding their applicability,
- Analysis of the hurdles encountered in the process of manufacturing of the element, and proposal of appropriate changes that would most efficiently lead to the alleviation of these issues,
- Application of material mechanics and knowledge about the behaviour of UHPFRC acquired during the literature study, in order to verify if some of the most demanding requirements applied to the elements are indeed fully justified,
- Redimensioning and reinforcement design of the new gate,
- Preparation and validation of NLFE models based on the UHPFRC used,
- Verification of the proposed design solutions through the application of numerical modelling,
- Comparison between the original FDN design and the newly proposed one.

To achieve the outlined objectives, both analytical and numerical design practices were applied, and a vast array of knowledge acquired both before and during the duration of this project, had to be drawn upon and used complementarily. With the ultimate goal of verifying whether the prior design proposal represented the limits of the capabilities of the UHPFRC, or if those could still be better utilized, and if so, how best to do so.

2 Literature study

This chapter presents an overview of ultra-high performance fibre-reinforced concrete (UHPFRC) as a material. Based on a literature review, it provides information on its basic material properties and describes the currently applied design methods and standards. It also provides information on the numerical modelling methods relevant to the design problem analysed in the project.

2.1 UHPFRC as a material

2.1.1 Basics of UHPFRC

Ultra-high performance fibre reinforced concrete (UHPFRC) is a result of decades of advancements in the development of cementitious materials. Probably its most obvious property is its substantially higher strength when compared with other materials in that group. As per (AFGC-SETRA, 2002) [1], the concretes' compressive strength has to be within the range of 150-250 N/mm^2 for it to be deemed an UHPC. However, the differences between UHPCs and normal strength or high-strength concretes go much deeper than that. Most of its superior properties stem from its extremely dense microstructure. UHPCs are characterized by porosity of below 6% (Resplendino & Toulemonde, 2013) [6]; for example, Ductal, according to (AFGC-SETRA, 2013) [2] reaches the porosity of 1.9%, significantly lower than the porosity of normal strength concretes (12-16%) and relatively close to the porosity of some of the densest rocks, such as granite (around 1%).

While the terms ultra-high performance concrete and ultra-high performance fibre reinforced concrete are not generally mutually exchangeable, in majority of practical applications - including the one that this project dealt with - UHPC is reinforced with fibres. While the superior compressive properties of UHPFRC come primarily from its extremely dense microstructure, the significantly higher axial tensile strength of around 7-11 N/mm^2 (Fehling et al. 2014) [7], and reduced cracking in tension, result from the presence of (usually) high-strength steel fibres. The fibres also provide concrete with improved ductility. Linked to much higher strength parameters is significantly higher modulus of elasticity of UHPFRC. Table 1 provides a comparison of some basic mechanical properties of different concrete types.

Property	**Unit**	**NSC**	**HSC**	**UHPC**
Compressive strength	[N/mm^2]	20-65	65-105	150-200
Tensile strength	[N/mm^2]	2,3-4,3	4,5-5,0	6,0-10,0
Modulus of elasticity	[N/mm^2]	28.000-38.000	38.000-41.000	50.000-60.000

Table 1: Basic mechanical properties of different concrete types. From Betoniek, (2017), Da's sterk! Betoniek Standaard, 1-12. [8]

Dense microstructures provide UHPFRC with very high durability. The significant presence of superplasticizers in composition of UHPC mixtures gives the fresh concrete very good workability, akin to that of self-compacting concretes.

2.1.2 Mixture composition

The design of the UHPFRC mixture composition is a much more complicated process than in the case of normal-strength concretes. To achieve the extremely high density from which the key properties of UHPFRC stem, the composition of the mix has to be very thoroughly analysed, often including multiple experiments and/or the use of grading optimization software [7].

Primary components of the mix include:

- **Cement:** CEM I low-alkali Portland cements of strength classes 42.5R and 52.5R with high sulphate resistance and low heat of hydration, are generally used as they reduce the risk of alkali-silica reaction and require relatively small amount of water. UHPFRC contains large amounts of cement, a significant part of which remains unhydrated and provides an additional boon to the structure in the form of self-healing ability.
- **Reactive admixtures:** Used to achieve optimum density packing. They additionally contribute to the formation of the concrete's microstructure through the creation of additional hydrate phases. Most often, silica fume and blast furnace slag are used.
- **Inert admixtures:** Similar to reactive admixtures, their primary goal is to improve the packing density of the mix, they remain uninvolved in the chemical reactions taking place during the hardening of the concrete. To best optimize the density of the mix, they must undergo a very selective grading process. Usually, quartz powder is used.
- **Superplasticizers:** These primarily deagglomerate cement and other fine particles and allow the mix to maintain good workability despite its high cement content and the fact that many admixtures, such as silica fume, also decrease workability. The choice of the superplasticizer must be carefully made based on the contents of the mix.
- **Fibres:** Fine fibres usually made from high-strength steel, are an important part of the mix. They usually make up around 2% of the mix (by volume) and are primarily introduced to improve the ductility of the hardened concrete.
- **Aggregate:** The composition of aggregate heavily influences the properties of the concrete, primarily through its packing density. To this end, much finer aggregates are being used, with approximate max size of 8mm. Some UHPFRC mixes can be characterized by the largest fraction of aggregate being as small as 0.5mm.
- **Water:** UHPFRC mixes are characterized by low water/cement ratio (usually less than 0.2). This requirement is crucial for the development of the key properties of the hardened UHPFRC, as even a relatively slight increase in the w/c ratio results in formation of capillary pores, which significantly increase porosity, and in turn, lead to significant drop in strength parameters and durability of the material.

2.1.3 Steel Fibers

Next to its high density and low porosity, the presence of fibres is the key source of the properties of UHPFRC. They influence the behaviour of the material in several ways:

- Increase ductility,
- Increase tensile strength,
- Offset the development of cracking,
- Provide good impact resistance.

Short fibres are crucial in providing concrete with strain-hardening behaviour. The main way in which they influence the mechanical properties of the concrete is by providing a sort of "micro-reinforcement", which becomes activated when the microcracking of the material begins. While in the case of normal concrete these micro cracks quickly progress, creating macro cracks resulting in strain-

softening behaviour, in the case of UHPFRC the fibres start to take over the load previously carried by the matrix. As a result of steel's higher tensile strength, material exhibits strain hardening behaviour.

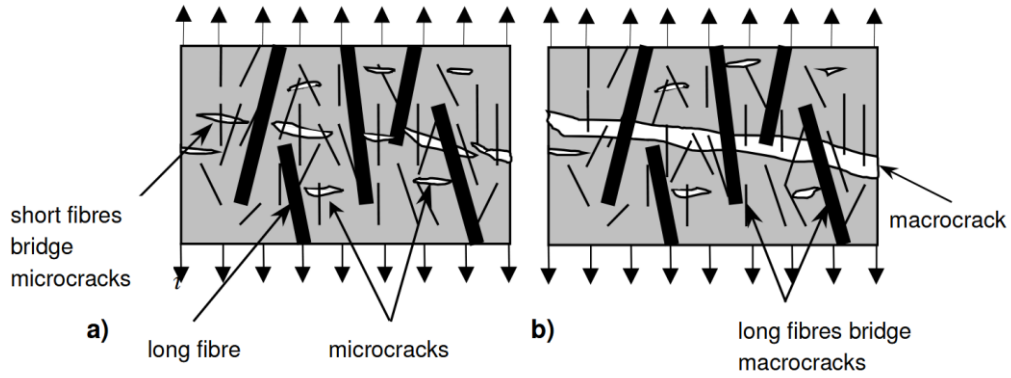

Fig. 1: Influence of fibres of different lengths on crack propagation process. a) Short fibres bridging the microcracks. b) Long fibres bridging the macrocrack. From Markovic, I. (2006). High-performance hybrid-fibre concrete - Development and utilisation [Doctoral thesis, Delft University of Technology]. Copyright [2006] by I. Markovic.

The properties of UHPFRC heavily depend on its fibre content. The fibres usually make up around 2% of the mix by volume. The higher the fibre content, the more strain-hardening behaviour the UHPFRC will usually exhibit. They can range in length from a few to several tens of millimetres. Research has proven (Markovic, 2006) [9] that fibre mixes containing fibres of varied lengths provide the material with the most optimal ductile behaviour and tensile strength. In those cases, when at higher strain levels cracks reach the pullout length of shorter fibres, the longer fibres still span the cracks, and they continue to provide substantial deformation capacity before the ultimate strength of the concrete is reached. This process is illustrated in Fig. 1. Fibers can be of different shapes (hooked, straight etc.). Sometimes, non-steel fibres are also utilized. Because of UHPFRC's significant fibre-bridging capabilities, it is usually used in structures dominated by flexure, shear or torsion.

Aside from the fibre type and content, the tensile strength of the concrete is also significantly affected by the orientation of the fibres [10]. The fibres contribute to the tensile behaviour of the concrete most effectively when they are aligned parallel to the direction of principle tensile stress. In most cases the flow of concrete during casting results in random fibre orientation, which in turn significantly decreases the fibres' crack-bridging potential, with fibre efficiency dropping by up to 30% [11].

2.1.4 Material properties of UHPFRC

2.1.4.1 UHPFRC under compression

Due to its incredibly dense microstructure, UHPFRC exhibits very high compressive strength and stiffness. In comparison to normal strength concrete, the stress-strain diagram of UHPFRC is characterized by a steeper inclination and a significantly larger range of essentially linear elastic deformation, ending shortly before the compressive strength is reached. The ultimate compressive strain is heavily dependent on the grading of the aggregate, with a tendency for smaller graded aggregates to provide higher values of strain at failure.

UHPC fails in compression in a more brittle way than normal strength concretes. This state of things is mostly linked to the fact that, as a result of its much more homogenous microstructure, the cracks in UHPC tend to propagate irrespective of the aggregate-matrix boundaries. The post-peak behaviour of UHPFRC can be influenced by its fibres (their content, geometry, orientation, etc.). However, precise prediction of post-peak material behaviour is very difficult, as it is influenced by a

multitude of factors. The scatter of post-peak behaviour of various UHPFRC samples was illustrated in Fig. 2.

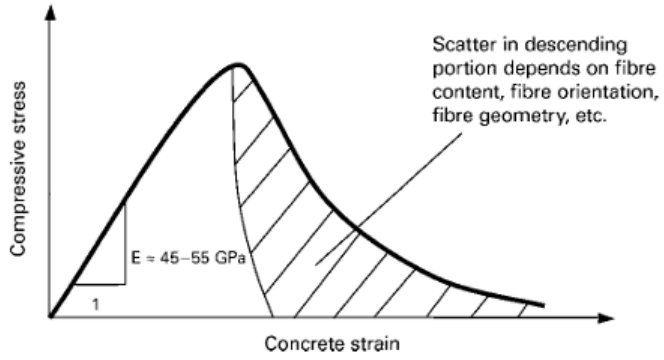

Fig. 2: Scatter in post peak behavior of UHPC in compression. From Ultra-High Performance Concrete UHPC (p. 26), by Fehling et al., 2014, Wilhelm Ernst & Sohn. Copyright [2014] by Wilhelm Ernst & Sohn.

2.1.4.2 UHPFRC in tension

Usually, the tensile strength value of UHPFRC lies in the range of 7-11 N/mm^2 (Fehling et al. ,2014) [7]. In the case of UHPC without, or with small amount of fibres, the tensile strength doesn't significantly increase above the values characteristic for normal strength concretes. It's the presence of fibres that span over the microcracks, temporarily "mending" them, that increases the tensile strength of UHPFRC. With different types and contents of fibres, a UHPFRC can exhibit strain-hardening or strain-softening behaviour. Depending on the length of the fibres, their influence can be present at different stages of the loading process, with longer fibres being able to increase the strength at larger strain values.

When concrete matrix first cracks, the fibres get activated and start to transfer part of the tensile load previously carried by the cracked area. More and more microcracks start to form throughout the concrete matrix. As the crack width increases, the embedded length of the fibres decreases, reducing the force that can be transferred through them. When the ultimate tensile strength is reached, the fibres start to be pulled out of the matrix, and a localized macrocrack appears. Including varied lengths of fibres into the mix provides it with more ductile post peak behaviour, as after the shorter fibres have already been pulled out, the longer ones still transfer part of the load. As a result, the tensile behaviour of UHPFRC depends significantly on the fibre contents, geometry, orientation, etc.

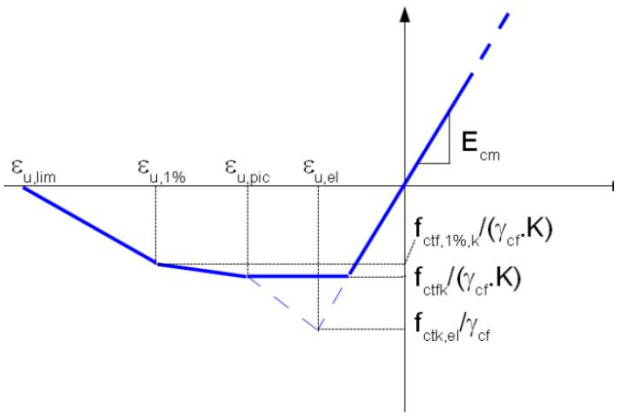

Fig. 3: Generalized tensile strain softening curve according to [2].

Tensile behaviour of UHPFRC is usually described by either a stress-strain curve or a stress-crack opening displacement relation. Most design standards separate UHPFRCs into those exhibiting strain-hardening behaviour and those characterized by strain-softening, and define a separate generalized tensile curve for each of them. Fig. 3 and Fig. 4 present those curves as per the French UHPFRC recommendations [2], where curve parameters are taken as:

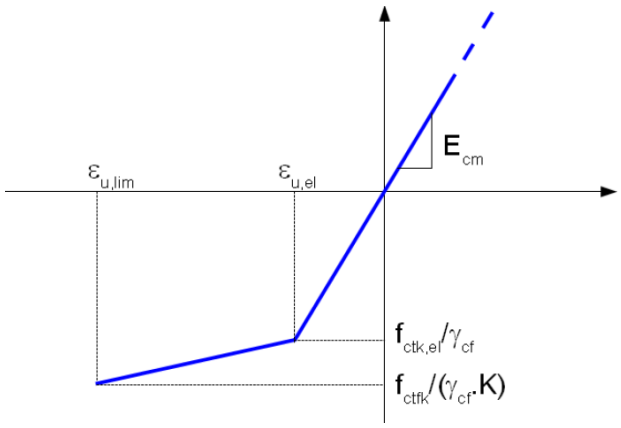

Fig. 4: Generalized ensile strain hardening curve according to [2].

E_{cm} - mean modulus of elasticity,

f_{ctfk} - characteristic maximal post-cracking stress,

$f_{ctk,el}$ - characteristic limit of elasticity under tension,

$\epsilon_{u,el}$ - elastic tensile strain at ULS,

$\epsilon_{u,pic}$ - ULS equivalent strain corresponding to the local peak in post-cracking phase or to a crack width equal to 0.3 mm if there is no peak,

$\epsilon_{u,1\%}$ - equivalent strain corresponding to a crack width of 0.01H where H is the depth of the tested prism with dimensions complying with the structure's dimensions at ULS,

$\epsilon_{u,lim}$ - ultimate strain beyond which fibres participation is no longer taken into account at ULS.

In the curve for strain softening UHPFRC four different stages can be identified:

$0 - \epsilon_{u,el}$ - elastic stage, tensile stress carried by the concrete matrix,

$\epsilon_{u,el} - \epsilon_{u,pic}$ - microcracking starts, cracks grow in number and width, fibres start to carry over the stresses,

$\epsilon_{u,pic} - \epsilon_{u,1\%}$ - crack localisation happens, one of the microcracks transitions into a macro crack fibres start to be pulled out of the matrix,

$\epsilon_{u,1\%} - \epsilon_{u,lim}$ - propagation of the macro crack, most fibres pulled out rapid strain growth and loss of load carrying capacity.

2.1.4.3 Modulus of elasticity

Modulus of elasticity usually reaches higher values in the case of UHPFRC than in the case of normal concretes. It typically lies within a range of 40 to 60 GPa. Its value depends on a multitude of factors such as:

- aggregate size,

- mix design,
- type and amount of fibres,
- curing method.

Due to that, prediction of the value of the modulus of elasticity of UHPFRC is difficult, and guidelines generally advice for it to be verified experimentally for the specific mix designs.

2.1.4.4 Shrinkage

Drying shrinkage, which occurs when moisture evaporates from the concrete, is significantly reduced [13] due to the low porosity of UHPFRC, as well as its low water/cement ratio and the assumption that most of the water is going to partake in the hydration process. It can however, be of significance in the case of very thin elements.

Autogenous shrinkage, on the other hand, is higher than in the case normal strength concrete [14], as UHPFRC contains larger amounts of cement and, as a result, larger volume change is to be expected due to the binder's hydration process. The shrinkage is significantly affected by heat treatment. In the case where no heat treatment is applied, the silica fume acts primarily as a filler and does not contribute to the autogenous shrinkage. However, shrinkage of UHPFRC can be effectively controlled by the application of heat treatment. It is then concentrated in the period of the treatment, and afterwards, no significant shrinkage occurs.

Typically, the total shrinkage of UHPFRC reaches the range of 0.7 to 0.84 mm/m [15]; however, it can reach as high as 1 mm/m in cases where no internal curing had been applied. These values are significantly higher than the range of 0.05 to 0.15 mm/m observed in normal concretes.

2.1.4.5 Creep

Due to its reduced porosity and generally much denser structure, UHPC is characterized by lower creep than normal strength concrete. According to (Liu et al., 2024) [16], the creep coefficient falls within the following ranges:

- Final creep coefficient (compression) for UHPC without heat treatment: φ = 0.5 … 1.5
- Final creep coefficient (compression) for UHPC with heat treatment: φ = 0.17 … 0.5
- Final creep coefficient (tension) for UHPC without heat treatment: φ = 1.2 … 2.38
- Final creep coefficient (tension) for UHPC with heat treatment: φ = 0.78 … 1.12

As seen, the creep coefficient can be significantly reduced by the application of heat treatment. The share of drying creep is low when compared with that of standard concrete, which is likely linked to UHPC's low porosity and its self-drying out effect.

2.1.4.6 Fatigue behaviour

Fatigue behaviour of UHPC is of concern, as it is in the case of normal concretes. While UHPC can withstand larger repetitive loads due to its generally higher strength, at higher stress levels fatigue deterioration of UHPC elements remains a significant problem. Models created for the assessment of fatigue behaviour of normal concretes do not provide accurate estimates in case of the UHPC [17]. For contemporary needs, the models present in the fib Model Code 2020 [5] can be used. However, models specific to UHPC are still being developed.

Fatigue performance is highly related to stress amplitudes, frequency, and cyclic loading characteristics. Generally, UHPC containing coarser aggregate performs worse regarding fatigue. Additional reinforcement can be used as a means of improving fatigue behaviour. (Fehling et al., 2014) [7] provides an overview of several research programs, which generally suggest that no statistically

significant difference was established between the fatigue performance of UHPC with fibres and without.

2.1.4.7 Dynamic actions

All concretes are characterized by an increase in compressive and tensile strength at high strain rates. This increase is usually described by the dynamic increase factor (DIF). (Millon et al., 2009) [18] evaluated the DIF for UHPC in tension to be within the range of 5-6. The improved impact performance of UHPC is primarily linked to the high strength of the concrete matrix and further increased by the presence of steel fibres. Drop-weight and projectile tests of UHPFRC confirm that the material exhibits much better energy absorption potential than normal concretes.

2.1.5 Durability

Thanks to its extremely dense microstructure, UHPFRC is characterized by significantly higher resistance to damage by most substances than the normal or high-strength concrete. Due to the very small presence of capillary pores in its microstructure, corrosive agents cannot infiltrate deep into the material. The porosity is small enough that even air permeability is relatively low; as a result, carbonation of UHPFRC progresses very slowly and tends to be heavily restricted in depth. Over the years, various tests and experiments (Fehling et al., 2014) [7] have proven that UHPFRC exhibits extremely high resistance to most substances that structures made of it can encounter, including chloride ions, ammonium nitrate, sodium sulphate, sodium sulphate, sulfuric acid, lactic acid. For example, its resistance to the influence of freezing/de-icing salts makes it viable for UHPFRC to be used in environments with exposure to those agents without the need for any additional protective measures. The outcome of this is that UHPFRC almost always satisfies the highest exposure classes (Khorami, 2023) [12].

For UHPFRC to exhibit these properties, it is crucial that its mix be characterized by a low water/cement ratio of preferably below 0.2, as increases above this value rapidly lead to the creation of capillary pores. Additionally, the durability of UHPFRC tends to be increased by the application of heat treatment during the hardening of the concrete.

2.2 UHPFRC in application

2.2.1 Mixing

UHPFRC has to undergo mixing in high-energy mixers to allow large amount of ultra-fine particles to become thoroughly solubilized with other ingredients of the mix. Alternatively, mixing in more traditional mixers is possible at the expense of longer mixing time. This solution, however, requires additional measures aimed at decreasing the temperature of the mix.

First, the dry materials are added to the mix, starting from the course ones. After the dry ingredients have been premixed, water already mixed with the superplasticizer is further added. The mixing continues until a stable mix with good workability is acquired. As the last part of the process, the fibres are added and mixed into the fluid concrete. It must be ensured that the mix is stable at the point at which mixing finishes and that no further fluidization occurs.

2.2.2 Casting

The casting procedure of the UHPFRC elements/structures has a significant impact on the final properties of the material, primarily on its tensile strength and tension-related behaviour. This characteristic results from the fact that the way UHPFRC is cast heavily affects the orientation of the fibres, which are responsible for the tensile performance of the element. Concerns about uniform fibre distribution also discourage the application of internal vibrators. However, use of external vibrators is

advised, as despite its self-compacting abilities, UHPFRC is not self-deaerating, and additional vibration energy is necessary to achieve proper deaeration.

2.2.3 Curing

Throughout the binding process, both the temperature and moisture level of the concrete has to be controlled. Immediately after the casting of the UHPFRC, its surface should be covered with plastic sheeting, a curing agent, or a watery mist; otherwise, a hardened outer layer quickly forms, which subsequently prevents the levelling of the concrete surface and its deaeration.

The final properties of hardened UHPFRC are heavily influenced by the application of heat treatment. (Fehling et al., 2014) [7] generally suggests heat treatment at 80-90 ^{o}C, during the period between 24-72 hours after casting. As a result, the binding process is accelerated and additional hydration phases form due to the reaction of the silica fume, leading to increased strength parameters and decreased porosity. Additionally, heat treatment allows the shrinkage to be concentrated in the period of treatment, with no significant further shrinkage occurring afterward. To protect the concrete from drying out completely, it should be covered airtight during the heat treatment process. After treatment, slow cooling process should be facilitated to prevent the development of microcracks.

2.3 Design in UHPFRC

2.3.1 Inadequacy of the standard concrete regulations

Design in UHPFRC presents different and additional challenges when compared with design in normal strength concrete. These differences stem from the described differences in the microstructure of the material.

Design codes dealing with normal concrete, for example, provide means to estimate the values of many material parameters based on the measured values of other parameters (for example, based on compressive strength). These formulas have been devised based on the results of experiments concerning concretes of specific strengths. Standards containing them explicitly mention the validity ranges of those formulas. UHPFRC's material parameters fall outside these ranges. Additionally, it is known that UHPFRC contains different mineral structures than normal concretes and is characterized by significantly lower porosity. These facts alone suggest that formulas created based on the performance of normal concretes cannot be expected to directly translate to the case of UHPFRC.

Another aspect significantly affecting UHPFRC's material performance is the presence of steel fibres. Design codes exist which deal with SFRCs, and they generally provide a good starting point to attempt the design of UHPFRC structures. However, they also have to be applied with care. Similarly, as in the case of standard concretes, whenever they refer to formulas estimating material parameters, UHPFRC might fall outside the range of applicability of such formulas. This is specifically the case when those formulas refer to the compressive strength of a UHPFRC.

Another area in which normal concrete standards cannot be efficiently applied to the design of UHPFRC structures is the requirements concerning the concrete cover of structural elements. These rules are based on the performance of a much less durable material. As described in Fehling et al. (2014) [7], UHPFRC's high resistance to most corrosive processes validates ascribing it the highest exposure classes (within the Eurocode framework) and often allows for a reduction in the thickness of the reinforcement's concrete cover.

These and many more similar issues clearly show the need for dedicated guidelines regarding design in UHPFRC.

2.3.2 Overview of available UHPFRC guidelines

Since UHPFRC was introduced, experience from conducted projects and academic research at various institutions has provided the foundation on which new regulations regarding the material could be formed. The first guidelines dealing with UHPFRC were introduced in the early 2000s. Since then, many guidelines dealing with the material have been published by various institutions from around the world. Table 2 provides an overview of those documents.

Year	Organization	Country	Title
2002	AFGC - L'Association Française de Génie Civil	France	''Ultra-High Performance Fibre-Reinforced Concretes - Interim Recommendations''
2006	JSCE - Japan Society of Civil Engineers	Japan	''Recommendations for Design and Construction of Ultra-High Strength Fibre-Reinforced Concrete Structures''
2008	DAfStb - Deutscher Ausschuss für Stahlbeton e. V.	Germany	DAfStb-Heft 561, Sachstandsbericht "Ultrahochfester Beton"
2013	Federal Highway Administration	US	''UHPC: A State-of-the-Art Report for the Bridge Community''
2013	AFGC - L'Association Française de Génie Civil	France	''Ultra-High Performance Fibre-Reinforced Concretes - Recommendations''
2014	KICT - Korea Institute of Civil Engineering and Building Technology	Korea	"Design Guidelines for K-UHPC"
2016	SIA - Swiss society of engineers and architects	Switzerland	SIA 2052 ''Ultra-Hochleistungs-Faserbeton (UHFB) - Baustoffe, Bemessung und Ausführung''
2016-2018	AFNOR - French standard institute	France	NF P18-470 "UHPFRC - Specifications, performance, production and conformity" NF P18-710 "Design of concrete structures - Specific rules for UHPFRC" NF P18-451 "Execution of concrete structures – Specific rules for UHPFRC"
2024	The American Association of State Highway and Transportation	US	"Guide Specifications for Structural Design with Ultra-High Performance Concrete"

Table 2: Overview of published UHPFRC guidelines

The AFGC-SETRA Recommendations (2002) [1] were the first French set of regulations regarding UHPFRC. They were the product of the work of the AFGC-SETRA Groupe de travail BFUP and were written as a reference for the use of UHPFRC in practice. The document focuses on the products that were commercially available at the time of the guideline's development. The recommendations cover topics such as:

- Characterization of the material,
- Determination of its mechanical properties,
- Product control and casting,
- Design of UHPFRC structures,
- Durability.

A revised version of the 2002 Interim Recommendations was published in 2013 [2]. The new document no longer bore the "interim" status. The updated recommendations incorporated the results of new developments in the field of UHPFRC and were implemented within the framework of Eurocode 2. At the time of its publication, the document was the most comprehensive guideline on the topic of UHPFRC.

Based on the 2013 Recommendations, three codes regarding UHPFRC were developed in France: NF P18-470, NF P18-710, and NF P18-451. They provided additional formal clarifications to some of the points made in the 2013 Recommendations, included complementary indications, and generally aimed to better integrate the recommendations into the Eurocode framework.

2.3.3 Work in progress

Various organizations are still working on developing their own UHPFRC guidelines. Some of them intend to create standards based on their own research programs, while others attempt to base their work on already published guidelines. An example of the latter would be the currently developed Spanish UHPFRC standards.

In Germany, DAfStb is working on creating a guideline on UHPC, primarily based on the results of the research program conducted beforehand. The guidelines are intended to be integrated into the framework of Eurocode 2.

One of the most recent developments in the field of UHPFRC-specific guidelines is the work of Task Group 4.2 on Ultra High-Performance Fibre-Reinforced Concrete of the International Federation for Structural Concrete. In November 2022, the group published the results of their work in the form of “fib BULLETIN NO. 105: Fibre Reinforced Concrete,” constituting the most recent publication on the topic.

2.3.4 Extensive process for determining material parameters

Even when dedicated UHPFRC guidelines are being applied in the design process, it is often necessary to support the process with additional documentation regarding the specific UHPFRC product used for the design. This is related to the fact that various commercial UHPFRC products can often be characterized by substantially different properties, especially those related to tensile behaviour, which depend on the fibre type and content.

Many of the UHPFRC guidelines call for various tests, sometimes even involving finished UHPFRC structural elements, in order to provide the most diligent design. Therefore, if such tests are deemed necessary during the design process, proper documentation regarding their results has to be added.

2.3.5 Flexural design

The flexural capacity of UHPFRC beams is usually evaluated using the method of sectional analysis (Yoo and Yoon, 2016) [21]. The method is based on dividing the cross-section into layers along its height. The tensile and compressive stress-strain models of the material are taken, and based on an assumed initial curvature, the position of the neutral axis of the cross-section is evaluated. The neutral axis is calculated through an iterative procedure. Based on the assumption that plane sections remain plane, the cross-sectional forces are calculated using the stress-strain relations assumed at the start, and their equilibrium is checked. With the accurate position of the neutral axis, the moments are calculated. When the assumed curvature results in the steel strain reaching the ultimate strain value, the calculations are completed, and the moment capacity of the cross-section is known. The stress-strain relations are usually taken based on the generalized variants available in the relevant UHPFRC

guidelines. Fig. 5 describes graphically the outlined procedure, and Fig. 6 presents an example of sectional division of a theoretical cross-section.

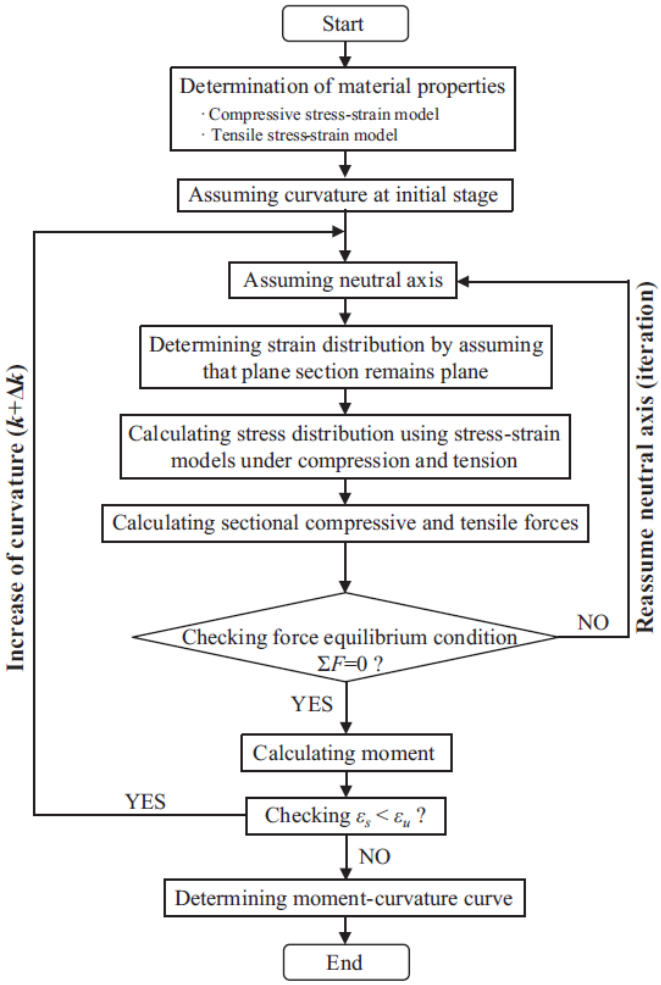

Fig. 5: Algorithm for sectional analysis. From Structural performance of ultra-high-performance concrete beams with different steel fibers (p. 419), by Doo-Yeol Yoo & Young-Soo Yoon, 2015, Elsevier. Copyright [2015] by Elsevier Ltd. All rights reserved.

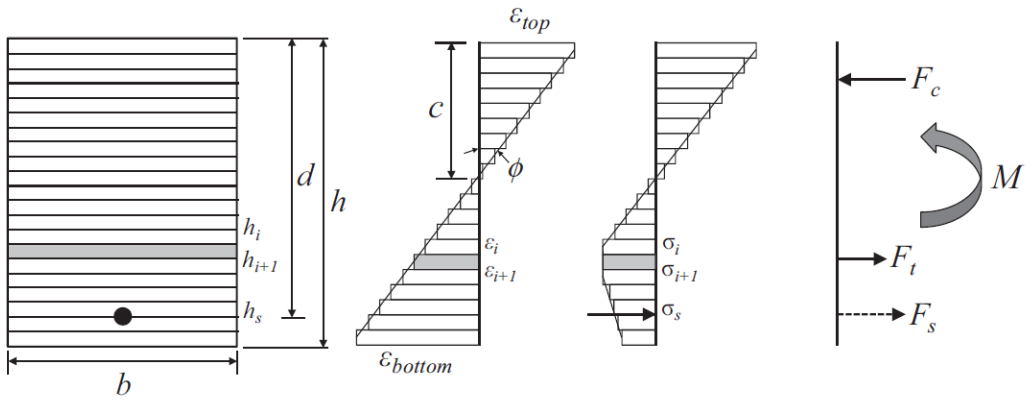

Fig. 6: Schematic description of stress and strain distributions in cross-section. From Structural performance of ultra-high-performance concrete beams with different steel fibers (p. 418), by Doo-Yeol Yoo & Young-Soo Yoon, 2015, Elsevier. Copyright [2015] by Elsevier Ltd. All rights reserved.

Fibre orientation has to be considered during the flexural design calculations, as it has been evaluated that in the vast majority of situations, it is heavily affected by the presence of reinforcement

or other factors. It is accounted for by the fibre orientation factor, which, according to AFGC's Ultra-High Performance Fibre-Reinforced Concretes – Recommendations [2], is equal to K = 1.25 if the global effects are considered and K = 1.75 for local effects

2.3.6 Shear design

Most design guidelines calculate the shear force capacity of UHPFRC elements by adding an additional term considering the resistance provided by the fibres. This includes AFGC's Ultra-High Performance Fibre-Reinforced Concretes – Recommendations [2], and the shear capacity assessment according to that guideline is discussed in this section.

[2] describes shear force capacity as equal to smaller of two values V_{Rd}, $V_{Rd,max}$. $V_{Rd,max}$ is the resistance of the concrete compressive struts. V_{Rd} is the tensile resistance of the ties in the concrete.

$$V_{Rd} = V_{Rd,c} + V_{Rd,s} + V_{Rd,f} \quad (1)$$

where:

$V_{Rd,c}$ is the contribution to the resistance provided by the concrete,

$V_{Rd,f}$ is the contribution to the resistance provided by the fibres,

$V_{Rd,s}$ is the contribution to the resistance provided by shear reinforcement.

Shear force resistance contribution from the fibres is equal to:

$$V_{Rd,f} = \frac{A_{fv}\sigma_{Rd,f}}{tan\theta} \quad (2)$$

where:

A_{fv} is the area of the fibre effect equal to $b_w \cdot 0.9d$ for rectangular and T sections, and $0.58 \cdot \phi^2$ for circular sections,

θ is the inclination angle between a diagonal crack and the longitudinal direction of the beam,

$\sigma_{Rd,f}$ is the residual tensile strength of the fibre-reinforced section and is defined depending on a type of UHPFRC for strain-softening or low strain-hardening UHPFRC:

$$\sigma_{Rd,f} = \frac{1}{K \cdot \gamma_{cf} \cdot w_{lim}} \int_0^{w_{lim}} \sigma_f(w)\ dw \quad (3)$$

where:

w_{lim} is equal to the larger of two values: w_u is the ultimate crack width attained at the ULS for bending combined with axial forces, w_{max} is the maximal admissible crack width,

K is the global fibre orientation coefficient,

$\sigma_f(w)$ is the experimental characteristic post-cracking stress for a crack width of w,

for strain-hardening UHPFRC:

$$\sigma_{Rd,f} = \frac{1}{K \cdot \gamma_{cf} \cdot (\epsilon_{lim} - \epsilon_{el})} \int_{\epsilon_{el}}^{\epsilon_{lim}} \sigma_f(\epsilon)\ d \quad (4)$$

where:

ϵ_{lim} is equal to the larger of two values: ϵ_u is the ultimate strain attained at the ULS for bending combined with axial forces, ϵ_{max} is the maximal admissible strain.

2.3.7 Torsion design

Research has shown that the inclusion of steel fibres is effective in improving the torsional performance (cracking, ultimate torsional capacity, ductility, post-cracking stiffness, and toughness). The response is further improved by the presence of stirrups and longitudinal reinforcement. AFGC's Ultra-High Performance Fibre-Reinforced Concretes – Recommendations [2] provide an updated approach for evaluating the torsional capacity of UHPFRC beams. The approach is based on Eurocode 2 [33], and it takes into consideration the fibres through $\sigma_{Rd,f}$ (residual tensile strength of the fibre-reinforced section).

2.3.8 Bond strength

Research has shown that the bond strength of steel bars embedded in UHPFRC is significantly higher than that of those embedded in normal-strength concretes. (Jungwirth and Muttoni, 2004) [19] found that it can be as much as 10 times higher.

The effects of fibre content and embedment length on bond strength were investigated by (Yoo et al., 2014) [20]. While bond strength remained largely unaffected by the fibre content and embedment length, it was clearly correlated with the compressive strength. The value of bond strength was evaluated to be approximately 2.5 times higher than predicted by relations established based on data considering standard concretes.

2.3.9 Slenderness and durability

These two aspects are the main features determining the attractiveness of UHPFRC structures despite UHPFRC's high material cost. It is imperative for a UHPFRC element design to take advantage of the material's excellent durability and adequately reduce the thickness of the concrete cover. Due to that apparent slenderness, it is, however, necessary to implement stringent crack control of UHPFRC elements in order to ensure that the microcracking that occurs does not negatively influence UHPFRC's long-term performance.

2.3.10 Consideration of fatigue performance

As outlined in [7], UHPC, as well as UHPFRC, were proven not to exhibit any improved fatigue performance when compared with more standard concretes. However, fatigue is potentially of greater significance for the long-term performance of UHPFRC elements than it is in the case of elements cast in normal concrete. In the case of standard concrete structures, temporary loads usually account for a relatively small portion of the total loading, and as a result, the stress/strain ranges induced by them are relatively insignificant when compared with the element dimensions. Due to the relatively higher slenderness of UHPFRC elements, these loads have more influence on their behaviour, and as such, fatigue is more likely to become a deciding factor in determining their long-term performance.

2.4 Numerical modelling of UHPFRC

2.4.1 Benefits of incorporating NLFEA into the design process

Nonlinear finite element analysis (NLFEA) is a powerful tool that, when properly applied, allows the analyst to significantly streamline usually multi-step design process of concrete structures. Standard concrete design procedures are based primarily on analytical methods and design codes, and are often supported by linear finite element analysis (LFEA) as a safe estimate for the internal force distribution. Depending on the complexity level of the applied NLFEA strategy, it can eliminate the necessity for conducting some of those analytical checks. A visualization of that relation in the context

of bridge deck slabs has been presented by (Plos et al., 2017) [22] and can be seen in Fig. 7. While most contemporary guidelines allow the NLFEA to be used as the basis for the design only in the case of existing concrete structures, e.g., (Hendriks & Roosen, 2019) [23]. fib Model Code for Concrete Structures 2020 (2024) [5] allows for the nonlinear design approach to be applied to the new structures, provided that the utilized solution strategy has been properly validated and its modelling uncertainty has been carefully estimated based on a set of relevant benchmark experimental data.

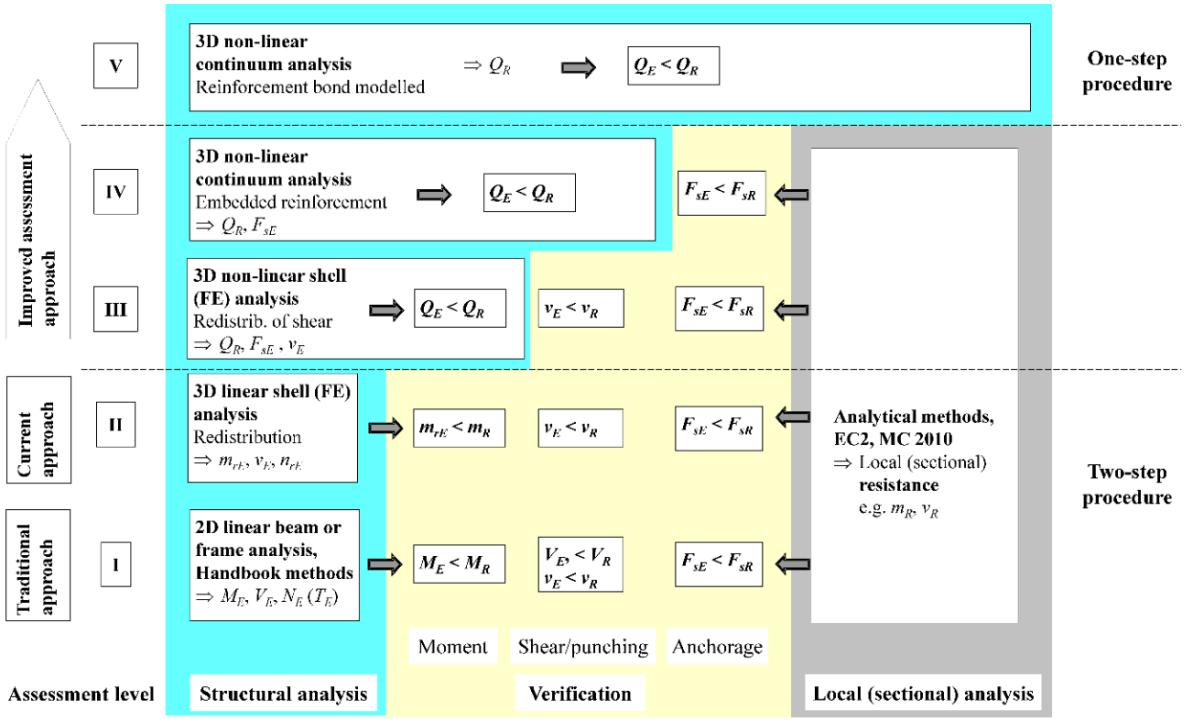

Fig. 7: Visualization of necessary design verifications depending on the type of FE approach applied (in the context of reinforced concrete bridge deck slabs). From A multi-level structural assessment strategy for reinforced concrete bridge deck slabs, by M. Plos et al., 2017, Taylore & Francis. Copyright 2017 by Taylore & Francis.

While experimental tests are usually needed to properly set up the nonlinear finite element method of analysis, this requirement is less problematic in the context of UHPFRC structures, as the relevant guidelines and standards already require many of the considered tests to be conducted, regardless of whether the NLFE approach is to be applied or not.

One of the crucial benefits offered by the NLFE design approach is the ability to assess the load redistribution effects in the concrete. Reinforced concrete exhibits inelastic behaviour, which, under high loading, can lead to significant load redistribution effects. When the concrete starts to crack, part of the load begins to be transferred through the surrounding parts of the structure, and the process continues until a failure mechanism is reached. Those effects can be especially impactful in case of structures with complex geometries, where the redistribution of the load can significantly alter the internal load paths inside them. The only way to take account of this effect is through an NLFE approach.

Load redistribution is of even more importance in the case of UHPFRC than in the case of standard concrete. Because of the higher modulus of elasticity and the very pronounced microcracking stage—during which the capacity to resist load continues to grow in a nonlinear way—the discrepancy between linear finite element method estimates and NLFE predictions is more pronounced.

2.4.2 Incorporating NLFEA into the design process

To facilitate the NLFE method of analysis, it is necessary to define the stress-strain tensile and compressive relations governing the behaviour of the analysed concrete. Proper definition of the nonlinear material behaviour is one of the most important parts of a utilized solution strategy. In the case of UHPFRC, defining the compressive nonlinear behaviour is often a secondary concern, and a linear compressive curve is sufficient for design purposes. This is duet to UHPFRC's significant compressive strength ($150\,MPa - 250\,MPa$) and as presented in Fig. 2 and described in the accompanying section, UHPFRC's essentially linear behaviour right up to failure in compression. Unless extremely high reinforcement ratios are used, most UHPFRC elements will not exhibit concrete crushing failure, and the failure mode will instead be linked to tensile cracking.

Proper definition of the concrete's tensile behaviour is, however, paramount. The fib Model Code for Concrete Structures 2020 (2024) [5] provides several "levels of approximation" for defining the behaviour of UHPFRC in tension. The highest, 4th level of approximation clearly advises on the approach for defining the tensile relation for the purposes of NLFEA. It recommends doing so through the application of an inverse analysis procedure, where the stress-crack width relationship is determined by fitting the results of the NLFEA to the force-CMOD curve acquired from three-point bending tests conducted according to NEN-EN 14651+A1 (2007) [24]. Inverse analysis is a widespread method used by researchers to evaluate material relations for the purposes of numerical analysis (Lee et al., 2017) [25].

A smeared crack approach is recommended for the definition of the material, in which the crack width is translated into tensile stain using a crack bandwidth that removes the dependence of the results on the utilized mesh size. The smeared crack approach has been widely confirmed by research (Fairbairn et al., 2006) [26], (Mezquida-Alcaraz et al., 2021) [15], to correctly model the behaviour of UHPFRC, provided that the underlying tensile relationships have been properly defined. It can however, provide non-conservative estimates of the concrete's behaviour, in the case of large-scale models, where the element type and size have not been correctly chosen for the problem at hand (van der Aa & van den Bos, 2021) [27].

The analyst must pay attention to the issue of scale transition in NLFE modelling of structures and structural elements of different sizes and geometries. Due to time and computational power restrictions – and the fact that often many consecutive analyses have to be performed – numerical analysis of concrete structures is often conducted utilizing rather large FE. In general, when concrete constitutive relations based on fracture energy and crack bandwidth are used, the results are considered mesh-independent when the crack bandwidth is dependent on the mesh size. This approach leads to objective results when the element size is smaller than the estimated average crack spacing and the model exhibits realistic crack spacing. However, when a large-scale model is applied, the energy dissipated within a finite element model should be related to both the size of the element and the average crack spacing (Hendriks & Roosen, 2019) [23]. That crack spacing can be calculated based on the available guidelines, such as fib MC2020 (2024) [5].

Other scale transition measures might be necessary. For example, because the large-scale model is unable to explicitly consider the bond-slip effect, it may be needed to implicitly consider the energy dissipated due to slip behaviour by modifying the fracture energy used for constitutive relations (Engen et al., 2014) [28].

Given that a specific solution strategy has been validated to reproduce appropriate failure modes and structural behaviour, it is then necessary to quantitatively evaluate its modelling uncertainty. (Engen et al., 2021) [29] present a detailed description of how this task should be handled

according to fib MC2020 (2024) [5]. The standard provides a set of prior parameters, which are then modified by the analyst in the procedure of Bayesian updating, based on the results of a set of relevant benchmark analyses. The evaluated mean and coefficient of variation are then used in the Global Factor method or the Partial Factors Method to assess the structural capacities of concern.

3 Original design of Robbengatsluis UHPFRC sluice doors

3.1 Design geometry

The subject of the project was a set of sluice gate doors, to be installed as part of the Robbengatsluis complex at the border between the provinces of Friesland and Groningen. FDN Engineering was tasked with designing a new pair of UHPFRC sluice gate doors as a replacement for an old pair of wooden-steel doors.

The gate is a typical mitre sluice gate. The UHPFRC gate's geometry was designed similarly to that of commonly utilized steel ones. The door's structure can be described as a large plate panel additionally strengthened with some beam segments. Additionally, to decrease the effective weight of the structure, the lower (submerged) part of the doors has two layers of plate segments to create an enclosed space between them, increasing the buoyancy of the structure. Fig. 8 presents an image of the UHPFRC gate taken during its installation at the Robbengatsluis complex. Following Fig. 9 presents the geometry of the structure as per FDN design.

Fig. 8: Photography of the original UHPFRC gate being installed

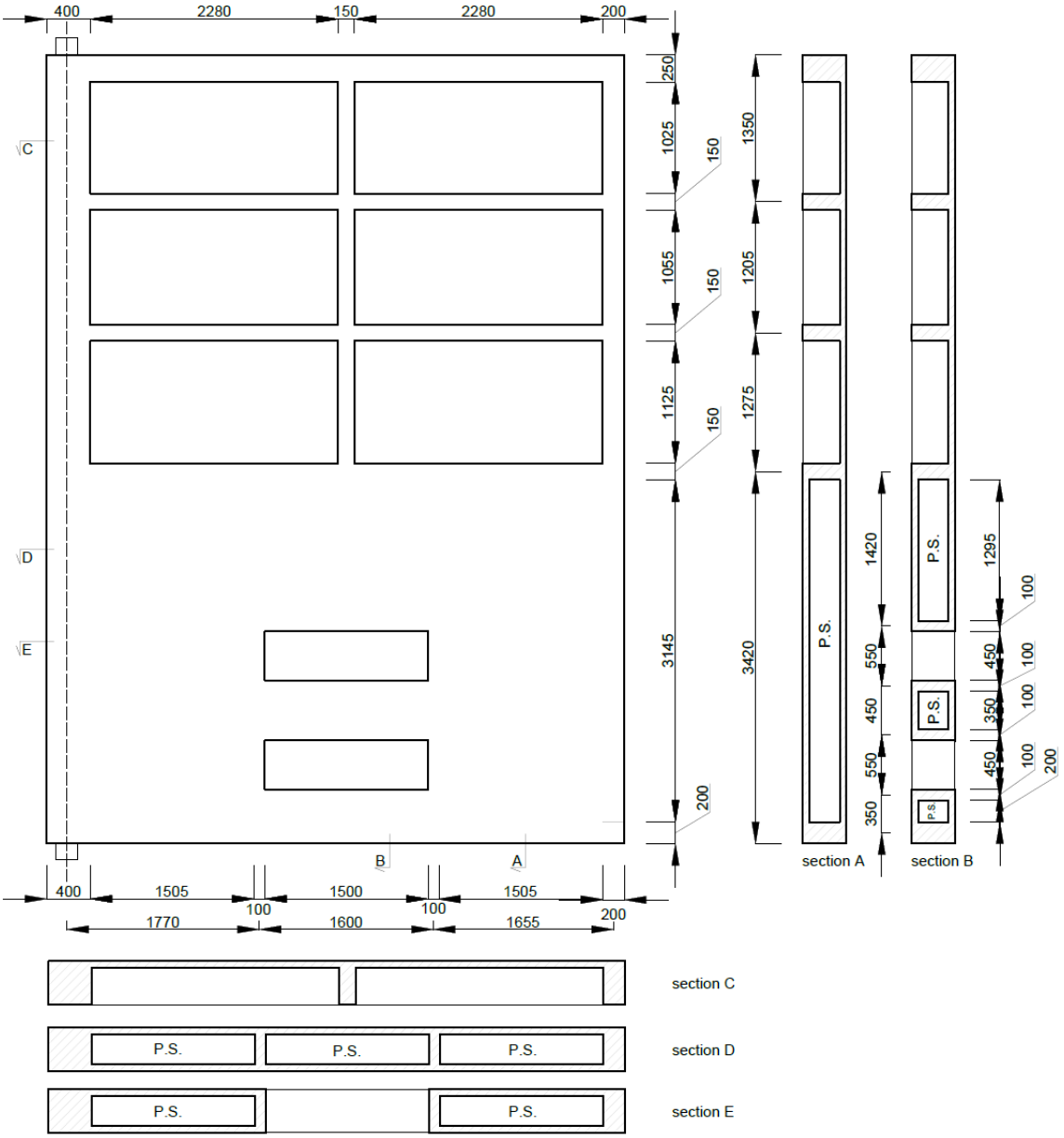

Fig. 9: Geometry of the original UHPFRC gate

3.2 Design loads

Design loads utilized in the original design process were based on a "Design note" provided by the province to FDN. The design note included the following loads:

- Dead wight of the structure,
- Water pressure,
- Wave load,
- Life load from a platform on top of the gates,
- Wind load,
- Water vessel propeller load,
- Ice load,
- Hawser load,
- Gate driving force,
- Impact loads.

The load combinations used for the design purposes were based on the guidelines included in Eurocode NEN-EN 1991-1 (2019) [31], [32] and Tables 5-8 and 5-9 in Rijkswaterstaat (ROK 1.4, 2017) [36].

3.3 Applied design standards

The internal forces in the structure were calculated with a linear finite element model of the gate. They were then used in the standard based analytical verifications to dimensions the reinforcement inside the plate and beam sub-segments of the gate. The standards and guidelines used to facilitate the process included:

- NEN-EN 1990+A1+A1/C2, Eurocode 0 - Basis of structural and geotechnical design, 2011, [30],
- NEN-EN 1991-1-1+C1, Eurocode 1: Actions on structures - Part 1-1: General actions - Densities, self-weight, imposed loads for buildings, 2011, [31],
- NEN-EN 1991-1-4+A1+C2, Eurocode 1: Actions on structures - Part 1-1: General actions – Wind actions, 2011, [32],
- NEN-EN 1992-1-1+C2, Eurocode 2: Design of concrete structures - Part 1-1: General rules and rules for buildings, 2011, [33],
- NEN-EN 1337-3, Structural bearings - Part 3: Elastomeric bearings, 2005, [34],
- AFGC/Setra, Ultra High Performance Fibre-Reinforced Concrete; Recommendations, 2013, [2],
- MC2010, Model Code for Concrete Structures 2010, 2010, [35],
- ROK 1.4, Richtlijnen Ontwerp Kunstwerken, 2017, [36],
- RVW 2011, Richtlijn vaarwegen, 2011, [37].

4 Preliminary analysis- alterations in the layout of the structure

4.1 Overview

The purpose of this chapter was to propose general alterations to the original design of the sluice gates, as presented in Chapter 3. There was uncertainty regarding the design choices implemented in the prior version. A proposal for changes was deemed necessary after evaluating the geometry of the structure and discussing the topic with FDN. After evaluating the prior design, it was subsequently concluded that a rearrangement and redimensioning of the existing segments of the structure would not have been a sufficient improvement for the new design.

In this chapter, the main principles guiding the proposal of these alternatives were first introduced. Next, the general approach to the process was outlined. Based on the guiding principles, the geometry of the structure was reevaluated, and three alternative designs were then proposed. Both simple analytical calculations and numerical analyses were subsequently utilized to verify the feasibility of these alternatives regarding some ULSs and SLSs. A comparison to the structural performance of the original design was also conducted. Finally, conclusions were drawn regarding which of the alternatives appeared most promising, and which one was chosen as the basis for the design process in the following parts of the project.

4.2 Main guiding principles

The alternatives that were the subject of the analysis are intended to fulfil the goals outlined below:

- provide a design that utilizes less material than the prior design,
- provide a design that is more efficient in terms of its structural performance,
- provide a design that is more easily manufacturable than the prior design.

Alongside these main goals the following priorities were taken into account when evaluating the considered alternatives:

- the new design choices should not be adversely affecting the durability and longevity of the structure,
- the alternative should not require increased maintenance measures to maintain its durability and performance,
- the new design choices should not disadvantage the functionality and usability of the gates,
- the alternative should not be introducing any hurdles to the manufacturing and installation processes of the gates,
- the new design should not require significant changes to the sluice structure in general in order to be implemented.

4.3 Approach towards proposing and evaluating the alternatives

To fulfil the outlined goals, while maintaining described requirements, an evaluation process consisting of several steps was conducted:

- **Step 1: Evaluation of the structure's geometric setup:**
  - first the structure's geometry was evaluated regarding the main issues identified as problematic with the original design of the gates (such as the distribution of the internal forces within specific segments of the structure and utilization rate of the unity checks in the standard analytical design process of these segments),

  - then the changes to the design that would alleviate these issues in the context of the outlined goals and priorities were suggested,
  - based on these changes, 3 new alternative designs for the gates were proposed,
  - lastly predictions were made regarding to what effect would the changes likely have on the behaviour of the structure.
- **Step 2: Evaluation of the buoyancy effect and measures** (changes decided upon in the prior step are affecting both the mass of the structure as well the impact of the buoyancy effect that the structure would be subject to. Therefore, it was necessary to evaluate if the changes would not adversely affect the performance of the gate regarding aspects related to its weight):
  - first calculations of the original designs mass and buoyancy effect's influence were presented,
  - next calculations of the mass and buoyancy effect's influence of the 3 alternatives were provided together with their comparison,
  - based on the available data the evaluation of the mass related performance of the alternatives was provided. That analysis touched on subjects such as:
    - verification of the ULSs of the steel parts that the gates were mounted on to,
    - verification of the weight related global deflections that could pose an issue to the proper functionality of the gates.
  - lastly conclusions were drawn as to the viability of the implemented changes regarding the weight related performance of the structure.
- **Step 3: Verification of the potential of the alternatives:**
  - First the approach chosen to propose the alternatives was outlined, and the reasoning behind it was provided,
  - Set up of the finite element models utilized in this section was provided and justified,
  - Comparison between the performance of the different alternatives and the original design was presented. This comparison was based primarily on the results of the analysis for:
    - Internal forces,
    - Deflections.
- **Step 4: Conclusion on the proposed alternatives:**
  - Discussion regarding which alternative was the most suitable one to be implemented as it pertained to the main guiding principles and goals presented at the start of the document was provided,
  - Conclusion in form of the alternative chosen as the basis of the analysis in the further part of the project based on the nonlinear analysis was presented.

4.4 Step 1: Evaluation of the structure's geometric setup

The basis for the original design process was the analytical design procedure centred around conducting unity checks for ULSs and SLSs of separate segments of the structure, combined with the design forces estimated based on the linear FE analysis of the doors under design standard defined load combinations.

The results of that process showed that the internal forces within the different parts of the original gate design were unevenly distributed throughout the structure. They exhibited concentrations within some parts of the structure while in other parts they reached relatively small values. This was true also for the plate segments of the gate. Those segments were also of particular significance in that context as all plate segments had been assumed to be reinforced with the same

reinforcement net all throughout the structure. This assumption will also be present throughout the rest of the design process as it significantly simplifies the manufacturing process. Also, there were requirements related to different aspects of the structures performance such as shrinkage behaviour that demanded certain minimal amounts of reinforcements to be present throughout the plates. The negative influence of the internal force distribution impacted the structural performance of the beam segments to a much lesser degree as the reinforcement was designed separately for every single one of them, so high relative difference between the internal forces in different beam segments did not lead to as severe over reinforcement as in the case of the plate segments.

Fig. 9 provided in chapter 3, presented the general view of the final gate design acquired in the original design process. The results of the linear FE analysis mentioned in this section were not presented in here, they were provided side by side with the analogical results for the new alternative designs in the later part of the chapter.

4.4.1 Proposal of the changes of the design

Based on knowledge about the material behaviour and characteristics of the UHPFRC and the loading that the gate was subject to, several proposals for changes in the design were considered. These changes have been mentioned below, after which short reasoning for either their inclusion in the redesign process or the abstention from doing so has been provided:

- Redesign of the gate as a curved mitre gate, the gate would take for of a plate structure without beam segments in this case,
- Redesign of the gate as a rolling flat gate,
- Redesign of the gate as a full plate structure (flat mitre gate),
- Change between the beam and plate segments set up of the flat mitre gate,
- Removal of the encased polystyrene cores from the structure,
- Inclusion of steel hollow beams as alternate means of providing buoyancy to the structure,
- Shifting the location of the levelling opening in the gate.

Curved mitre gate solution was primarily considered since it provides for the most effective utilization of the UHPFRC as a material. This approach would most certainly result in the most lightweight structure, as well as possibly could even require no additional reinforcement beyond the steel fibres. However, the curved design of the gate would demand the complete redesign of the lock heads. Moreover, the manufacturing of the curved gate would be significantly complicated, so this solution would only be warranted if it was known that a significant amount of the gates would be expected to be produced. As this design didn't fulfil many of the stated principles guiding the process it was not considered any further.

Rolling flat gate solution would relieve any buoyancy related issues, that the structure could face. However, this approach would also require the complete redesign of the lock heads. This was not possible in the primarily considered situation as well as in general, the rolling gate is not the most often utilized sluice gate solution so neither would it be possible in most cases of refurbishing of many other sluice structures. As this design did not fulfil the stated principles guiding the process it was not considered any further.

Full plate flat mitre gate option presented high potential in regard to reducing the complexity of the manufacturing process of the structure. This option could be viable if the gate was loaded primarily by the distributed loads. However, the considered loading conditions included several concentrated and line forces, strongly encouraging the presence of beam segments throughout the structure coinciding with the locations of application of those forces. Additionally, the water tightness

of the structure could be more difficult to be achieved in case of the generally thinner plate structure then in the case of a plate-beam structure with significantly thicker beams provided at the bottom and side edges of the gates. Due to those reasons the full plate flat mitre gate design was not considered any further in this document.

The changes in the setup of the beam and plate segments within the gate structure could be well justified since the setup of the beams in the original design did not exactly coincide with the location of respectively ice and impact loads considered. Additionally, the inspection of the internal force distribution in the previous design revealed that in the upper half of the structure the internal forces in the plate segments were significantly lower than in the bottom half. This suggested that the reorientation of the beam segments in the upper part of the gate to coincide with the mentioned loads and increasing the spacing in between them could provide clear benefits to the structural performance of the gates. The thicker beams at the outer edges of the structure should still be present as the means for providing the water tightness to the structure.

The presence of the polystyrene cores encased in between two layers of 60 mm UHPFRC plates had been justified by the need to increase the buoyancy force acting on the gates. These cores, however, unavoidably complicated the manufacturing process of the gates (floating of the cores) as well as the reinforcement patterns for the adjacent elements. The need for the second layer of the 60 mm UHPRFC plate also to a certain degree offsets the benefit coming from the increased buoyancy force acting on the gate. It could also likely be the case that the single layer of the plate loaded in both directions by the loads from the opposing sides of the gate would perform better than two separate layers loaded just in a single direction.

Inclusion of the steel hollow sections in the structure of the gate could provide for another way of increasing the buoyancy force acting on the structure. This approach would quite likely be more easily applicable during the manufacturing of the gates as well as considering the loading that the structure is subject to it would also provide better, buoyancy force increase/additional weight ratio then the polystyrene core solution. The appropriate interaction between the concrete and steel parts of the structure would be ensured by the anchoring of the steel beams into the concrete part and its reinforcement. The disadvantage of this solution would be however the need for periodical recoating of the steel beams to ensure their durability over time.

Moving the levelling openings present in the structure could be necessary due to the shifting of the other segments of the structure. This did not affect the structure negatively in terms of its functionality. It could however, depending on the nature of that shift introduce negative effects in terms of stress concentrations around the openings.

4.4.2 Postulating alterative designs

Based on the changes described in the previous section, 3 alternative designs for the sluice gate were proposed in this section. The designs were presented below one after another with short descriptions and justifications.

4.4.2.1 Design alternative 1

This alternative includes the least number of changes in comparison to the original design of the sluice gates. The only alteration introduced was the removal of the polystyrene cores present in the bottom part of the structure, as well as the removal of the second layer of the 60mm UHPRFC plates (lower water level side). Fig. 10 depicts the simplified front and side views of the updated structure.

Introduced changes were predicted to simplify the manufacturing process of the structure as well as improve the structural behaviour of the plate segments in the lower part of the gates. This solution would however decrease the buoyancy force acting on the structure, resulting in the higher effective weight of the gates.

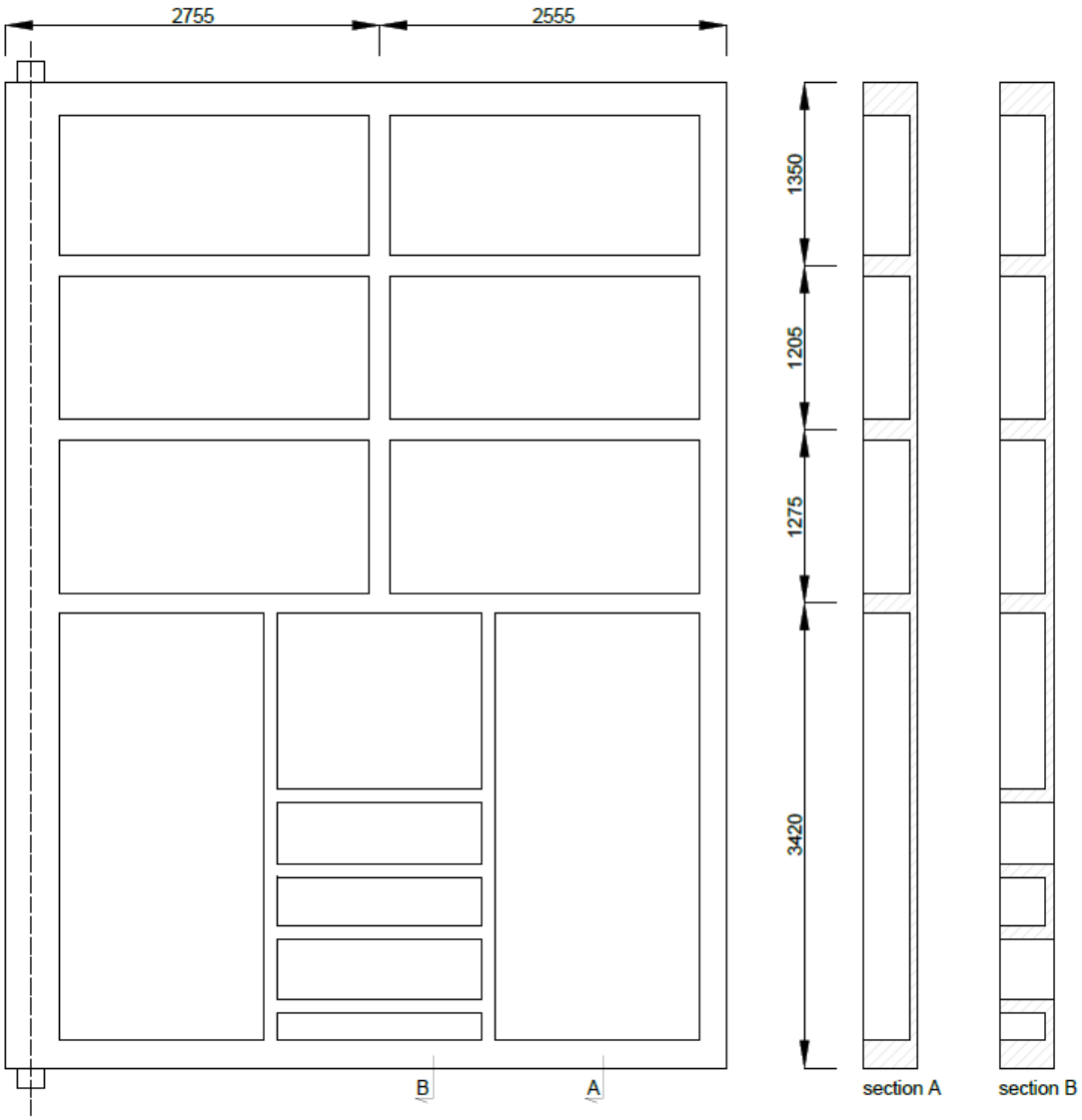

Fig. 10: Design alternative "1"

4.4.2.2 Design alternative 2

Alternative “2” included both the changes related to the polystyrene cores removal described in the case of the proposal “1”, rearrangement of the setup of the beam and plate segments within the structure and as well linked to this, the shifting of the positioning of the levelling openings. Fig. 11 provides a visualization of the front and side views of the variant “2”.

All edge beams were kept without introducing changes and were meant to both increase the general rigidity of the structure as well as ensure the water tightness of the gates. The central vertical beam was extended and now passes through the whole height of the structure. The original design had contained 3 main horizontal beams all located in the upper part of the structure. As the internal forces in the upper plate segments of the gates had been of very small value it was deemed

appropriate to significantly reduce support provided to those plates by the beams. The number of the main horizontal beams was kept the same, but they have been shifted significantly downwards. The lowest beam was shifted below the minimal water level in order to provide a slight increase to the buoyancy force acting on the gates, while the remaining beams were located roughly in between. Due to the shifting of the horizontal beams downward it was no longer possible to mount the bollards on those beams (as done in the original design). Due to this the bollards were to be mounted on the central vertical beam. The levelling openings have been positioned side by side next to the central vertical beam and lower horizontal beam.

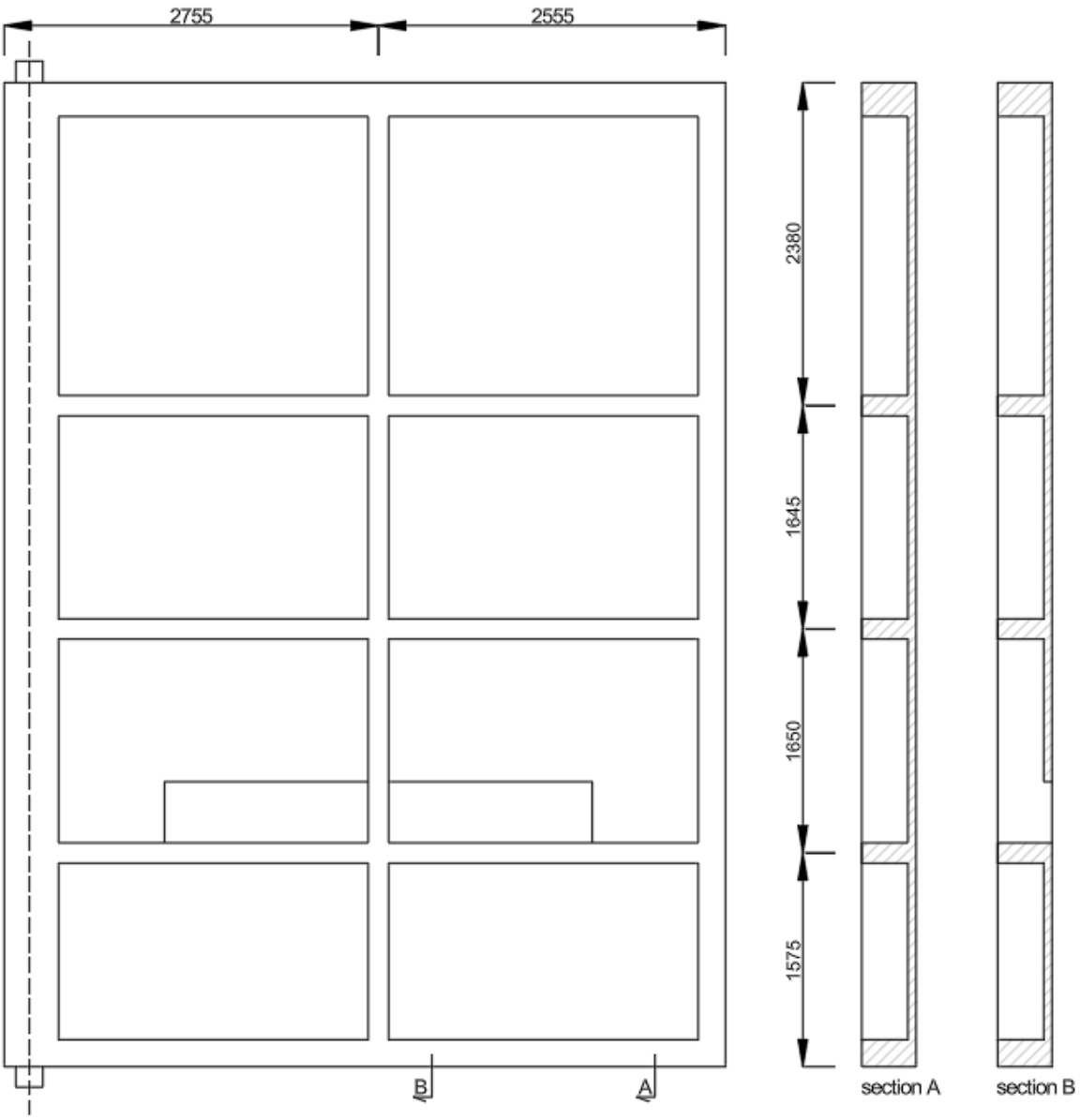

Fig. 11: Design alternative "2"

This solution resulted in a decreased effective weight of the gate as the general volume of the gate got smaller while the volume of the permanently submerged part of the gate became slightly higher. The adjustment of the location of the beam segments within the structure should also provide a more effective distribution of the loads acting upon the structure.

4.4.2.3 Design alternative 3

This alternative included the changes described in the sections relevant to proposals “1” and “2” as well as the inclusion of the steel sections in the bottom most part of the structure. Fig. 12 depicts the simplified front and side views of the updated structure.

Introduced changes would have increased the buoyancy effect acting on the gates as well as decrease the forces, deflections, cracking in the lowest plate segments of the structure.

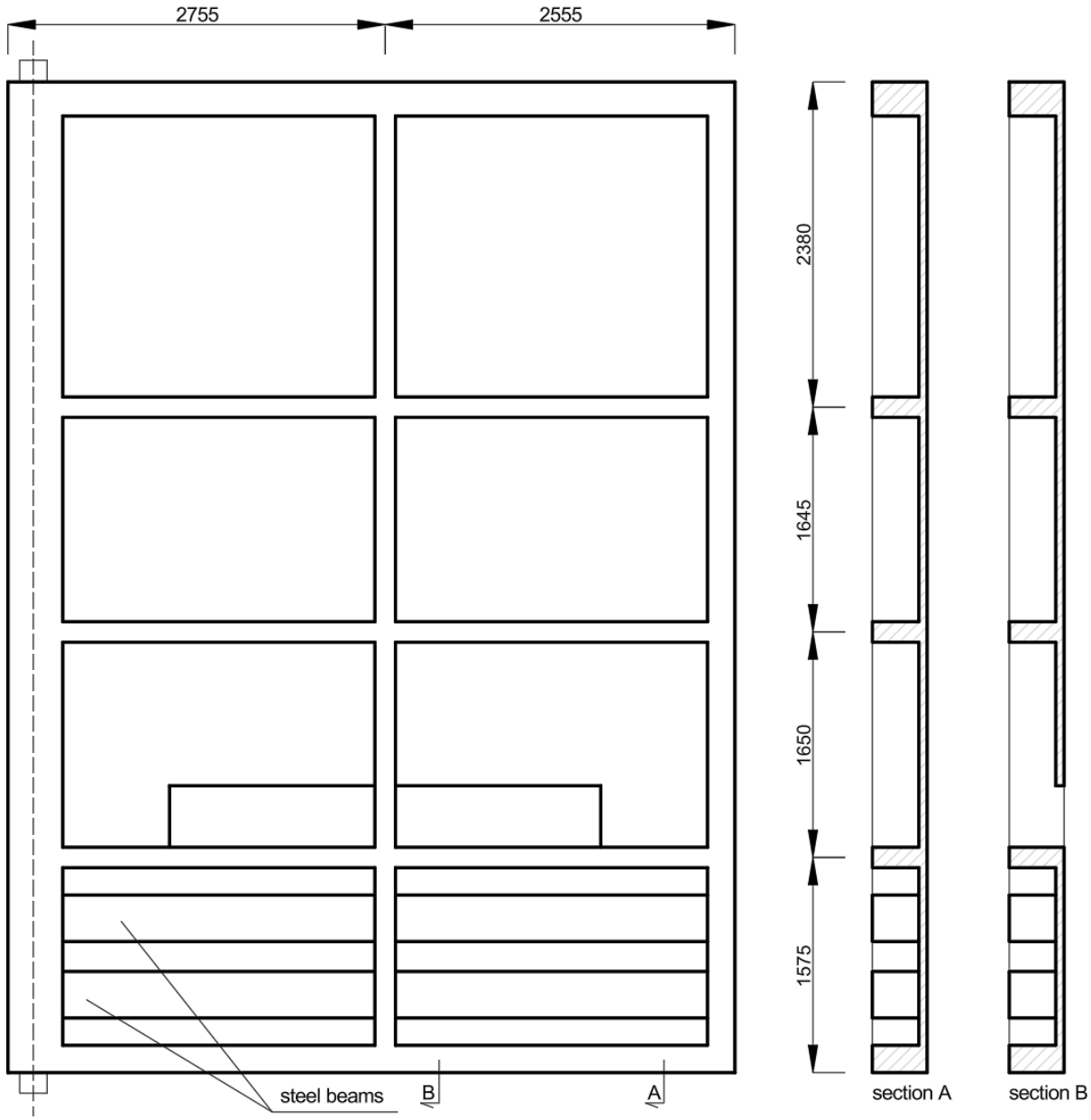

Fig. 12: Design alternative “3”

4.4.3 Prediction of the influence of implemented changes

The updated designs were compared in terms of their structural behaviour with the original design (and one another) through the means of comparing the results of the linear FE analysis based on the same principles as originally (internal forces, deflections). However, the changes introduced potentially significantly alter other aspects of the structure’s performance.

Changes included in the alternative “1” were expected to simplify the manufacturing process of the structure as well as improve the structural behaviour of the plate segments in the lower part of the gates. The former were not quantitatively evaluated while latter were discussed in the section of the report based on the results of the FE analyses. However, the changes also radically affected the buoyancy force acting on the structure and therefore also its “effective” weight in the submerged conditions.

Alternative “2” resulted in a decreased effective weight of the gate (compared to “1”) as the general volume of the gate became smaller while the volume of the permanently submerged part of the gate got slightly higher. The adjustment of the location of the beam segments within the structure should also provide a more effective distribution of the loads acting upon the structure (compared to “1” and “2”). While in case of the alternative “3” further increased the buoyancy effect acting on the gates as well as decreased the forces, deflections, cracking in the lowest plate segments of the structure. However, the manufacturing process would be more complicated than it would have been in the case for alternative “2”, as well as the periodic recoating of the steel sections would be required.

For the original design process, it was stated that the single gate piece cannot exceed the total mass of 20 t, as well as it should not exceed the weight corresponding to 15 t after subtracting the effect of the buoyancy force on the structure. As all proposed changes most likely affected the “effective” weight of the structure in a significant way it was necessary to consider this aspect alongside the mentioned changes in the internal force distributions and deflections (based on FE results), before the viability of the specific alternative as the basis for the more detailed design process could be established.

4.5 Step 2: Evaluation of the buoyancy measures, effect and its influence

As outlined in the previous section, in the original design process there was a requirement mentioned that a single gate piece can have a maximal mass of 20 t, and the “effective” mass (after factoring in the buoyancy effect) of the 15t shouldn’t be exceeded. The changes introduced in the considered design alternatives alter the mass/”effective” weight (“effective” understood as after subtracting the effect of the buoyancy force) of the gate and as such these properties had to be evaluated before the alternatives could undergo any further analysis. It was dictated by the fact that in the case when the mass of the door would be too high, there could arise problems in regard to aspects like, failure of the elements that the gate is mounted on to, or significant global deflections in the structure that would prevent the gates from proper functioning (issues with proper water tightness, opening/closing procedure).

It was deemed that the suitability of the alternatives in regard to their mass and related aspects, could be assessed by first calculating the alternative’s mass/”effective” weight, and later evaluating its effect in the form of specific ULSs of the steel tubes that the gates will be mounted up on, as well consideration of the global deflections present throughout the structure. These steps for the mentioned alternative designs had been described in the following sections of the document.

4.5.1 Original design’s mass/buoyancy

The requirements regarding max mass/”effective” weight of the gate mentioned at the start of the chapter, resulted in the inclusion of the polystyrene cores in the lower part of the gates as the means for providing increased buoyancy force compensation. Calculations regarding the verification of the mentioned requirement in the prior design process had been provided in the Table 3.

Element	Width	Height	Thk.	Nos	Volume	Unit
60mm thick plate	5.3	7.25	0.06	1	2.3055	m3
60mm thick plate	5.3	3.5	0.06	1	1.113	m3
150mm ribs-middle	5.3	0.15	0.34	3	0.8109	m3
200mm rib -bottom	5.3	0.2	0.34	1	0.3604	m3
250mm rib-top	5.3	0.25	0.35	1	0.46375	m3
Support column	6.35	0.4	0.36	1	0.9144	m3
Edge column	6.35	0.22	0.36	1	0.50292	m3
Reduction for opening	1.5	0.45	0.06	2	0.081	m3
Total Concrete Volume					6.389	m3
Density of concrete (concrete+rebar+glassfibre)					3000	Kg/m3
Selfweight of the door					**19140**	**kg**
Water weight					1025	kg/m3
Minimal water height from bottom					1.65	m
Buoyancy uplift weight (1025*1.65*5.27*0.4)					**3565**	kg
Total weight (buoyancy incl.)					**15575**	kg
				=	**15.57**	t
Weight limit					**15.00**	t
Check					acceptable	

Table 3: Calculation of the mass of the single door piece incl. the influence of buoyancy - (Appendix 4- UO Ontwerp - Ebdeuren Robbengatsluis)

Apparently, this calculation contained an inaccuracy related to the fact that the levelling openings had been omitted when evaluating the value of the buoyancy force acting on the structure. Due to that the values were recalculated. The density of concrete was assumed identical as in (Appendix 4-UO Ontwerp - Ebdeuren Robbengatsluis) as 3000 kg/m3. This led to slightly higher mass of the gate of 20.389 t. After factoring in the buoyancy effect the newly evaluated “effective” mass of the gate stood at 17.150t.

4.5.2 Alternative “1” mass/weight

The next step was the calculation of the mass and “effective” mass properties for the considered alternative designs. For the alternative “1” the mass before subtracting the effect of the buoyancy force was evaluated as 18.139 t. After factoring that into the weight of the structure the “effective” mass of the gate was established as equal 16.729 t.

4.5.3 Alternative “2” mass/weight

For alternative “2” the mass before subtracting the effect of the buoyancy force was evaluated as 17.369t. The value of the buoyancy force was estimated as equal to 15.261 kN. After factoring that into the weight of the structure the “effective” mass of the gate was established as equal 15.812 t.

4.5.4 Alternative “3” mass/weight

The depth of the gate after subtracting the 60 mm thick plate was equal to 340 mm. Based on that the initial assumption was taken of incorporating two (throughout the height) square steel beams of outer cross section size 340 mm and wall thickness of 10 mm. The increase to the buoyance force acting on the gate was evaluated equal to 10.458 kN, while the mass of the structure has been

increased by the total of 0.473 t. Based on that the “effective” mass of the alternative “3” reached the value of 15.219 t.

The benefit from including the steel beams hasn’t been proven to reduce the “effective” weight of the structure in a very meaningful way. The decrease achieved due to the inclusion of the steel section could be possibly increased if relevant structural checks would allow to decrease the beam volume/steel volume ratio for the applied beams. However, since both alternative “2” and “3” achieved the “effective” weight parameter lower than that of the original gate design and the alternative “3” would require the need to perform maintenance works on the gate as well as it would complicate the manufacturing process, it was deemed unnecessary to conduct such calculations and instead it was decided that the alternative “2” would ultimately be more suitable than “3”. To confirm that alternatives “1” and “2” could have indeed been applied and ensure the proper functioning of the structure, in the next section simple analytical checks for the ULSs of the parts that the gates would be mounted up on were verified, the global deflections present throughout the structure have also been considered.

4.5.5 Evaluation of the mass related performance of the structure

Most important aspect regarding the weight of the structure was the risk of the too high weight resulting in failure of the parts that the gate is mounted upon. This risk was evaluated in this section primarily by evaluating the shear force ULS of the steel tube that connects the gate to the lock head. In general, it would also be necessary to verify the risk of crushing of the concrete of the lock head that the tube interacts with, but this calculation was not considered as in the prior design process the resistance of this concrete to crushing was determined as significantly exceeding the necessary value.

4.5.5.1 Shear ULS – steel tubes

The shear force acting on the steel tubes was estimated based on the simple static equilibrium for the gate as equal to:

$$H_1 = \frac{\left(F_{weight} - F_{buo}\right) * \frac{w}{2}}{h} \tag{5}$$

where:

F_{weight} - weight of the gate,

F_{buo} - buoyancy force acting on the gate,

w - width of the gate,

h - height of the gate.

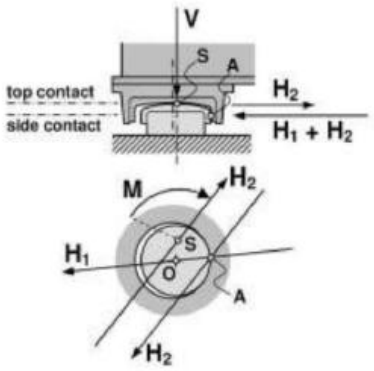

Fig. 13: Shear force on a pivot point. From ROK 1.4 (p. 72), by Rijkswaterstaat, Ministerie van Infrastructuur en Milieu, 2017.

This calculation yielded the value of $H_1 = 56.895kN$. This value had to be further increased as outlined in Rijkswaterstaat (ROK 1.4, 2017) [36] and depicted in Fig. 13, by $H_2 = V * \mu$, where μ was equal to the static steel on steel friction coefficient (assumed as 0.3). The orientation of H_1 and H_2 was not known so the maximally unfavourable condition was assumed, and the values were added up. Assuming the steel section CHS168.3x12.5 for the tube as done in the prior design this yielded the stress in the steel section at the value of:

$$\sigma_{steel,H} = \frac{H_1 + H_2}{A_{steel}} = \frac{56.895kN + 46.521kN}{0.000490m^2} = 210.678MPa$$

, in the case of the alternative "2", and 241.681 MPa in the case of the alternative "1". Considering steel grade S355H (as in the case of the original design) this meant that both alternatives may be safely applied regarding steel tube's strength considerations.

4.5.5.2 Global deflection of the gate

Additionally, to the steel tube ULS verification it also had to be checked whether the deflections related to the weight of the gate do not exceed values that could hinder the structure from properly fulfilling its function. Excessive deflections could for example prevent the gate from maintaining its water tightness or cause malfunction of the gate's opening mechanism. The deflections were evaluated based on the results of the FE analyses conducted for the purpose of the next section of the document (comparison of the internal force distribution of the prior and alternative designs). Fig. 14, presents the deflections for the alternative "1", while Fig. 15 presents the deflections for the alternative "2".

As visualized in these figures the deflections in the structure reached relatively small values, below 0.22 mm for alternative "1" and below 0.21 mm for alternative "2". These values are below the range of accuracy that the manufacturing and mounting process of the gates is subject to. Due to that they will not introduce any issues that could disrupt the proper functionality of the structure.

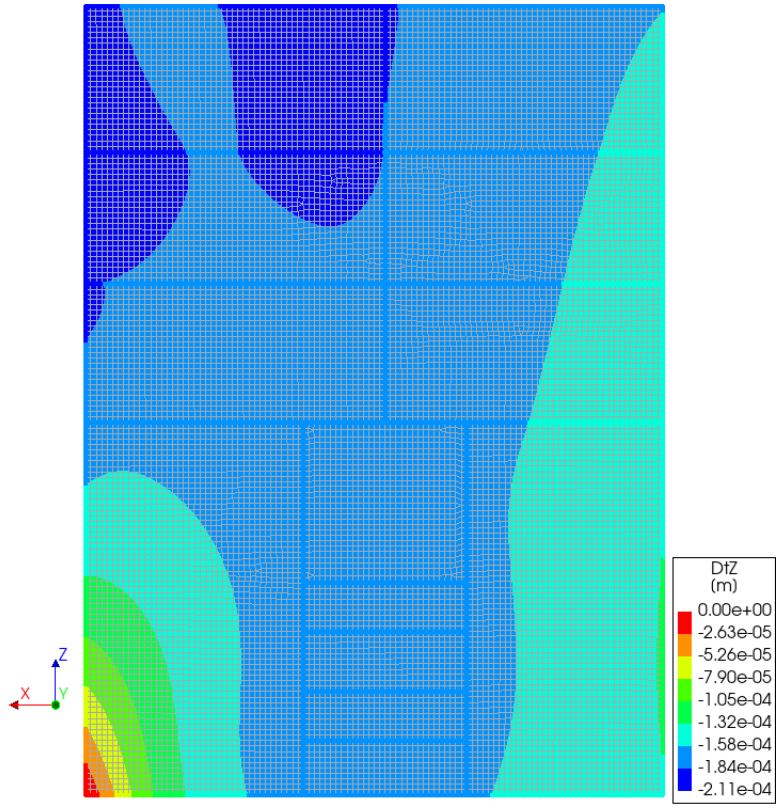

Fig. 14: Deflections of alternative "1"

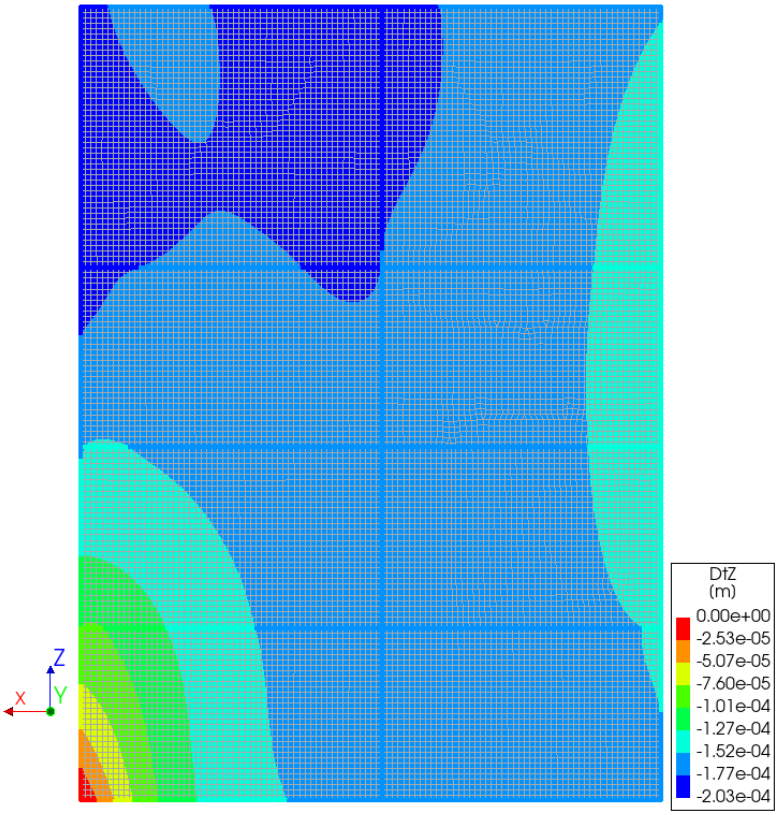

Fig. 15: Deflections of alternative "2"

4.5.6 Conclusions in regard to the mass/buoyancy force changes

Both the alternative “1” as well as “2” did not increase the “effective” weight of the structure in a way that would be detrimental to the safety and proper serviceability of the sluice. They are therefor considered in the following sections as viable, alternate designs from these standpoints.

4.6 Step 3: Verification of the potential of the alternatives

4.6.1 Approach

The general approach applied to evaluate the potential of the alternatives regarding the original design and one another was the comparison of the internal force values and distribution within the specific segments of the structure.

This comparison was conducted based on the results of the linear finite element analyses generally analogical to that applied in the prior design process. To have a more direct means of comparing the results for the alternatives with those of the original design a new model of the original structure was prepared in Diana FEA software [38]. Since the original model was prepared in SAP2000 and this software was unavailable now the preparation of the analogical model in Diana FEA software allowed for more flexibility in data post processing. The fact that this model was based on verifiably the same assumptions as the new models for the alternatives, also ensured that there were no changes in the results sourcing from any potential differences in those assumptions.

The results for the new model were initially compared to the results of the old model and it was generally ascertained that while there were small differences in between them the differences were in the range of few percent and were therefore deemed negligible.

The comparison was conducted both for the plate segments as well as the beam segments of the gates. Plate segments were of particular significance in that context as all plate segments had been assumed to be reinforced with the same reinforcement net all throughout the structure. This assumption was also present throughout the rest of the design process as it significantly simplified the manufacturing process. Additionally, the internal force distribution within the plate segments was particularly uneven throughout the structure. Due to that the sub goal was that the alternative designs should provide better force distribution throughout the structure as well as lower maximal values globally.

The internal force distribution impacted the structural performance of the beam segments to a much lesser degree as the reinforcement was designed separately for every single one of them, so high relative difference between the internal forces in different beam segments did not lead to over reinforcement in the same way as in the case of the plate segments. Due to that the general goal was to simply maintain the internal forces in the beam segments in the similar value range as in the case of the original design.

4.6.2 Setup of the FE models

This section provides the general description of how the finite element model for the analyses has been set up. The structure was modelled through the use of beam elements for the beam segments of the gate and flat shell elements for the plate segments of the door. More specifically the three node, three dimensional class III beam elements (CL18B) and eight node quadrilateral isoperimetric flat shell elements (CQ48F).

For every design (original, alternatives) there were 2 separate models prepared, one simulating the support and loading conditions when the gates are closed and another simulating the conditions when the doors are opened/during movement.

In the case of the closed variant the gate was supported in both horizontal directions on its sides and in the horizontal direction perpendicular to the gate surface on the bottom edge, additionally it was supported in all directions at the bottom pivot point.

In the case of the open variant the gate was supported in both horizontal directions at the top pivot point and in all 3 directions at the bottom pivot point. At the latter the rotation around the vertical axis was also considered fixed.

The structure is load with the same loads and design load combinations as described in chapter 3. The material parameters were also assumed the same as in the case of the original model: Young's modulus 6e+10 N/m^2, Poisson's ratio 0.2, mass density 3000 kg/m^3.

The model included dummy plates implemented in the position of the levelling opening that are supposed to provide the means of loading the gate with full considered load. Those plates were considered to be fully fixed at the edges to the neighbouring UHPRFC plates, they were assumed to be made out of steel.

The mesh size was assumed to be based on the size of the smallest elements (due to geometry modelling) that was approx. 5cm elements.

4.6.3 Comparison of the performance of the alternatives

4.6.3.1 Internal force comparison in the plate segments

Figures below present the comparison between the internal force distributions and values in the plate segments of the original design and those of design alternatives "1" and "2". The results were presented in the form of contour plots, the colour scale of the plots is adjusted to be the same for all 3 designs.

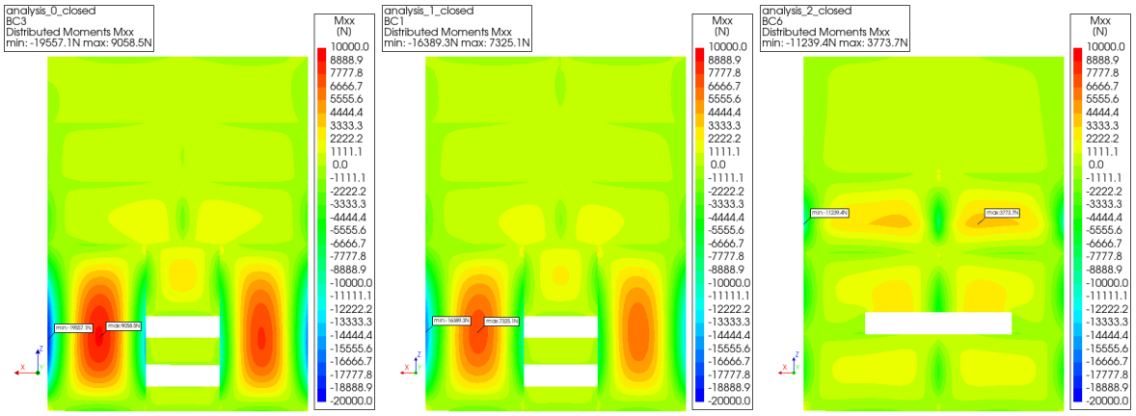

Fig. 16: Moments Mxx (about global "z" axis) in the plate segments of the structure. Left to right: original design, alternative 1, alternative 2

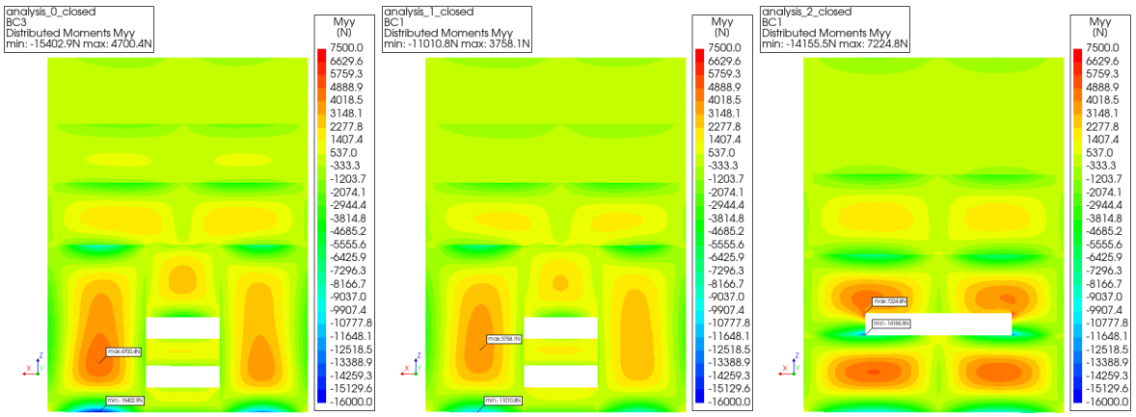

Fig. 17: Moments Myy (about global "x" axis) in the plate segments of the structure

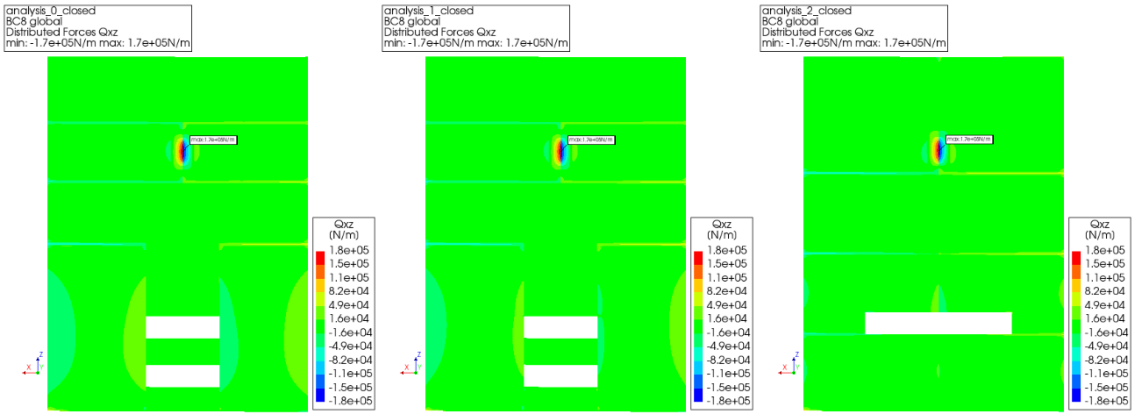

Fig. 18: Distributed shear forces Qxz in the plate segments of the structure

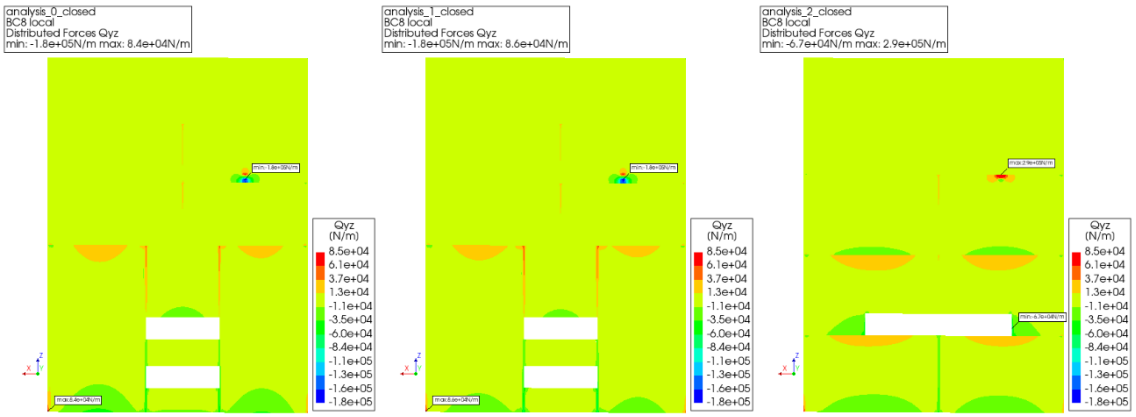

Fig. 19: Distributed shear forces Qyz in the plate segments of the structure

The moments in the plates reached lower values in both design alternatives than in the original one. The shear forces reached basically the same values as in the case of the original design (those values were used in the prior design procedure), the value of the distributed shear force Qyz in the case of alternative "2" reached significantly higher value though. However, the extreme values of the shear forces for these models are not real forces that will be present in the real structure. Their values are related to the presence of impact loads, that in reality would be located over the location of beams and would not induce such extreme local stress concentrations as they would not directly load the

plate segments (here beam segments do not have width regarding the special discretization of the structure). If on the other hand the impact load was applied away from the beam the load would be more evenly distributed throughout the plate segment. This approach to analysing results was however utilized in the original design procedure so for the means of comparison it is also implemented in this document.

4.6.3.2 Deflection comparison in the plate segments

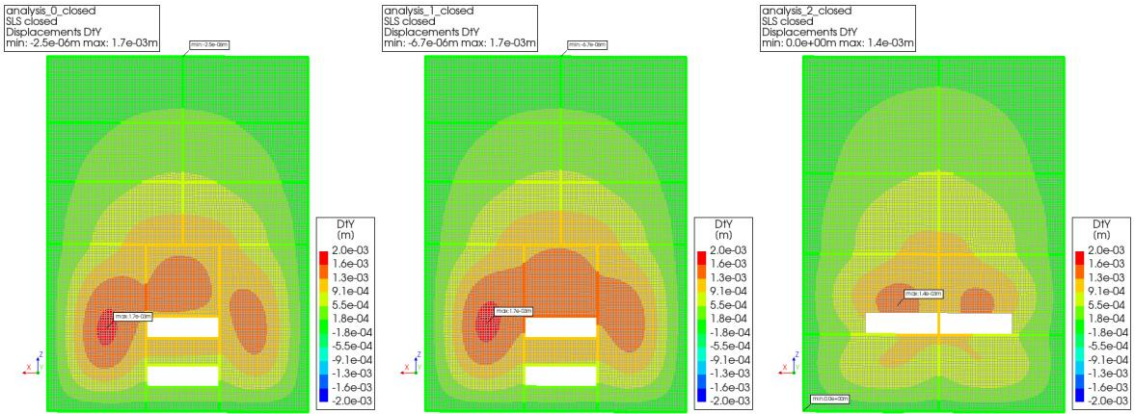

Fig. 20: Deflections in the plate segments

The global deflections that the variants underwent were smaller than in the case of the original design.

4.6.3.3 Internal force comparison in the beam segments

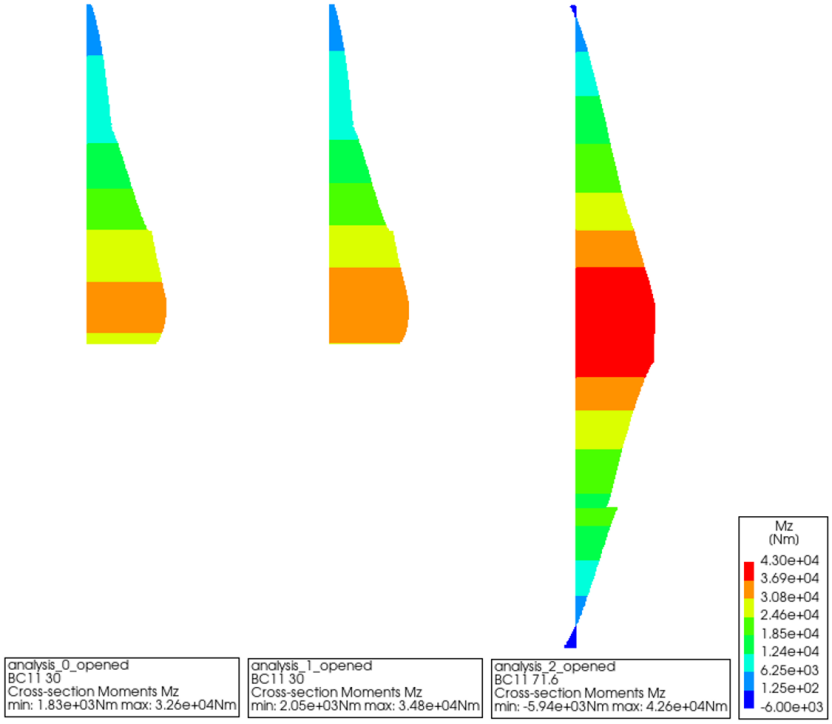

Fig. 21: Moments about major axis in the central vertical beam

This section of the report contains only the results of the analyses for the central vertical beam. The results for that part were the least beneficial in comparison to the original design, therefore the conclusions to this section can be well substantiated based just on these results. Presenting the results for all the beam segments in this report would take an excessive amount of space and not provide much added value in terms of additional information.

In general, the forces in the beam segments for alternative 1 were relatively similar to those in the case of the original design. In the case of the alternative 2, forces in beam segments in the middle of the structure were higher than in the case of original design (horizontal beams). The most significant increase in forces was encountered in the case of the vertical central beam, the extent of it was presented in Fig. 21-Fig. 25.

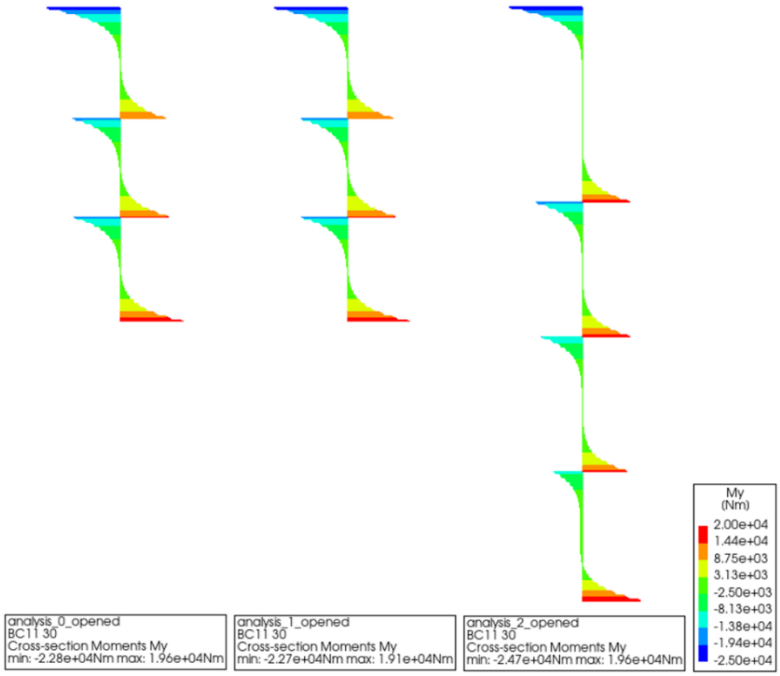

Fig. 22: Moments about minor axis in the central vertical beam

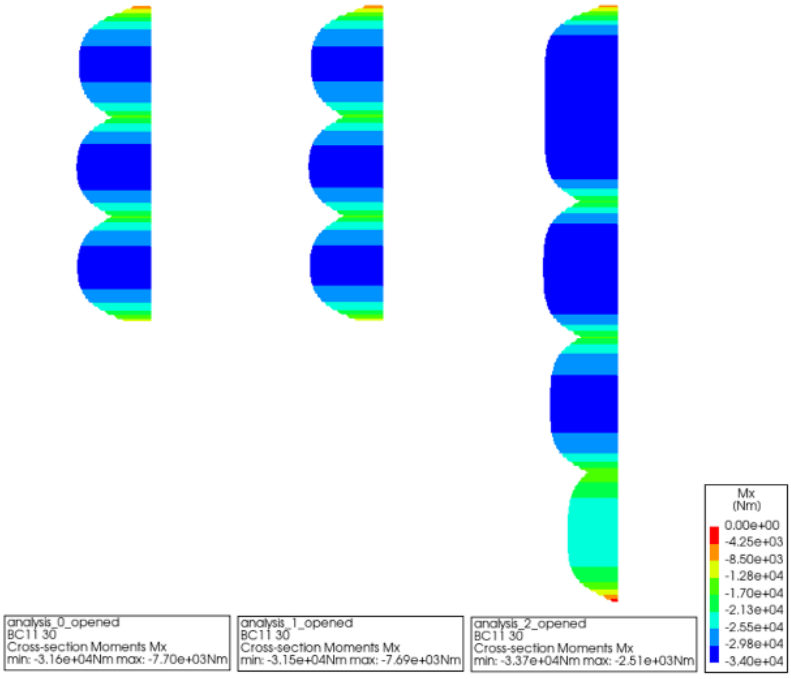

Fig. 23: Torsional moments in the central vertical beam

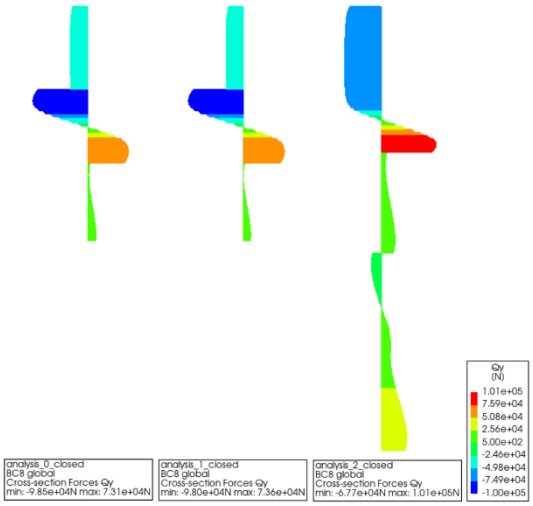

Fig. 24: Transverse force (out of the plane of the gate) in the central vertical beam

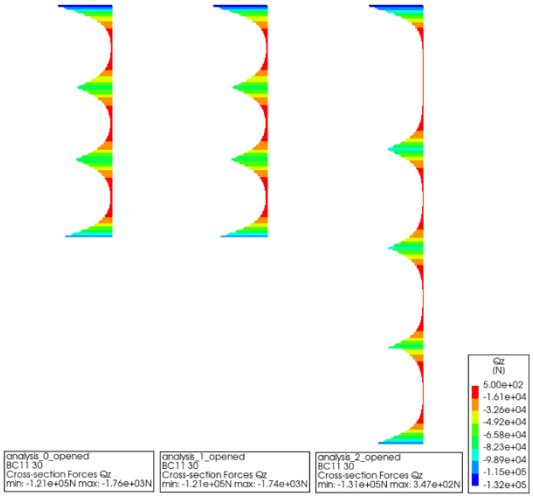

Fig. 25: Transverse force (in the plane of the gate) in the central vertical beam

As seen in the figures in alternative “2” the internal forces exceed the original values to the degree of around 10% and in the cases of bending moments about the major axis 20% and in the case of the transverse force (out of the plane of the gates) 30%. Therefore, the reinforcement or beam design would have to be increased in this beam or its sections. However, the new design would provide savings in the reinforcement throughout the rest of the structure.

4.7 Step 4: Conclusion on the proposed alternatives

Based on the results of the analyses conducted and it was evaluated that the changes to the “effective” weight of the structure do not introduce effects significantly detrimental to the safety and functionality of the structure. The alternatives “1” and “2” simplify the manufacturing process of the structure, reduce the volume of the UHPFRC used as well as based on the comparative analysis with the original designs FE results almost certainly do not negatively affect the structural behaviour of the gate. Alternative “2” provides larger benefits in all above aspects than alternative “1”, however due to lack of strengthening around the openings in the case of the alternative “2” it was decided that the significant deflection in these areas could hamper the functionality of the levelling openings. Because of that it was decided that alternative “1” would be a safer design option. Alternative “3” has been put aside as it provides similar benefits to “2” but introduces issues with manufacturing and maintenance, while the increased buoyancy force measures were deemed not necessary during the conducted

analyses. As such, alternative “1” was assumed as the basis for the design process for the following parts of the project.

5 Methodology of the design procedure

5.1 Overview

As established in the proceeding chapters, the task of the efficient and optimal design of the UHPFRC sluice gate structure presents a challenge in the form of the novelty of the applied material solution. The results of the original design process suggested that the utilized analytical formulas provided overtly conservative estimations of at least some of the calculated capacities. Having that in mind, it was decided that a two-pronged approach for providing an alternate design procedure was to be conducted.

On the one hand, the literature on the topic was evaluated in order to verify if there are more adequate analytical formulas available that could substitute the overtly conservative ones that were used before. These potential newfound verification methods were to be applied in the analytical approach generally corresponding to the one conducted for the original design.

UHPFRC is characterized by significant material property differences based on the contents of the concrete mix, especially depending on the amount, length and shape of the fibres used. Due to that, analytical formulas can be applied with limited effectiveness to some of the mix variants, depending on the experimental data, based on which they were developed. As such, the other approach is focused on the development and application of an NLFE model of the utilized material. Establishing an accurate NLFE model and applying it in the design process could alleviate the inefficiency described above, would provide the means of accounting for the force redistribution effects in the structure, and provide a framework that could be successfully applied to various UHPFRC mixes in the future.

This chapter presents the methodology applied to the design process in case of both of the approaches described above.

5.2 Methodology- NLFE approach

5.2.1 Principles for conducting the NLFE – based analysis

A design procedure based on an NLFE model could prove to be a robust solution that would alleviate the issue of inadequacy of some of the available analytical formulas and allow for the effective design of similar structures for various UHPFRC mix variants. However, to that end, such a design approach has to be based on a set of coherent principles ensuring a comprehensive design process, leading to verified and safe results.

It was decided that the framework for the proposed approach will be based on the guidelines regarding NLFEA-based design provided in the newly released Model Code for Concrete Structures 2020 (2024) [5].

The guidelines state that several steps need to be taken in order to ensure the analysis provides comprehensive, reliable and safe results. First, the analyst has to define a solution strategy for NLFEA, that is, a detailed description of an applied NLFEA method and model, suitable for the problem at hand. The solution strategy should contain all the relevant information about the applied FE approach, such as, among others:

- Finite element types,
- Finite element sizes,
- Method for verifying the equilibrium,
- Description of the material models,
- Modelling of boundary conditions,

- Displacement versus force-controlled analysis,
- Structural geometry.

After deciding on the applied solution strategy, the analyst must validate its accuracy and objectivity. The first step on the pathway to this goal is the validation of the material model applied. NLFE models for concrete can include different aspects such as its tensile/compressive behaviour, effects of confinement, concrete-concrete interaction, concrete steel interaction, effects of cyclic loading, etc. [5]. All features applied have to be validated by comparing the simple FE model results with experimental data. Mesh refinement analysis should also be conducted to establish that the material model can produce reliable results upon element mesh size change.

When the material model has been established and validated, it is next necessary to validate the solution strategy regarding the structure or structural element being the main subject of the analysis. This has to be done by comparison to the experimental results of either the full problem or its structurally relevant subpart exhibiting similar behaviour and failure mechanisms.

Before the solution strategy is used to form any conclusions, its modelling uncertainty should be evaluated by means of the statistical analysis of the results of a set of benchmark experiments relevant to the problem at hand.

Procedure including all of these activities can be systematized and presented using the flow chart as depicted in Fig. 26. The outlined steps are described in more detail in the following subsections and their application in the gate design procedure presented in Chapter 6.

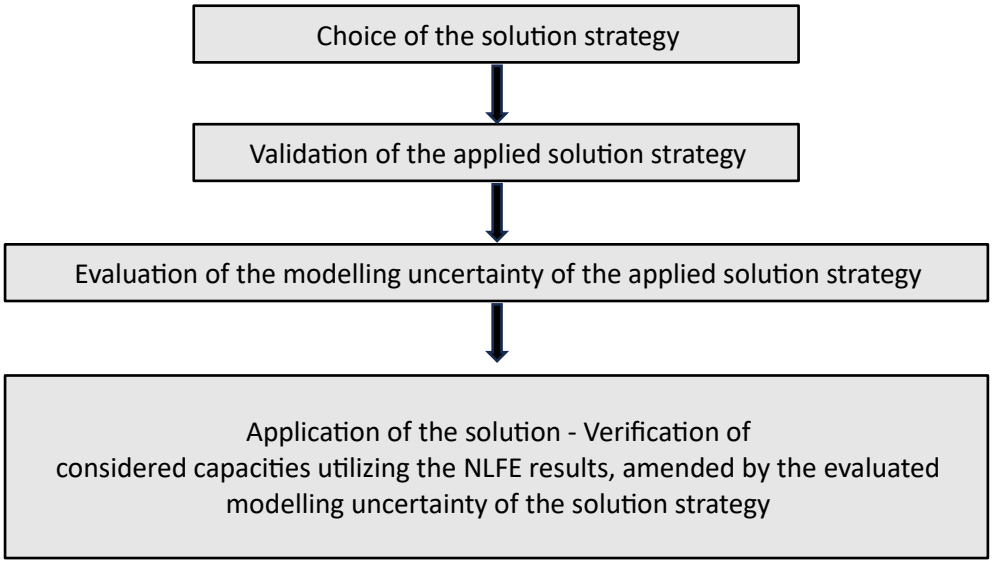

Fig. 26: Flow chart of the NLFE based approach

5.2.2 Choice of FEA software

The solution strategy applied is heavily dependent on the finite element software used, as different software can offer varied capabilities. For the purpose of this project, DIANA FEA BV's, DIANA FEA software was applied [38].

5.2.3 Procedure- developing NLFE design approach

5.2.3.1 General

According to the assumptions described in Chapter 4, gate structure is composed of plate and beam segments. Applying NLFEA approach to the gate as a whole, despite being the most robust of the possible approaches, would have been extremely cumbersome, as the above-described steps of

validation and assessment of modelling uncertainty would have required extensive and complicated tests. As such, it was decided to split the structure into the beam and plate segments and treat them generally separately throughout the process.

5.2.3.2 Establishing solution strategy

The first part of the NLFE design approach is the choice of the solution strategy. In the context of the project, the most complex task within that step was the development of the material model of the considered UHPFRC. As stated in earlier sections, UHPFRC can exhibit wide range of material behaviour depending on many factors. As such, a proper non-linear material model was of paramount importance for the usefulness of the devised approach.

To accurately model the considered UHPFRC, material tests had been conducted and then were used in an inverse analysis procedure to arrive at the final material model used throughout the approach.

In terms of other aspects of the solution strategy, two separate solution strategies were developed: one for the beam segments of the gate and one for the plate segments. Their details were described in Chapter 6.

5.2.3.3 Validation of solution strategy

Validation of the applied solution strategy is necessary to ensure that the analysed finite element models behave in ways corresponding to the considered real structural elements under various loading conditions, and that they experience the same failure mechanisms and similar stress-strain responses. Validation is done by comparing the results of analyses of simple models (applying the specific solution strategy) to the experimental data from corresponding tests.

The second part of the NLFE procedure was applied separately for the beam- and plate-segment-related approaches. Both experimental and literature-based data have been utilized. Corresponding reinforced UHPFRC beams and plates were modelled, and the response of the NLFE models, utilizing the developed UHPFRC material model, was compared with the gathered experimental data in terms of aspects such as deformation, crack pattern, and attained failure modes.

5.2.3.4 Evaluating uncertainty of the proposed solution strategies

The third step, evaluating modelling uncertainty, is necessary if any NLFEA-based approach is to be used for design purposes. The analyst must establish how accurate the assumed solution strategy is at predicting the capacity of the concerned structural elements. The assessment takes the form of a quantitative comparison between the capacity predicted by the solution strategy and a set of benchmark experiments. Those experiments should represent a structurally significant sub-part of the considered problem, exhibiting similar behaviour and failure mode.

Sections 30.10.2.2-30.10.3.4 of MC2020 (2024) [5], were assumed as the basis for the modelling uncertainty assessment within the project. The standard lists three main methods for that purpose:

- Partial Factor Method,
- Global Factor Method,
- Sampling-based method.

The assumed solution strategy included the step of conducting an inverse analysis to establish the UHPFRC's tensile curve as an exponential one, defined according to DIANA FEA. In this process, the variables defining the material properties were manipulated through a curve-fitting procedure. As such, there are no material variables available that could be used as random variables in the Partial

Factor Method. For a similar reason, and to avoid elaborate probabilistic analysis, the Sampling-based Method was also disregarded. Therefore, the Global Factor Method was chosen for the assessment of modelling uncertainty within the project, as the remaining applicable safety format available in the MC2020 (2024) [5]. The calculated global factor will be applied to the specific capacity results of the NLFE models to arrive at the final design values of those capacities.

5.2.4 Application of NLFE design approach

After the assumed solution strategy has been validated and its modelling uncertainty has been quantified, the approach can be applied to the design of specific structural elements within the gates. The scope of application of the approach is dependent on the assumed solution strategy. The application with regard to the project was described in detail in Chapter 6, following the detailed description of the utilized solution strategy.

5.2.5 Assessment of modelling uncertainty- Global Factor Method

The structure's capacity to resist the load is verified in general as:

$$F_d \leq R_d \tag{6}$$

where:

F_d is the design value of the load variable,

R_d is the design value of the capacity variable, which is estimated by the means of Global Factor Method.

The uncertainties for the load and capacity are separated. In the Global Factor Method, the design capacity is equal to the global capacity divided by the global factor γ_R. It is assumed that the NLFEA run with mean values of basic variables, gives the mean value of the capacity R_m. The design value of the capacity R_d is defined as:

$$R_d = \frac{R_m}{\gamma_R} \tag{7}$$

where:

R_m is the mean value of capacity,

γ_R is the global factor.

Since the structure is not sensitive to geometrical variability, for the considered problem the mean capacity R_m is basically assumed equal to the result of the NLFEA run with expected in situ material properties:

$$R_d = \frac{R_{NLFEA}}{\gamma_R} \tag{8}$$

For single failure mechanism, which is the case in the considered problem, global factor is equal to:

$$\gamma_R = \frac{1}{\mu_\theta} exp(\alpha_R \beta_{LS} V_R) \tag{9}$$

where:

μ_θ is the mean value of the modelling uncertainty,

α_R is the FORM sensitivity factor for the capacity,

β_{LS} is the target reliability index of the limit state of interest,

V_R is the global coefficient of variation.

Based on Rijkswaterstaat guidelines (ROK 1.4, 2017) [36] for 100-year reference period for new structures $\beta_{LS} = 4.3$. FORM sensitivity factor α_R is equal to 0.32. θ is the modelling uncertainty, log-normally distributed random variable defined as $\theta = R_{exp}/R_{NLFEA}$. μ_θ and $V_R = V_\theta$ are acquired through a Bayesian updating process, based on results from a pool of n benchmark analyses that are used to update prior parameters for modelling uncertainty.

s_y'	v_y'	$\overline{y}'$	n'
0.10	6.2	0.02	1.4

Tablere 4: Prior parameters for the distribution of y=ln𝜗

The updated parameters are calculated as:

$$n'' = n' + n \tag{10}$$

$$v_y'' = v_y' + v_y + 1 \tag{11}$$

$$\overline{y}'' = \frac{1}{n''}\left(n\overline{y} + n'\overline{y}'\right) \tag{12}$$

$$s_y''^2 = \frac{1}{v_y''}\left(v_y s_y^2 + v_y' s_y'^2 + \frac{nn'}{n+n'}\left(\overline{y} - \overline{y}'\right)^2\right) \tag{13}$$

where:

$\overline{y}$ is the mean of the sample,

s_y is the variance of the sample,

$v_y = n - 1$ is the number of degrees of freedom.

Using equations (14), (15), the mean and the coefficient of variation of the modelling uncertainty can be approximated as:

$$\mu_\theta \approx exp\left(\overline{y}''\right) \tag{14}$$

$$V_\theta \approx s_y'' \sqrt{\frac{v_y''\left(v_y'' + 2\right)}{\left(v_y'' - 2\right)\left(v_y'' + 1\right)}} \tag{15}$$

5.3 Methodology-analytical approach

5.3.1 Overview

One of the goals of the project was to provide an alternate design that would better utilize the advantages of the material, as well as make the manufacturing process of the structure easier. With the resources available, this goal could not be fully realized within the scope of the project solely through the utilization of the NLFE approach, due to the extent of the tests that would have had to be performed. As such, the analytical design process has also been conducted to provide an alternate design that would meet the necessary safety and serviceability design requirements. This analytical procedure, in some areas, supplements the NLFEA-based derivations and, in others, solely addresses the concerned design checks.

5.3.2 Principles for conducting the analytical analysis

The background for conducting the analytical design process was primarily the MC2020 (2024) [5], as well as BetonKalender, Ultra-High Performance Concrete UHPC, Fundamentals – Design – Examples by Fehling et al. (2014) [7].

As the first step in analysing the structure, linear finite element models of the gates were prepared. Based on the results of the LFEA, the internal forces within the structures were estimated. For design purposes, the structure was then divided into beam and plate segments. Sectional analysis of those segments was subsequently conducted, in which all of the distinguished segments underwent limit state analysis to verify their ultimate and serviceability limit states. Most of the limit states were verified based on the specifications within MC2020 (2024) [5]; the bending ULS of both beam and plate segments was verified based on Fehling et al. (2014) [7]. The procedure has been illustrated utilizing the flow chart presented in Fig. 1, and more information on its steps is provided in the following subsections.

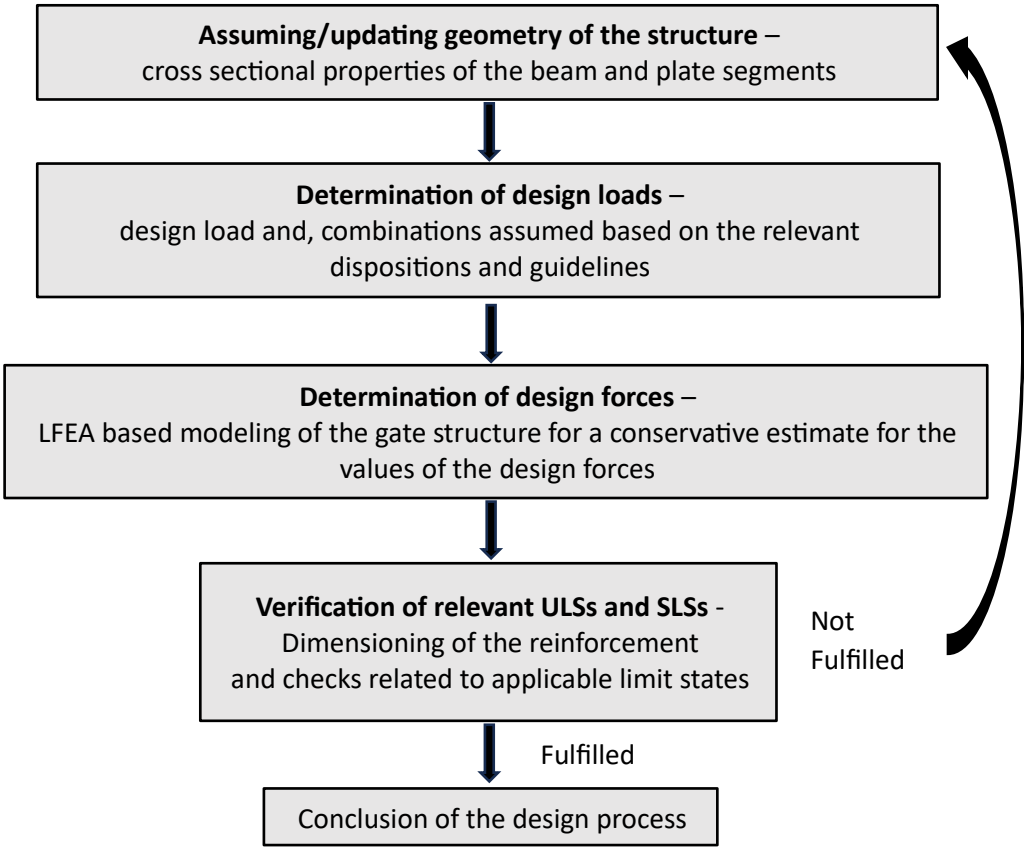

Fig. 27: Flow chart of the analytical design procedure

5.3.3 Analytical design process

5.3.3.1 Determination of design loads

The loading applied to the gates was determined based on the Design Note supplied to FDN by the Province of Groningen, when the original project was contracted. The loads specified in the note included:

- Dead wight of the structure,
- Water pressure,
- Wave load,
- Life load from a platform on top of the gates,

- Wind load,
- Water vessel propeller load,
- Ice load,
- Hawser load,
- Gate driving force,
- Impact loads – equivalent static loads as specified in the Design Note.

The loads outlined in the Design Note were then incorporated into Eurocode NEN-EN 1991-1-1 (2019) [31] and Rijkswaterstaat (ROK 1.4, 2017) [36] based load combinations. Therefore, the loading combinations took the same form as in the case of the original design.

5.3.3.2 Linear FE modelling of the structure

The "design alternative 1" presented in Chapter 4 had been used as the basis for the design of the gates. The geometry of alternative 1 was not altered any further (with the exception of the ratio of cross-sectional dimensions of some of the internal beams) throughout the process, as its geometrical parameters heavily influenced serviceability aspects such as water tightness, buoyancy, etc. The assumed gate dimensions were determined to provide good performance in the case of all these aspects. The rest of the design process is concerned with the reinforcement design for the structure.

Two FE models of the structure were prepared: one representing support and loading conditions of the gates in the closed position, the other corresponding to the open position. The models are generally the same as in the case of alternative 1 in Chapter 4, with the cross-sectional dimensions of some of the beams being different.

The structure was modelled through the use of beam elements for the beam segments of the gate and flat shell elements for the plate segments of the door. More specifically, three-node, three-dimensional class III beam elements (CL18B) and eight-node quadrilateral isoparametric flat shell elements (CQ48F) were used.

In the case of the closed variant, the gate is supported in both horizontal directions on its sides and in the horizontal direction perpendicular to the gate surface on the bottom edge. Additionally, it is supported in all directions at the bottom pivot point.

In the case of the open variant, the gate is supported in both horizontal directions at the top pivot point and in all three directions at the bottom pivot point. At the latter, the rotation around the vertical axis is also considered fixed. Fig. 28 presents the geometry and support conditions of both variants of the model.

The material parameters were also assumed to be the same as in the case of the original model: Young's modulus of 6e+10 N/m², Poisson's ratio of 0.2, and mass density of 3000 kg/m³. The mesh size used was approximately 5 cm.

The model includes a dummy plate implemented in the position of the levelling opening, which is intended to provide the means of loading the gate with the full considered load. These plates are considered to be fully fixed at the edges to the neighbouring UHPFRC plates and are assumed to be made out of steel.

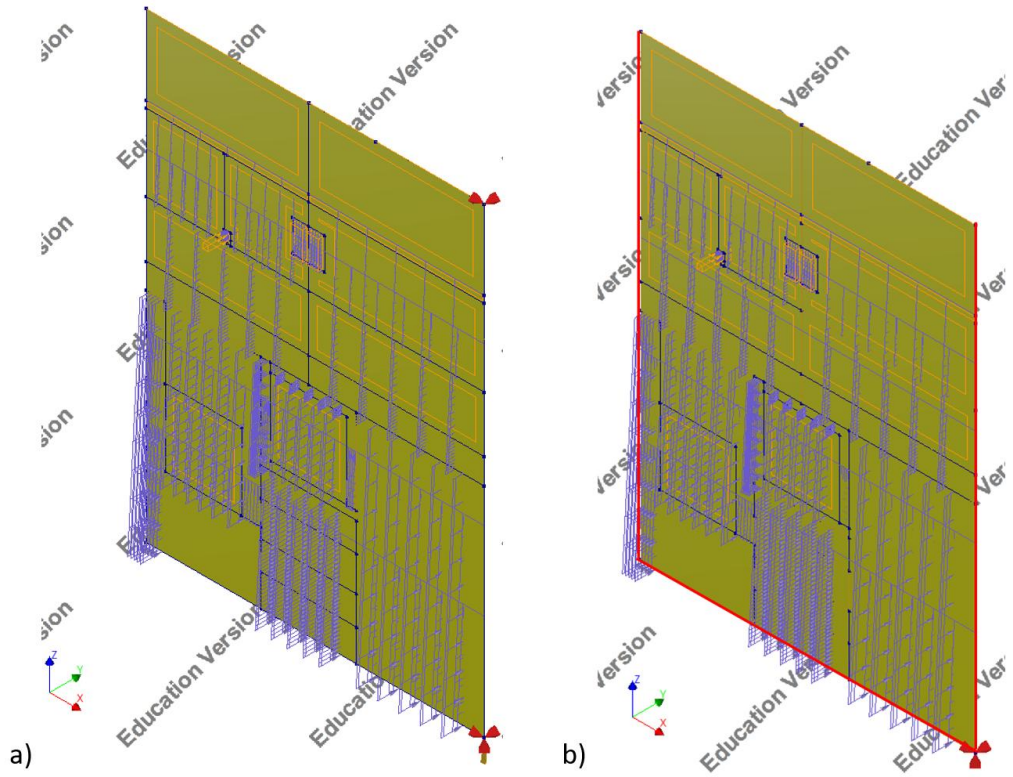

Fig. 28: Geometry of the FE models. a) Open gates model, b) closed gates model. Red lines depict line supports

5.3.3.3 Determination of design forces

For the purpose of the cross-sectional analysis, the gate structure was divided into a set of sub-elements: plate segments and separate beam segments for the continuous beams throughout the structure. Fig. 29 presents a schematic view of the structure with the sub-elements marked and annotated with the names by which they were referred to throughout the project:

- Plate segments,
- Internal horizontal beams 1&2,
- Internal horizontal beam 3,
- Internal vertical beam,
- Beams around the openings,
- Top beam,
- Seal beam,
- Pivot beam,
- Bottom beam.

Plate segments were all considered together. This approach was chosen to ensure that the plates are capable of resisting the generally unpredictable nature of the impact load, as well as to simplify the manufacturing of the gates. The two top “internal” beams were treated together in the cross-sectional analysis, as they have the same cross-sectional dimensions and are located in the part of the gate exposed to the smallest loads. It was likely that neither would require much, if any, reinforcement. Similarly, the beams around the openings in the bottom part of the gates were also treated as a group, as they were identical and the forces present in them were relatively small compared to other parts of the gates.

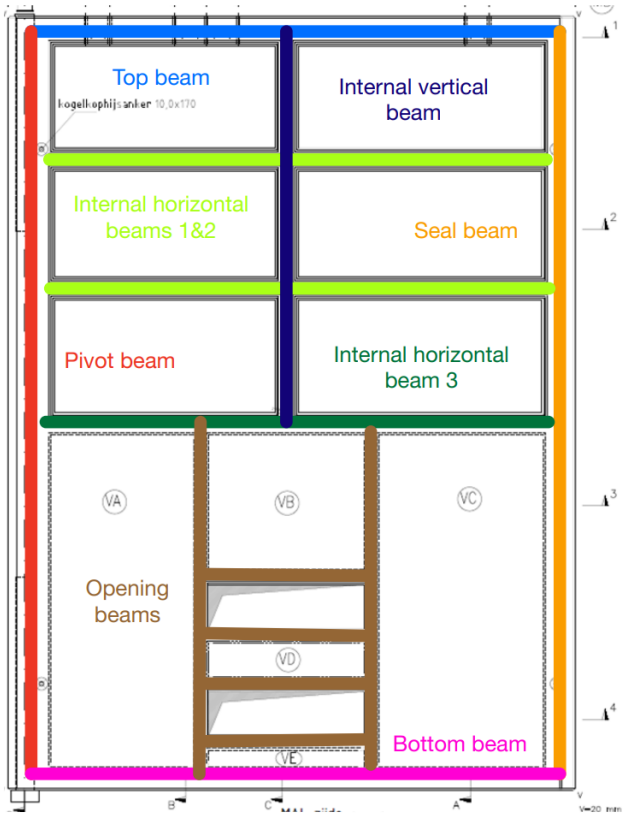

Fig. 29: Division of the gate structure into sub-elements considered separately in the design process

The FE models described in the previous section were used to evaluate the design forces present in the identified sub-elements of the gate structure. That is, distributed moments and shear forces for the plate segments, and moments, shear forces, and axial forces for the beam segments. For each of the identified sub-elements, only one set of forces representing the extreme loading conditions was considered.

5.3.3.4 Cross-sectional, limit state analysis

For the identified sub-elements of the structure, the adequate ULSs and SLSs were verified in a cross-sectional analysis process. For the plate segments, these limit states included: bending ULS, shear force ULS, punching shear ULS (adapted for the purpose of considering safety with regard to statically equivalent impact loads), and crack width SLS. For the beam segments, the limit states included: bending ULS, shear force ULS, torsion ULS, and crack width SLS. The deformation SLS was also evaluated. The following sub-sections describe the theoretical and standard background utilized for the specified ultimate and serviceability limit states.

5.3.3.4.1 Bending ULS

Bending ULS verifications are based on the UHPFRC cross-sectional behaviour model described in Fehling et al. (2014) [7]. The model discussed in the publication was created based on the analysis of test results of UHPFRCs characterized by 20 mm long fibre contents of 0.5%–1.5% by volume and mean compressive strengths of approximately 190 MPa, which corresponds well with the UHPFRC utilized in the case of the project. The model is evaluated to provide sufficient accuracy for the evaluation of the bending moment capacity for similar UHPFRCs. The model assumes stress distribution and resulting internal forces in the form of stress blocks, as presented in Fig. 30.

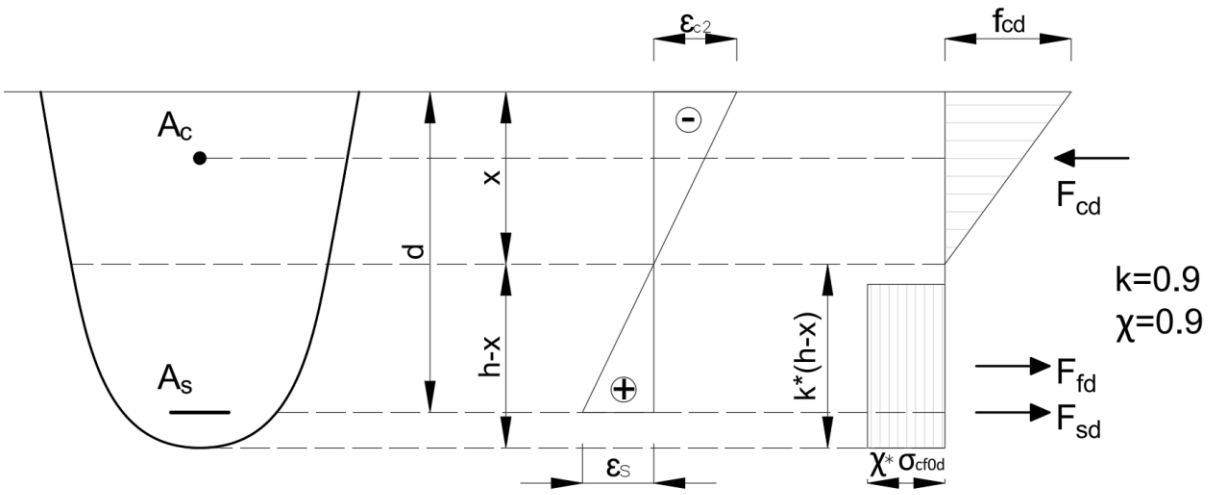

Fig. 30: Model for cross-sectional bending ULS analysis of the considered UHPFRC

The bending moment capacity of the analysed beam is then calculated based on the equilibrium conditions of the considered beam:

$$\Sigma F = 0 = N_{Ed} - F_{sd} + F_{cd} - F_{fd} \tag{16}$$

$$\Sigma M = 0 = M_{Ed} - F_{cd} \cdot (d - x/3) + F_{fd} \cdot (d - 0.45x - 0.55h) \tag{17}$$

where the corresponding forces are equal to:

$$F_{cd} = 0.5 \cdot b \cdot x \cdot f_{cd} \tag{18}$$

$$F_{sd} = A_s \cdot f_{yd} \tag{19}$$

$$F_{fd} = 0.81 \cdot b \cdot (h - x) \cdot \sigma_{cf0d} \tag{20}$$

where:

σ_{cf0d} is design fibre efficiency.

5.3.3.4.2 Shear ULS

Shear force ULS verifications were based on chapter 30.7.4.2 of MC2020 (2024) [5]. The design shear resistance of the beams was evaluated as:

$$V_{Rd} = V_{Rd,F} + V_{Rd,s} \tag{21}$$

where:

$V_{Rd,F}$ is the design shear resistance in SFRC members with conventional longitudinal reinforcement,

$V_{Rd,s}$ is the design shear resistance provided by shear reinforcement,

Design shear resistance for SFRC members with conventional longitudinal reinforcement is equal to:

$$V_{Rd,F} = \left\{ \frac{0.18}{\gamma_c} \cdot k \cdot \left[100 \cdot \rho_l \cdot \left(1 + 7.5 \cdot \frac{f_{FTUk}}{f_{ctk}} \right) \cdot f_{ck} \right]^{\frac{1}{3}} + 0.15 \cdot \sigma_{cp} \right\} \cdot b_w \cdot d \tag{22}$$

where:

k is a factor taking into account the size effect, equal to:

$$1 + \sqrt{\frac{200}{d}} \leq 2$$

ρ_l is the longitudinal reinforcement ratio,

f_{FTUk} is the characteristic value of residual tensile strength corresponding to $w_u = 1.5mm$.

f_{ctk} is the characteristic value of the tensile strength for the concrete without fibres,

f_{ck} is the characteristic value of cylindrical compressive strength [MPa],

σ_{cp} is the average stress acting in the cross section for an axial force, due to loading,

b_w is smallest width of the cross-section in the tensile area.

When shear reinforcement is necessary its contribution to the design shear resistance of the beam is equal to:

$$V_{Rd,s} = \frac{A_{sw}}{s_w} z_v \cdot f_{ywd} \cdot cot\theta_F \tag{23}$$

θ_F is evaluated using ϵ_x and they respectively are calculated as:

$$\epsilon_x = \frac{1}{2E_s A_s}\left(\frac{M_{Ed}}{z_v} + V_{Ed} + \frac{N_{Ed}}{2}\right) \geq 0 \tag{24}$$

$$\theta_F = 29° + 7000 \cdot \epsilon_x \tag{25}$$

where:

A_s is main longitudinal reinforcement area,

ϵ_x is the longitudinal strain at the mid depth of the effective shear depth, shall not be taken larger than 0.003,

$z_v = 0.9d$ is effective shear depth.

Additionally, $V_{Rd,max}$ is taken as:

$$V_{Rd,max} = \frac{k_\epsilon \cdot f_{cd} \cdot b_w \cdot z_v}{cot(\theta_F) + tan(\theta_F)} \tag{26}$$

where:

$$k_\epsilon = min\left(\frac{1}{1 + 110\epsilon_1}, 1\right) \tag{27}$$

$$\epsilon_1 = \epsilon_x + (\epsilon_x + 0.001) \cdot cot(\theta_F)^2 \tag{28}$$

In all sections the shear minimum reinforcement condition had been taken into consideration:

$$0.08 \cdot \sqrt{f_{ck}} \leq f_{FTUk} \tag{29}$$

In section where it is fulfilled no minimum shear reinforcement is necessary.

Plate segments

Plate segment's shear capacity is evaluated through distributed shear forces in form of a condition:

$$v_{Ed} \leq v_{Rd} \tag{30}$$

Design shear resistance v_{Rd} has been evaluated according to the II Level of Approximation and is equal to:

$$v_{Rd} = \tau_{Rd,cF} \cdot h = \left(\eta \cdot \frac{0.6}{\gamma_c} \left(100 \rho_l \cdot f_{ck} \frac{d_{dg}}{d} \right)^{\frac{1}{3}} + f_{FTUd} \right) \cdot h \tag{31}$$

where:

$$\eta = max\left(\frac{1}{1 + 0.43 f_{FTUk}^{2.85}}; 0.4 \right) \tag{32}$$

$$d_{dg} = 16mm + d_g \leq 40mm \tag{33}$$

$$f_{FTUd} = k_G \cdot \frac{f_{FTU;ef}}{\gamma_F} \tag{34}$$

where:

d_g is the maximum size of the aggregate,

k_G is factor scaling the residual tensile strength for non-local case.

Residual tensile strengths f_{FTUk} and $f_{FTU;ef}$ are respectively taken as:

$$f_{FTUk} = \frac{f_{R3k}}{3} \tag{35}$$

$$f_{FTU;ef} = k_0 \cdot f_{FTUk} \tag{36}$$

According to Danish guideline "Design Guideline for structural applications of steel fibre reinforced concrete" (SFRC Consortium, 2014) [39], fibre orientation factor k_0 for thin slabs can be assumed as 1.

5.3.3.4.3 Torsion ULS

Torsion ULS has been verified based on resistance on chapter 30.1.4 of MC2020 (2024) [5]. In the case of rectangular cross-sections, the maximum resistance is verified by a requirement that:

$$\left(\frac{T_{Ed}}{T_{Rd,max}} \right)^2 + \left(\frac{V_{Ed}}{V_{Rd,max}} \right)^2 \leq 1 \tag{37}$$

Calculation of torsional resistance of solid cross section is based on an ideal hollow cross section. Analysed cross-section is conceptualized as "effective hollow cross-section" of the shape of analysed cross-section and wall with effective panel thickness of t_{ef}, equal to:

$$t_{ef} \leq \frac{d_k}{8} \tag{38}$$

where:

d_k is the diameter of a circle that can be inscribed at the thinnest part of the cross section.

A minimum t_{ef} can be considered equal to twice the distance between the concrete surface and centre of longitudinal reinforcement. The area of the cross-section enclosed by the centrelines of the effective panels is denoted as A_k and utilized to evaluate the torsional resistance:

$$T_{Rd,max} = k_\epsilon \cdot \frac{f_{ck}}{\gamma_c} \cdot t_{ef} \cdot 2 \cdot A_k \cdot sin(\theta_F) \cdot cos(\theta_F) \quad (39)$$

5.3.3.4.4 Serviceability limit states

Verifications of serviceability limit states included: design crack width verifications, minimum reinforcement for crack width as well as deflections verifications. Design crack width w_d was evaluated as:

$$w_d = \frac{1}{2}\frac{\phi_s}{\rho_{s,ef}} \cdot \frac{f_{ctm} - f_{Ftsm}}{\tau_{bm}} \cdot \frac{1}{E_s} \cdot (\sigma_s - \beta \cdot \sigma_{sr} + \eta_r \cdot \epsilon_{sh} \cdot E_s) \quad (40)$$

where:

ϕ_s is the diameter of longitudinal reinforcement,

σ_s is the steel stress in the crack,

τ_{bm} is mean bond strength between reinforcing bars and concrete,

β is empirical coefficient to assess the mean strain over the length over which slip between concrete and steel occurs,

η_r is a coefficient taking into account shrinkage contribution,

ϵ_{sh} is shrinkage rate,

σ_{sr} is the maximum steel stress in a crack in the crack formation stage:

$$\sigma_{sr} = \frac{f_{ctm}}{\rho_{s,ef}}(1 + \alpha_e \rho_s)$$

where:

α_e is ratio E_s to E_c,

ρ_s is longitudinal reinforcement ratio,

$$\rho_{s,ef} = \frac{A_s}{A_{c,ef}}$$

$A_{c,ef}$ is the effective area of concrete in tension.

f_{Ftsm} was taken as equal to $0.45 \cdot f_{R1k}$.

Minimum reinforcement of $A_{s,min}$ was applied:

$$A_{s,min} = k_\epsilon \cdot k \cdot (f_{ctm} - f_{Ftsm}) \cdot \frac{A_{ct}}{\sigma_s} \quad (41)$$

where:

k_ϵ was assumed as 1,

k was assumed as 1,

A_{ct} is the tensile part of the concrete cross-section, evaluated by considering a stress field at elastic limit,

σ_s is considered equal to the yielding stress of the steel.

6 NLFE approach in the design of the sluice gates

6.1 Overview

This chapter describes how the principles outlined in Chapter 5 were applied to the UHPFRC sluice gate structure to develop an NLFE-based procedure that can be reliably used in the design process. It also presents the procedure's verification and the scope within which it can be safely applied in the design of the sluice gates.

The first few subsections describe the specifics of the applied solution strategies. Next, those strategies are validated, and their modelling uncertainty is evaluated. The final part of the chapter presents how the developed solution strategies were utilized directly in the design process to calculate some of the design capacities of the structure, etc.

6.2 Development and validation of a NLFE UHPFRC modelling approach

6.2.1 Establishing the material model

6.2.1.1 Materials present in the nonlinear finite element model

UHPFRC can be conceptualized as a composite consisting of three main distinguishable sub-materials: the UHPC matrix, steel (usually) fibres, and any potential traditional reinforcement. The distinction between the concrete matrix and the fibres is made only in finite element models that are utilized to study the behaviour of the material itself and not of any macro-scale structural elements or structures. In cases such as this project, the scale of the analysed problem allows the fibres and concrete matrix to be treated as a single “fused” material. As such, the materials directly considered in the conducted finite element analysis are UHPFRC and the reinforcing steel.

6.2.1.2 Material model of UHPFRC

6.2.1.2.1 Principles for the material model development

One part of a solution strategy is the material model used to facilitate a NLFEA. Depending on the problem being analysed, the nonlinear finite element material model can describe a varied set of effects.

As the UHPFRC mix design is not a topic of this project, only one concrete mix is considered throughout the entirety of the project—the same as the one utilized in the prior design.

In this project, a total strain-based crack model is utilized. The primary reason for that choice is that the approach studied here is intended to be generally applicable to various UHPFRC structures, and the total strain-based crack model has been deemed the most robust solution, as it does not require information on the cracking pattern exhibited by a structure prior to the model’s creation.

As one of the most crucial characteristics governing concrete’s behaviour, the material model contains a nonlinear description of tensile behaviour in the form of a tensile curve. No other additional effects are included in the model. This is due to the fact that the inclusion of every additional physical phenomenon in the model requires a set of tests providing experimental data regarding that specific phenomenon.

The project does not aim to establish a “ready-to-use” design procedure, as due to time and resource constraints, this was simply not possible. Instead, the goal is to provide an outline of a procedure in which the NLFE procedure is used for the design of the UHPFRC structure and to assess the usefulness of the chosen approach. Due to a lack of resources for conducting extensive tests concerning other aspects of the material behaviour, it was decided that the definition of just the material tensile curve will suffice to acquire relatively accurate UHPFRC material behaviour within the analysed structure.

6.2.1.2.2 Experimental tests

The tensile behaviour of the analysed UHPFRC mix has been evaluated based on three-point bending tests of prisms conducted according to NEN-EN 14651+A1 (2007) [24] in an independent laboratory. Three 550 mm × 150 mm × 150 mm UHPFRC prisms were cast at the production plant on the day the gate structure, according to the prior design, was cast. The test results are provided in Annex 2 to the report; they were recorded in the form of the load-deflection relationship.

As the vibrating table was not available at the location on the day the samples were cast, the beams had to be compacted using internal vibrators. Unfortunately, as a result of that vibration procedure, it was noted after demoulding that two of the beams were insufficiently compacted. Due to this, in the following parts of the project, the results of the test of only one of them were further utilized, as they exhibited consistency with the flexural strength results of previous tests. The flexural strength, as an average of three tests conducted before the prior design was made, was equal to 14.00 N/mm², while the now considered sample exhibited a flexural strength of 13.54 N/mm².

6.2.1.2.3 FE simulation of the 3-point bending tests of the utilized UHPFRC

The UHPFRC material model was developed by simulating the conducted three-point bending tests in the DIANA FEA software. The test was simulated with a 2D plane stress element-based model utilizing symmetry conditions. The symmetry condition was applied as a horizontal X-translational constraint along the middle of the beam. The notch in the beam was modeled by excluding that horizontal constraint throughout the height occupied by the notch (25mm). The beam support was

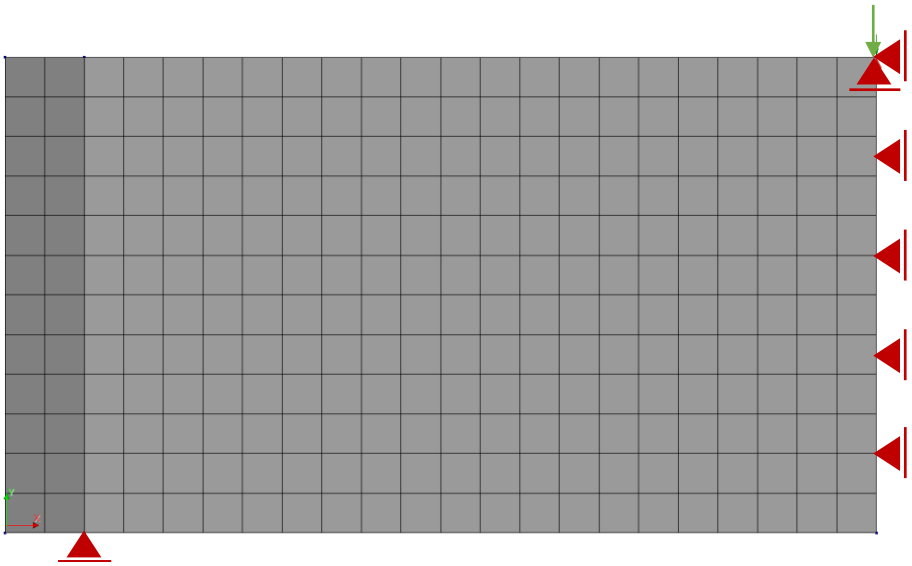

Fig. 31: Geometry, BCs and loading conditions of the model of the tested beam

modelled as a point translational constrain in the vertical Y direction. The loading took form of a displacement applied at the top of the beam in its centre. Fig. 31 represents the geometry, loading, and boundary conditions of the considered FE model. CQ16M eight-node quadrilateral isoparametric plane stress elements, based on quadratic interpolation and Gauss integration, were used. The nonlinear finite element procedure included only physical nonlinearities. It was based on a modified Newton-Raphson iterative method with 100 iterations. Energy and out-of-balance force norms with convergence tolerances of 0.001 and 0.01, respectively, were applied.

Concrete behaviour was modelled using a total strain-based rotating crack model. Tensile behaviour is described by a tensile curve. DIANA software offers a multitude of options for the choice of that tensile curve. It was decided that, for the purpose of this project, a crack bandwidth-based

tensile curve would be utilized to provide a mesh-independent solution to the problem. The tensile curve for UHPFRC is characterized by a significantly different shape than those of normal strength concretes. Each tensile curve is defined within the program by a specific set of parameters that modify the shape of the curve within a predefined range. As such, it is natural that only some of the available curve choices have shapes that correspond to that of a specific type of concrete.

The procedure to define the material model of the UHPFRC was based on the following set of steps, presented in a diagram in Fig. 32. To that aim, the fracture energy of the studied concrete was

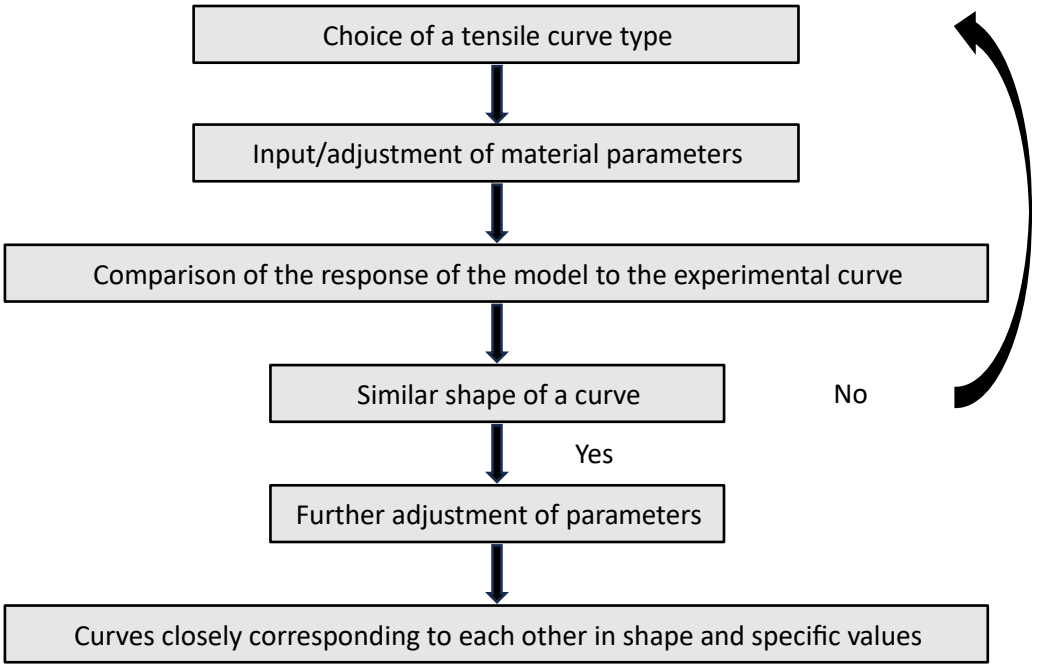

Fig. 32: Procedure applied to define the material model of UHPFRC

calculated from the test as the area under the force-displacement diagram. This fracture energy and tensile strength were subsequently input into several different predefined tensile curve options available in the software. However, none of the options provided satisfactory results in the form of a model response closely matching the behaviour of the tested sample. Some results of that process can be seen in Fig. 33, which depicts the comparison between the experimental load-deflection curves and corresponding curves acquired through NLFEA using exponential and Hordijk tensile concrete curves. The possibility of inputting a completely new user-defined tensile curve was deemed to be outside the scope of the project. As such, it was decided that the most suitable predefined curves (in terms of their shape), based on a crack bandwidth concept, would have their input parameters arbitrarily modified to find the best-fitting load-displacement curve. To that end, the calculated fracture energy was assumed as a "constant parameter," and the input tensile strength was then modified. Through a trial-and-error procedure, the best-fitting load-displacement curve was acquired. The exponential tensile curve exhibited the shape most closely corresponding to that of the experimental curve. Fig. 33 depicts some of the curves acquired during that process.

As the result, exponential tensile curve defined by tensile strength of 5.5 N/mm^2 and fracture

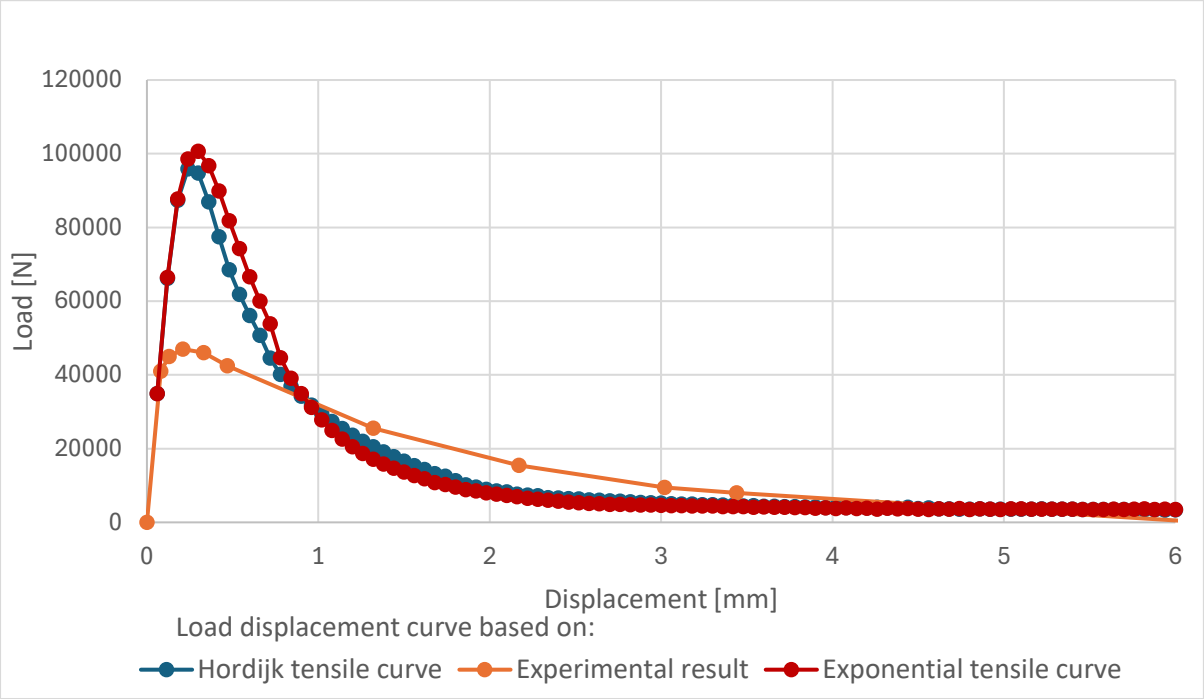

Fig. 33: Tensile curves for experimentally evaluated material parameters

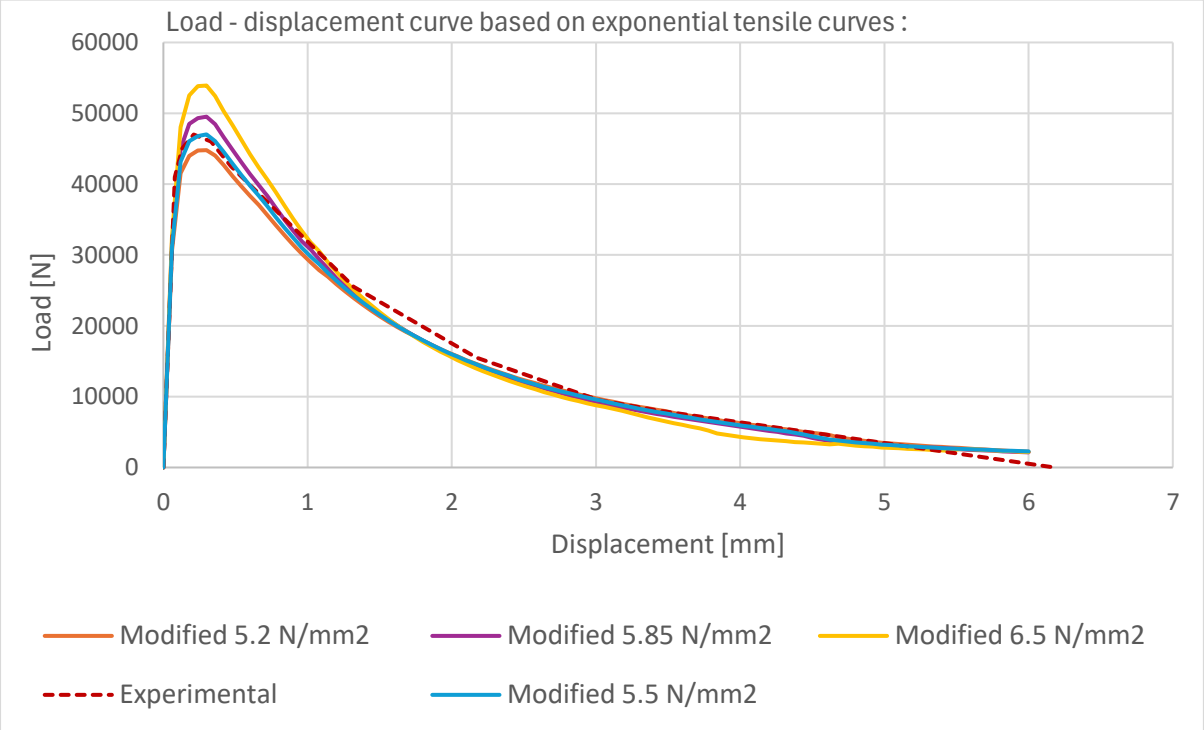

Fig. 34: Curves acquired during curve fitting process

energy of 4.844 N/mm was determined to result in the best fit for the load-displacement curve. The model utilizes Rots crack bandwidth specification. It doesn't include any residual tensile strength specifications or poison's ratios reductions. As described earlier in the chapter compressive behaviour of the concrete is defined by a linear compressive curve.

The mesh size for the analyses conducted was defined as approximately 12.5 mm. Afterwards, a mesh sensitivity study was conducted to determine if the results were indeed mesh independent. One coarser and one finer mesh were analysed, with sizes of approximately 25 mm and 8 mm, respectively. As seen in Fig. 33, the results are indeed mesh size independent. Responses for the mesh

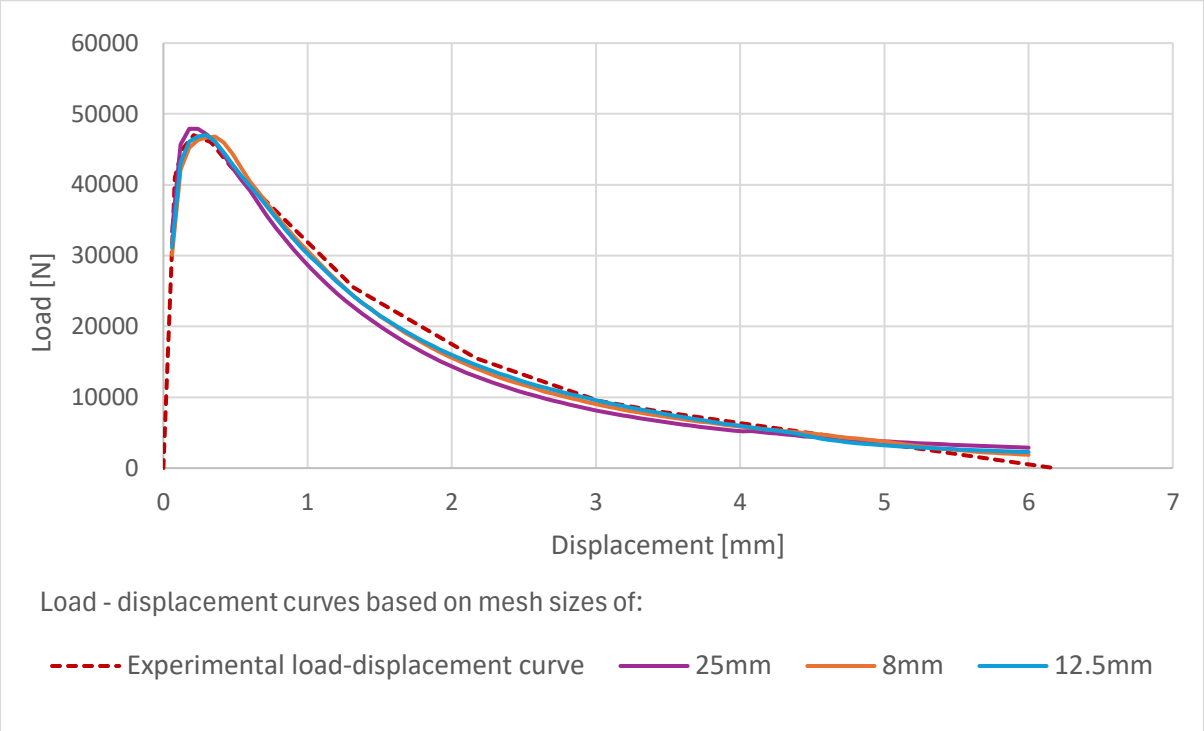

Fig. 35: Load-deflection curves depending on the applied mesh size of the model

sizes of 12.5 mm and 8 mm closely corresponded to one another. In the case of the 25 mm mesh size, there was a slight discrepancy, but it was still relatively insignificant and can be attributed to the fact that the mesh size approaches the geometrical parameter of the model (depth of the notch) and is not a result of the method through which the fracture behaviour of the concrete was modelled.

6.2.1.3 Material model of reinforcing steel

Steel fibres were modelled as part of the UHPFRC matrix and, as such, are not explicitly included in the considered FE models. Traditional reinforcement, on the other hand, is considered directly in the project and has been modelled throughout as a plastic material with no hardening included.

6.2.2 Description and validation of plane stress and shell element solution strategies

Validation of the applied solution strategy is necessary to ensure that the analysed finite element models behave in ways corresponding to the considered real structural elements under various loading conditions, and that they exhibit the same failure mechanisms and similar stress-strain responses. Validation is performed by comparing the results of analyses of simple models applying the specific solution strategy with experimental data from corresponding tests.

For the purpose of the project, the material model of the UHPFRC was applied in two separate solution strategies. The first strategy utilized shell elements and was used to calculate internal forces in the plate segments of the gates, as well as to verify the SLS (deflections) of the structure. The second solution strategy was based on 2D plane stress element models similar to that described in Section 6.2.1.2.3. This sub-chapter presents the validation of both solution strategies.

6.2.2.1 Plate element approach

Solution strategy

This approach is based on eight-node quadrilateral isoparametric curved shell elements (CQ40S). The UPFRC is modelled using the same material model as the one in section 6.2.1.2, while reinforcement is included in the form of embedded reinforcement grid. The material models correspond to those described in section 6.2.1.

Experimental data

To validate the solution strategy, experiments conducted by FDN on plate segments are utilized. The experiments included bending tests of two UHPFRC plates fabricated from the same UHPFRC material, with the only difference being a lower content of steel fibres (100 kg/m³ instead of 150 kg/m³). The specimens tested were two slabs measuring 5 m × 3 m × 0.045 m. The plates were reinforced with standard reinforcement bars of Ø12 and Ø10. Fig. 36 presents the cross-section of the

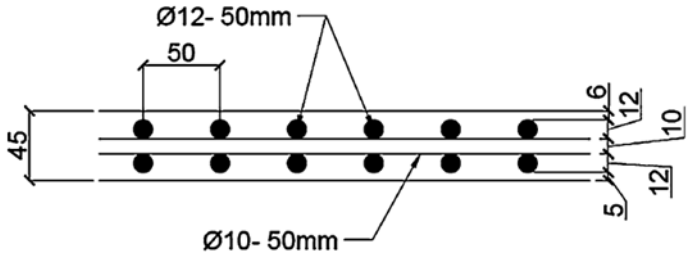

Fig. 36: Cross-section of tested plates. From Bending Capacity of Thin UHPC Plates Based on Theoretical Predictions and In-situ Testing (p. 440) , by Jan Falbr, 2018, Springer International Publishing. Copyright [2018] by Springer International Publishing.

plates. The plates were simply supported at both shorter edges, 0.3 m from the ends. The plates underwent bending tests loaded by 2150 kg concrete blocks. The schematization of the experiments is presented in Fig. 37. The experiments were described in detail in the article (Falbr, 2016) [40].

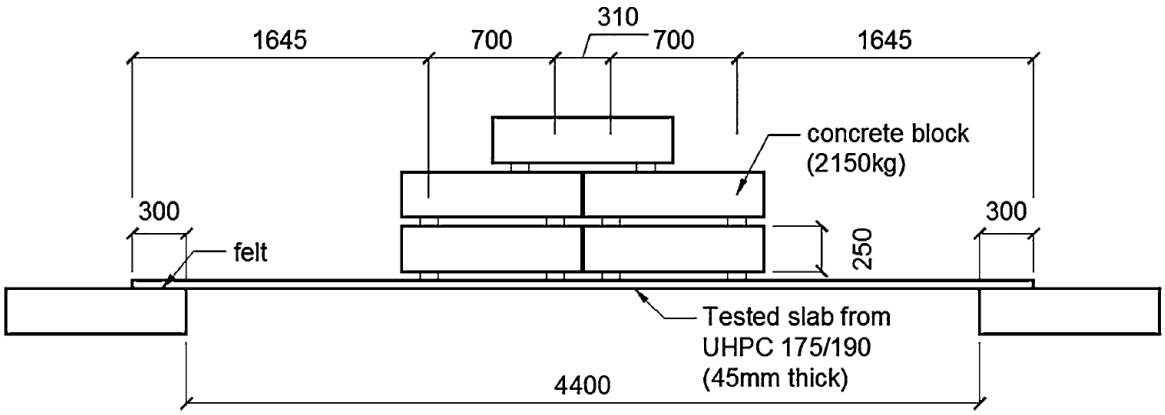

Fig. 37: Experimental setup for plate bending tests. From Bending Capacity of Thin UHPC Plates Based on Theoretical Predictions and In-situ Testing (p. 441) , by Jan Falbr, 2018, Springer International Publishing. Copyright [2018] by Springer International Publishing.

Numerical model

As mentioned, the applied solution strategy is based on eight-node quadrilateral isoparametric curved shell elements (CQ40S) and the material models established previously. Using the symmetry of the testing setup, only half of it is modelled in the FE software. Fig. 38 represents the geometry, loading, and boundary conditions of the considered FE model. The referenced coordinate system is a right-handed one. The symmetry condition was included as a horizontal X translational constraint and a Y rotational constraint along the middle of the plate. The supports were modelled as a line translational constraint in the vertical Z direction, located 300 mm from the leftmost edge of the slab. Points A and B are connected by a "link" of significantly higher stiffness than the rest of the model. This is to properly simulate the loading conditions caused by the concrete blocks stacked on top of the slab. The link's endpoints were connected to the main plate such that their nodes had identical Z translations. The remaining degrees of freedom at these nodes were left independent to allow

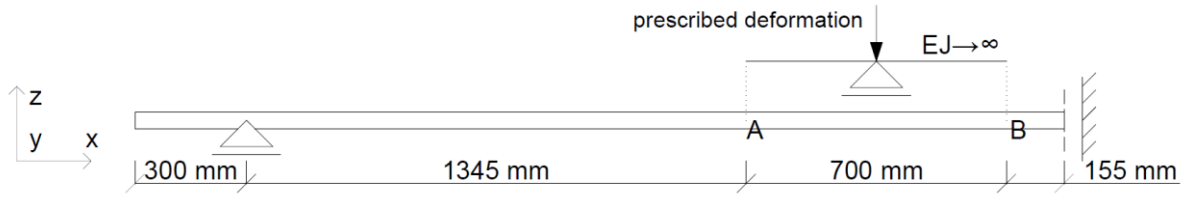

Fig. 38: Geometry, BCs and loading conditions for plate FE model

deformation freedom for the slab. The loading took the form of displacement in the Z direction applied at the middle of the link (−0.5 m). The nonlinear finite element procedure included only physical nonlinearities. It was based on a modified Newton-Raphson iterative method with 100 iterations. Energy and out-of-balance force norms, with convergence tolerances of 0.001 and 0.01 respectively, were applied.

Validation

In experiments conducted by FDN [40], the plates failed under a load corresponding to 7–8 concrete blocks, that is, under a load of 148 kN–169 kN. The results of the experiments were available primarily in the form of a load-displacement curve for the middle of the plate, as well as photographs of the crack pattern on the bottom of the plate. The results of the numerical model were compared with the experimental ones.

In the experiments, the plates first started cracking in the lower part, and the deflections increased as the reinforcement began to reach the yield strength. Failure took place relatively shortly after the yield strength of the reinforcing net was reached, which can be seen in the load-displacement curve. Failure occurred through crushing of the concrete in the top layers of the slabs. The bottom surface of the plates experienced the most significant cracking in the middle of the span. The width of the cracks quickly decreased with distance from the centre. The spacing between the macro cracks observed was approximately 50 mm. Fig. 39 presents the load-displacement curve acquired from the experiment and its comparison with the numerically acquired one.

The failure of the numerical models was defined as the point where the stresses in the top layer of the plate reached the value of 175 MPa (the compressive strength of the UHPFRC used). As the concrete was modelled using a linear compressive curve, when the compressive stresses in the element began to exceed 175 MPa, the overall response of the model quickly diverged from that of the real structure. Past that point, the results should be disregarded, and it was assumed that failure takes place at that point.

As seen in Fig. 39, the numerical model provided a generally similar response to that recorded in the experiments, with the load capacity of the numerical model being consistently slightly higher over the whole applicable range. For example, at approximately 220 mm of plate deflection, the real plate resisted a load of 106 kN, while the modelled one resisted 113 kN. This can likely be attributed to the fact that the UHPFRC mix on which the utilized material model is based had a slightly higher steel fibre content, which should offset the transition from micro- to macro-cracking and thus decrease the rate at which deflection grows. In the FE model, failure occurred at a load of 140 kN, under 289 mm of deflection. The failure occurred as a result of concrete crushing in the upper part of the plate at mid-span. This capacity is lower than the 148 kN (at 407 mm deflection) observed in the test result.

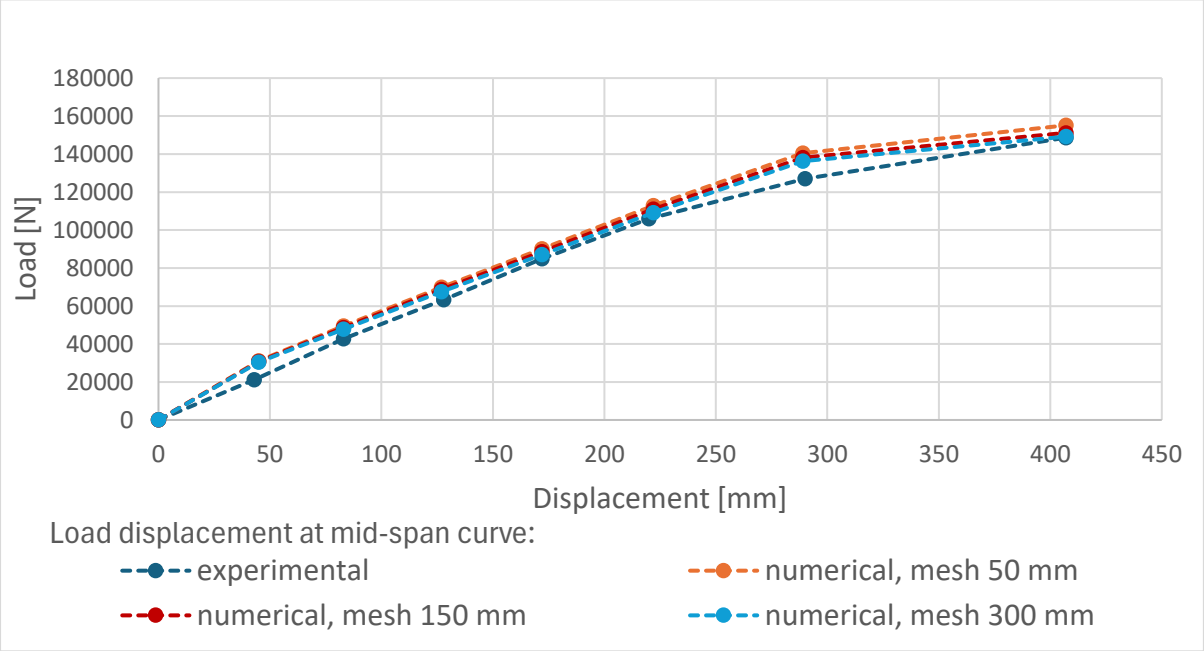

Fig. 39: Comparison of numerical and experimental results for plate bending tests

The numerical model experiences concrete crushing at the same stage as the onset of ductile behaviour occurs (at 289 mm). This divergence supports the validity of the applied numerical model. The modelled UHPFRC mix had a slightly higher steel fibre content. Again, if the numerical model is appropriately set up, this should result in a slightly delayed transition between micro- and macro-crack development, and therefore delayed yielding of reinforcement, as the macro-crack stage must be reached first. As the tested specimen reached ductile behaviour (reinforcement yielding) only shortly before the failure point, the apparent finding that the numerical model reaches it almost exactly simultaneously with the onset of concrete crushing suggests that it correctly describes the mechanical behaviour of the considered UHPFRC mix. The general shape of the load-deflection curve also supports the validity of the model, as the only difference in the shape of the curve is the later onset of ductile behaviour, causing the curve to flatten at a larger deflection than otherwise.

Three different mesh sizes were utilized (50 mm, 150 mm, 300 mm). There was no significant difference in the behaviour of the model depending on the size of the mesh.

Fig. 40 presents a photograph of the crack pattern acquired in the tests, as well as graphics presenting the crack pattern exhibited by the numerical model. In the tests, cracks reached their largest width at the mid-span of the plate (decreasing in width with distance from the centre). They developed with spacings of approximately 50 mm and were most clearly visible up to a distance of approximately 300 mm from the centre. In the rest of the plate, they were only slightly noticeable—visible only partially through the width of the plate, or completely invisible to the naked eye. At the

mid-span, there was one major crack attributed to the behaviour of the element after concrete crushing.

In the numerical model, the cracks reached widths between 0.2–0.3 mm (clearly visible to the naked eye) at a distance of 600 mm from the mid-span, with the most significant width up to a distance of 200 mm. The crack pattern of the numerical model also generally corresponds with the one acquired experimentally.

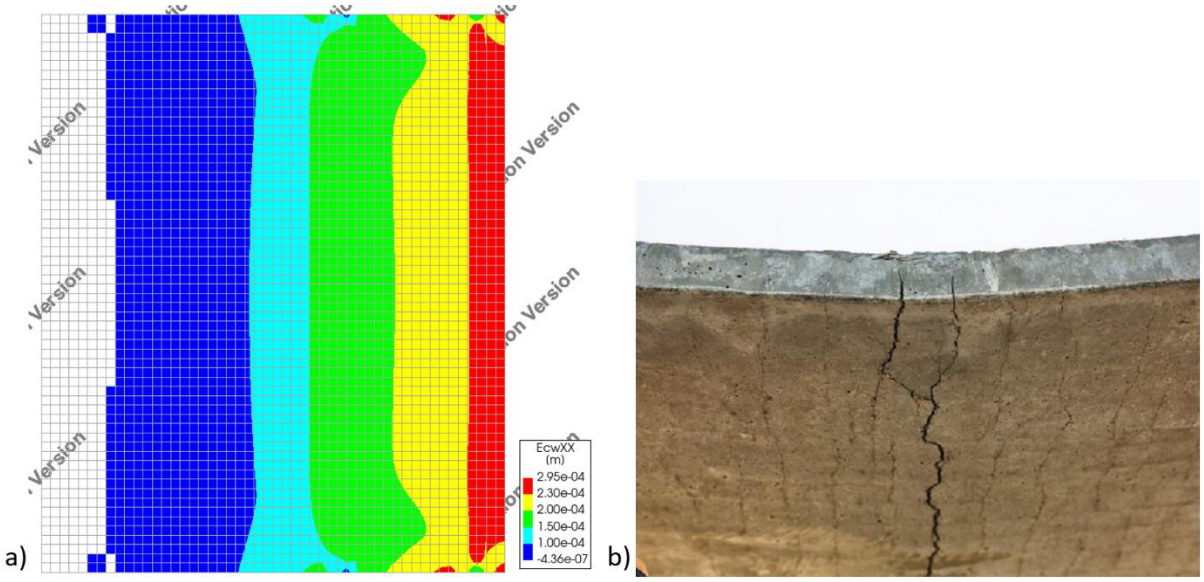

Fig. 40: Crack pattern of the plate. a) Numerical results. b) Experimental results. From Bending Capacity of Thin UHPC Plates Based on Theoretical Predictions and In-situ Testing (p. 441) , by Jan Falbr, 2018, Springer International Publishing. Copyright [2018] by Springer International Publishing.

Due to the methodology of the conducted experiments, the data acquired is not extremely precise; however, for the purpose of validating the general behaviour of the developed solution strategy, it allows for establishing conclusions that the numerical models properly describe the behaviour of the real material. With the requirement of monitoring when the concrete compressive strength is reached, it properly describes the failure mode and behaviour of the structure.

Due to the unsatisfactory precision of the data, it cannot be used to reliably assess the modelling uncertainty of the applied solution strategy.

6.2.2.2 Plane stress element approach

Solution strategy

This approach was based on eight-node quadrilateral isoparametric plane stress elements (CQ16M). The reinforcement was included in the form of embedded reinforcement bars. The UHPFRC material model was based on a tensile exponential curve and was established for the specific mixes utilized in the cited studies in the same way as in Section 6.2.1.2..

Experimental data

The utilized experimental data Yoo & Yoon (2015) [41], Yang et al. (2010) [42] was used both for the validation of the solution strategy as well as for evaluating its modelling uncertainty. For that purpose, a wider range of experimental data from the literature was used. Altogether, tests of five different UHPFRC steel-reinforced beams were considered. This includes beams produced from two different UHPFRC mixes. Generally, the mixes were very similar to the one used in the case of the flood gates. They had the same steel fibre content (2% by volume) and contained a similar fibre type (steel

fibres 13 mm in length and 0.2 mm in diameter) as that of the FDN UHPFRC mix (12.5 mm in length and 0.2 mm in diameter). The literature mixes had slightly higher compressive strengths (approx. 190 MPa). For the purpose of solution strategy validation, reference will be made to only one of the studied experiments.

The test data utilized included the load-deflection/load-CMOD curves acquired by the researchers for their UHPFRC mixes in three-point bending tests, as well as the load-displacement curves from four-point bending tests of steel-reinforced beams fabricated from these mixes. Fig. 41 presents the experimental setup used for the four-point bending tests in (Yoo & Yoon, 2015) [41].

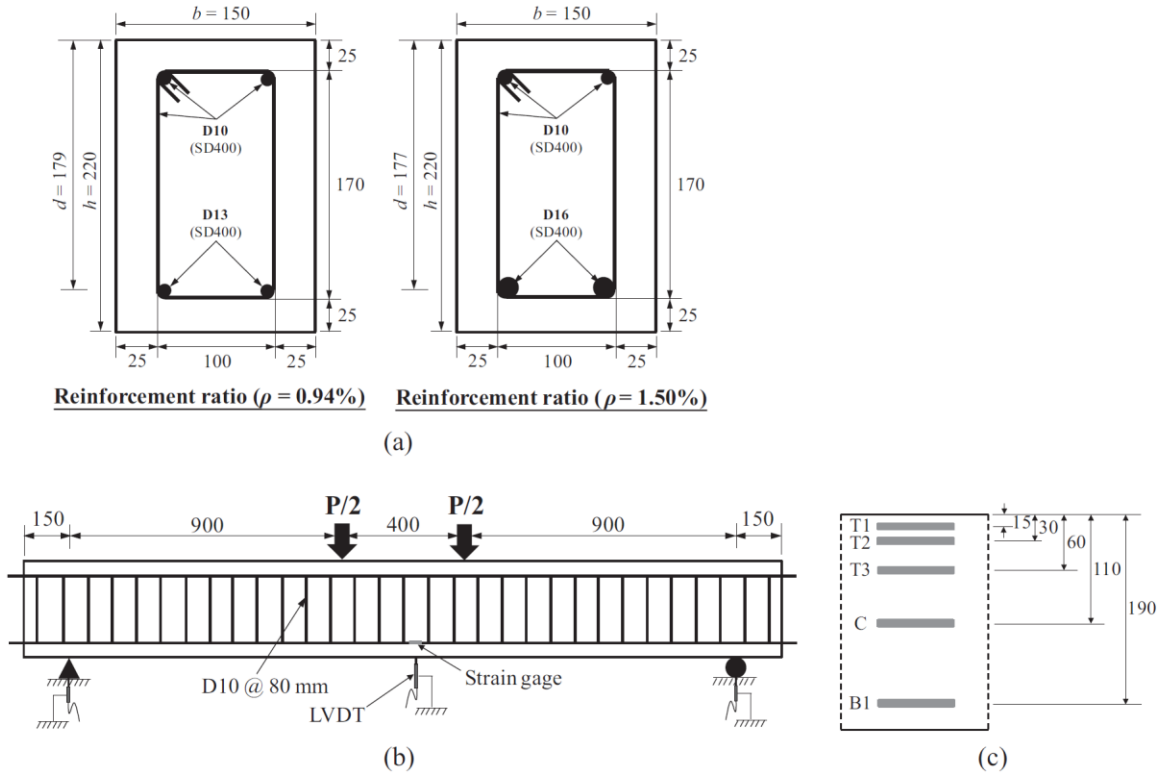

Fig. 41: Experimental setup used for the 4-point bending tests. From Structural performance of ultra-high-performance concrete beams with different steel fibers (p. 412) , by Doo-Yeol Yoo & Young-Soo Yoon, 2015, Elsevier. Copyright [2015] by Elsevier Ltd. All rights reserved.

Numerical Model

As mentioned, the applied solution strategy was based on eight-node quadrilateral isoparametric plane stress elements (CQ16M), and the material model established in an analogical inverse analysis procedure to that described in section 6.2.1.2.3, applied to the load-deflection diagram from the 3-point bending test of UHPFRC mix with 13mm long fibres in [41]. Fig. 42 depicts that load-deflection curve as well as the corresponding one acquired in the inverse analysis procedure.

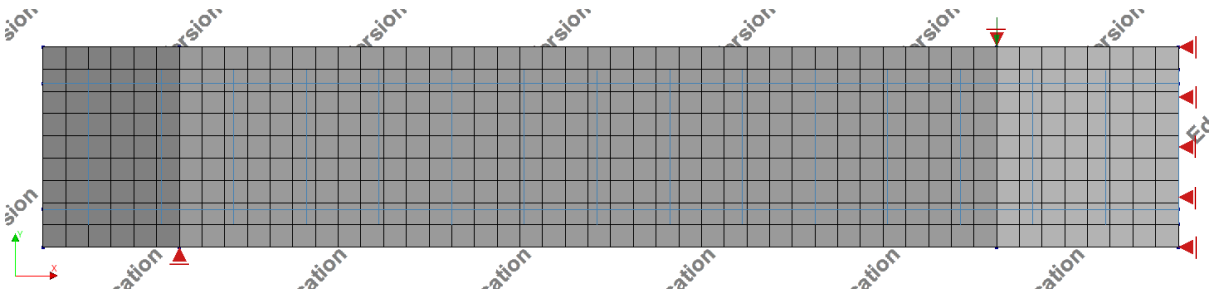

Fig. 42: Geometry, BCs and loading conditions for beam 4-point bending tests

Using the symmetry of the testing setup, only half of it was modelled in the FE software. Fig. 43 represents the geometry, loading, and boundary conditions of the considered FE model. The referenced coordinate system is a right-handed one. The symmetry condition was included as a horizontal X translational constraint throughout the middle of the beam. The beam support was modelled as a point translational constraint in the vertical Y direction. The loading took the form of a displacement (50 mm) applied at the top of the beam, 200 mm from its centre. Reinforcing steel is modelled using embedded reinforcing bars. Both longitudinal and shear reinforcement are modelled. Steel is modelled as an ideally plastic material (no hardening). The nonlinear finite element procedure included only physical nonlinearities. It was based on a modified Newton-Raphson iterative method with 100 iterations. Energy and out-of-balance force norms with convergence tolerances of 0.001 and 0.01, respectively, were put in place.

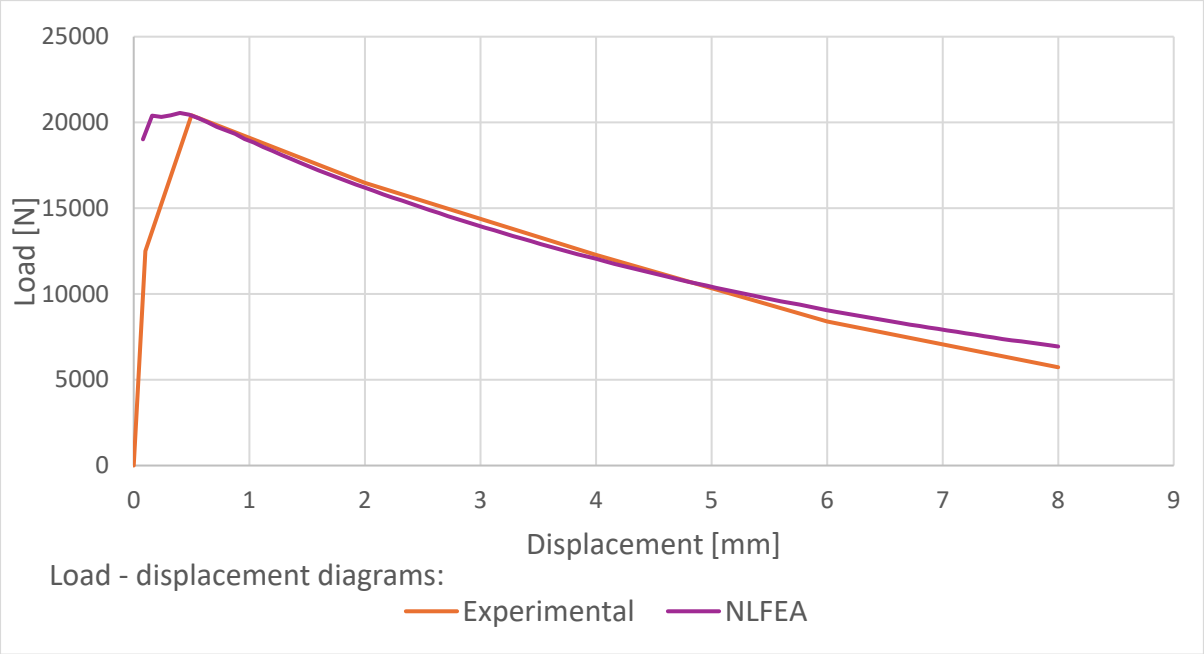

Fig. 43: Load-deflection curves for the tested UHPFRC and assumed material model

Validation

Validation takes form of a comparison between the experimental and numerical results of 4-point bending test of the beam with reinforcement ratio $\rho = 0.94\%$ from [41]. Fig. 44 presents the comparison between these load-deflection curves.

The numerical model experienced a bending failure mode, with one dominant crack forming in the zone between the point where the load was applied and the mid-span of the beam. The general shape of the numerical deflection curve corresponds very well to that of the experimental one. However, a significantly lower ultimate bending capacity was reached. The experimental setup failed at a load of 87.3 kN, while the numerical model reached an ultimate capacity of 72.5 kN (−17%).

(Yang et al., 2010) [42] was utilized to provide a comparison in terms of the cracking pattern. Fig. 45 presents the comparison between the crack pattern and crack development process of the numerical model and the test results. It depicts an approximately 500 mm segment of the beam to the left of its mid-span at three different stages in the loading process. The sub-figures on the left show the primary crack width results for the numerical model, while the sub-figures on the right show photographs of the crack pattern taken at different stages of the test.

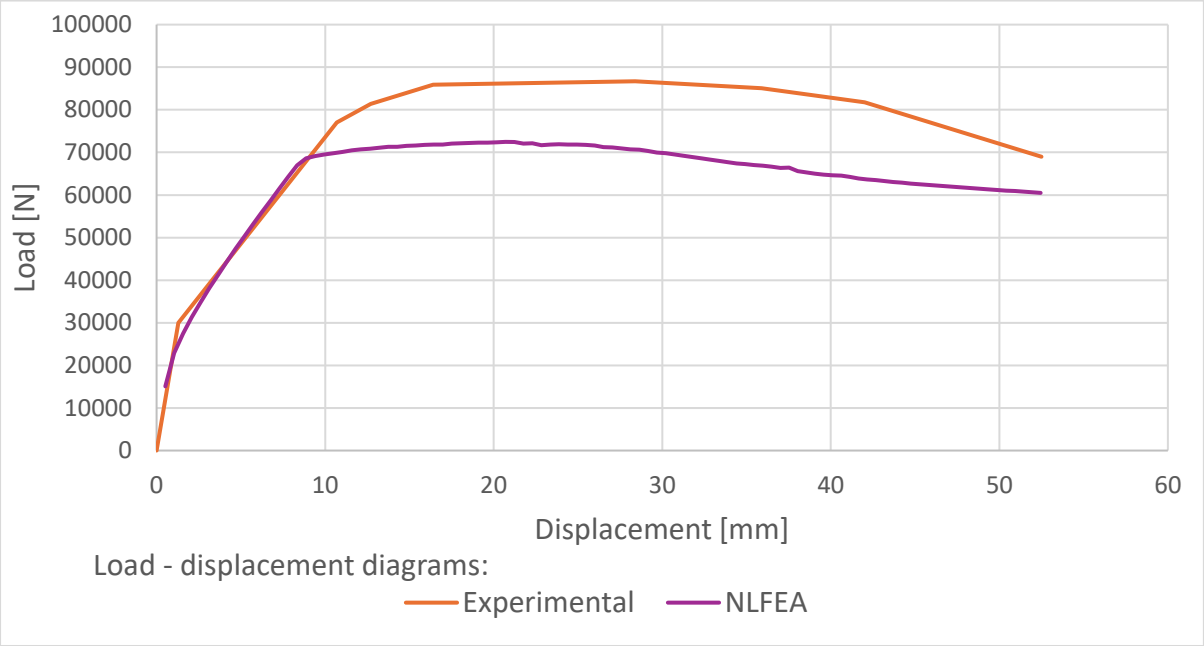

Fig. 44: Experimental and numerical load-deflection curves for considered reinforced beam

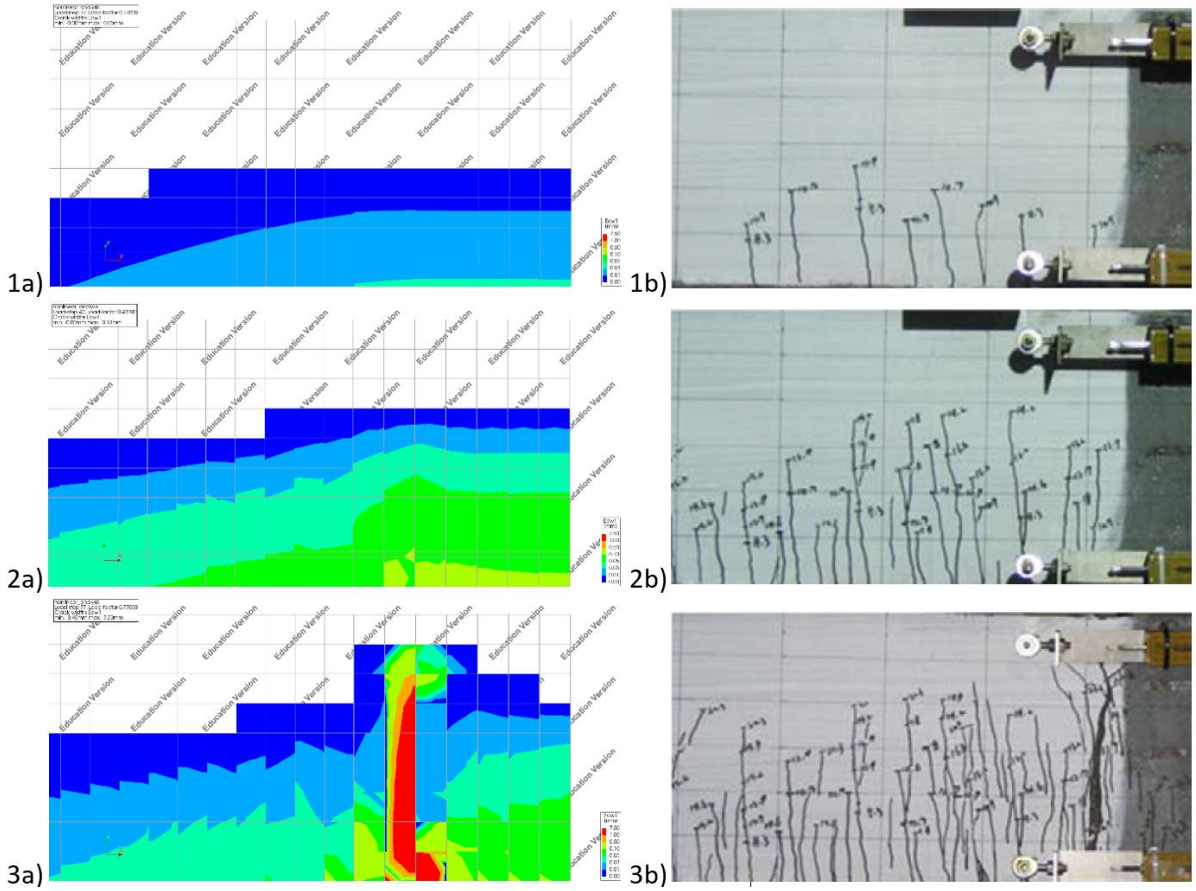

Fig. 45: Crack pattern and development acquired using NLFEA and through experiments. From Structural behavior of ultra high performance concrete beams subjected to bending (p. 3483) , by Hwan Yang, Changbin Joh & Byung-Suk Kim, 2010, Elsevier. Copyright [2010] by Elsevier Ltd. All rights reserved.

It can be seen in sub-figures 1a) and 1b) that at the early loading stage, micro-cracks start to develop throughout the central area of the beam. Then, in 2a) and 2b), they slowly propagate through the height of the beam and grow in number without increasing significantly in width (transitioning to

macro-cracking). This behaviour is typical of UHPFRC. The micro-cracks continue to propagate in number and through the height of the beam until, at a later stage of the loading process, critical fibres in one of the micro-cracks (3a), 3b)) start being pulled out from the concrete. That crack then transitions into a macro-crack, and the deflection of the beam begins to grow quickly. Traditional reinforcement reaches yield strength, and soon after, the beam experiences failure.

While the macro-crack appeared in a slightly different location in the numerical simulation, this can be attributed to the microstructure of the concrete. In general, the cracking pattern and development process exhibited by the model correspond very well to those recorded in the experimental test.

The assumed solution strategy correctly predicts the failure mode of the considered elements as well as reliably predicts the behaviour of the UHPFRC elements throughout the loading process. However, in order to be used for any design processes, the solution strategy has to be evaluated in terms of its modelling uncertainty.

6.2.3 Assessment of modelling uncertainty

Unfortunately, experiments on plate segments manufactured from the considered UHPFRC mix could not be conducted for the purpose of this project. The only relevant data available was used in section 6.2.2.1 to qualitatively assess the validity of the assumed solution strategy. However, due to the scarcity of data (only two test samples) and the imprecise nature of the data collected, a quantitative assessment of the strategy's modelling uncertainty is impossible. As such, the modelling uncertainty of the first solution strategy (the shell element-based one) described in section 6.2.2.1 could not be performed, as no relevant data was found in the literature either. The available literature [41], [42] contained, however, a supply of reinforced beam 4-point bending test results of relatively similar UHPFRC mixes. Therefore, the data available in the literature will be used to assess the modelling uncertainty of the solution strategy described in section 6.2.2.2 with regard to predicting the ultimate moment capacity of reinforced beams experiencing bending failure mode. If relevant experimental data for plate tests were available, an analogous process to that described in the following parts of this section could then be applied to the shell element-based solution strategy. That strategy could then be utilized for design purposes.

Sections 30.10.2.2-30.10.3.4 of MC2020 (2024) [5], were assumed as the basis for the modelling uncertainty assessment within the project. References [41] and [42] constitute the pool of benchmark experiments utilized to assess the solution strategy from section 6.2.2.2 (the plane stress element-based one), with regard to predicting the ultimate moment capacity of reinforced beams experiencing bending failure mode.

As outlined in section 5.2.3.4, Global Factor Method was utilized to evaluate the modelling uncertainty.

6.2.3.1 Modelling uncertainty of the solution strategy for assessing reinforced beam bending capacity

References [41] and [42] constituted the pool of experimental data utilized for assessing the modelling uncertainty. The utilized models were all based on the same principles as those described in section 6.2.2.2. In the case of [41], only results related to the beams containing 13mm long fibres were used. Three of the test specimens from [42] were utilized. Annex 3 contains detailed results of the beam bending simulations and final results of the inverse analyses conducted for the UHPFRC mixes. For the purpose of the modelling uncertainty assessment, Table 5 contains the results of the NLFEAs in the form of the critical loads reached by each of the beams and the corresponding peak experimental loads.

Experimental capacity [kN]	Numerical model capacity [kN]	Beam
86.7	72.5	S13, $\rho = 0.94\%$ [41]
123.5	93.1	S13, $\rho = 1.50\%$ [41]
206.8	182.6	R14-2 [42]
163.1	163.0	R13C-1 [42]
121.7	100.0	NR-1 [42]

Table 5: Benchmark bending capacities

As a result of the analysis conducted according to the outline presented in Section 5.2.5, the modelling uncertainty was evaluated based on the data contained in Table 5. The detailed calculations for that process are contained in Annex 4. Consequently, the final measure for quantification of the modelling uncertainty takes the form of a global factor for the capacity of a beam experiencing bending failure mode, equal to:

$$\gamma_R = 1.041$$

The global factor reaches a value very close to unity. This is caused by the fact that the solution strategy consistently underestimated the capacity of the modelled beams, as evident in Section 6.2.2.2 and Annex 3.

6.3 Application of the NLFE approach in the design process of the sluice gates - results

6.3.1 Overview

NLFEA is a powerful tool that, when properly applied, allows the analyst to significantly streamline the usually multi-step design process of concrete structures. Standard concrete design procedures are based primarily on analytical methods and design codes and are often supported by linear finite element analysis. Depending on the complexity level of the applied NLFEA strategy, it can remove the necessity for conducting some of those analytical checks. In the case of nonlinear solution strategies based on shell elements, such as the one described first in this project, the NLFEA removes the need for analytical verification of moment and shear ULSs. However, such a solution strategy can only be applied for design purposes after it has been successfully validated that it can properly predict bending and shear failure modes, and its modelling uncertainty has been properly assessed. With the range of available experimental data, the second of these tasks could not be fulfilled. As such, the shell element-based solution strategy described in section 6.2.2.1 cannot be applied reliably to the design procedure.

However, the prepared solution strategies can still be utilized in the design process in a more limited way. The shell element-based strategy will be utilized to evaluate the internal forces in the plate segments of the gates. The plane stress element-based strategy will be utilized to evaluate the bending ULS of the structure's sub segments.

6.3.2 Application of the NLFE approach- design forces in plate segments

NLFEA is a useful tool for determining the load effects experienced by a concrete structure for further capacity control of their critical sections, in cases when the loading paths and/or magnitudes are significantly affected by concrete cracking/reinforcement yielding. UHPFRC exhibits a large capacity for load redistribution. Owing it primarily to the fibre bridging effect and the resulting processes of micro- and macro-cracking, as well as to its significant compressive strength. As such, load effects on UHPFRC structures examined through the application of NLFEA substantially differ from those evaluated based on LFEA.

In the project, the shell element-based solution strategy described in section 6.2.2.1 was applied to the gate structure. The developed material model was applied to the gate model developed in chapter 4. As stated before, the strategy should not be used for design purposes, as it could not be properly verified. However, the following design procedure is based on sectional analysis, where structural capacity is evaluated using a reliability-based approach. The loads applied to the NLFE model are also properly evaluated, considering design load factors and combinations. The experiments used to validate the solution strategy were based on very similar material properties and plate geometric properties to those in the case of the considered UHPFRC sluice gates. Although the modelling uncertainty of the strategy could not be quantitatively assessed, section 5.2.4.1 clearly showed that the strategy provided a good estimation of the behaviour of the structure.

Based on the geometry and dimensions of the structure, it can be evaluated that the load paths within the structure generally lead from the plates, through the beam segments, to the supports. As such, a finite element model in which the plates are modelled using the presented nonlinear approach and the beams using a linear one should accurately simulate load redistribution within the plate segments.

In summary, due to all these factors, it can be confidently stated that the developed solution strategy can be safely applied to evaluate the internal forces in the sluice gates' plate segments. Even if the resulting internal forces were to come out on a slightly nonconservative side, the UHPFRC's substantial capacity for load redistribution should further provide a safety margin, ensuring the viability of the approach.

Scope of application of the shell model

As reasoned above, due to the issues with assessing the modelling uncertainty, the shell element-based model was used only to calculate the internal forces within the plate segments of the sluice gates.

It was assumed that all plate segments throughout the structure would have the same thickness and the same grid of steel reinforcement present in them. Due to that, only one plate segment experiencing the most extreme loading conditions had to be analysed using the NLFE approach for the dimensioning and design of their reinforcement. Based on the results of the linear FE analysis for all the load combinations experienced by the structure according to its design note, it was evaluated that two specific loading combinations, identified as "BC1" and "BC2" (these being symmetrically analogous to one another), induced the most extreme response. The plate experiencing that response is further referred to as the "critical plate" and has been marked in Fig. 46. Load combination "BC1" is referred to as the "critical load combination". Only this critical plate was modelled with the nonlinear material model, and only the loading conditions represented by the critical combination were considered. The resulting internal forces are assumed to be the extreme forces present throughout all plate segments, and further analytical design of the plates is based on them.

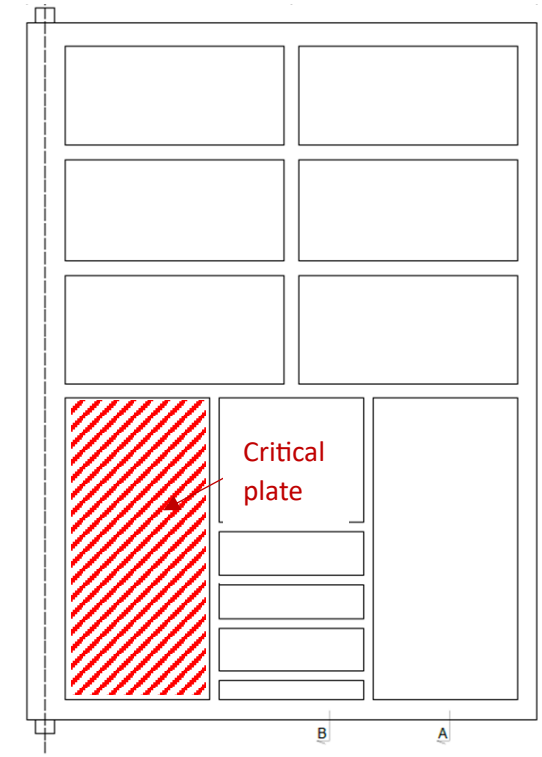

Fig. 46: Critical plate segment

Sluice gate FE model

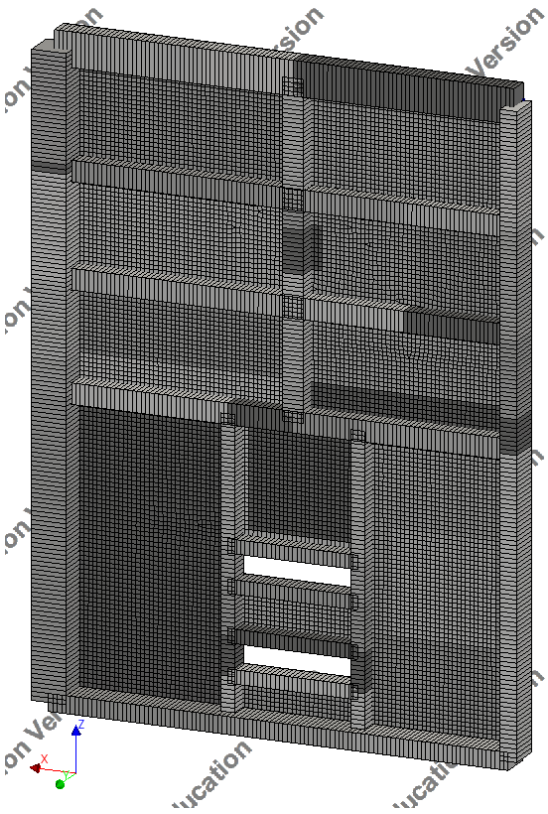

Fig. 47: Finite element mesh of the shell-based gate model

The model of the sluice gates utilizing the shell elements was based on the model used in the "preliminary analysis" and the linear finite element one used to calculate the internal forces in the

beam segments for the analytical design procedure. Boundary conditions consist of line supports in the vertical direction at the bottom beam, a line support in the out-of-plane direction at the bottom and side beams, and a point support in the horizontal in-plane direction at the bottom pivot point. Fig. 47 presents the meshed model of the gates. The geometry of the model is the same as the final one presented in Chapter 7. The difference from the linear model lies in the three layers of grid reinforcement present in the critical plate.

Almost the entire gate was modelled using a linear material model as described in Chapter 4. The only segment utilizing the nonlinear material model discussed throughout Chapter 6 was the critical plate segment.

Load combination "BC1" was utilized as the loading applied to the model. The nonlinear analysis was conducted using the force control method, where all the loads contributing to the critical combination increased from 0 to the design value over 100 steps.

Force-controlled analysis could be applied because the load combination used should not lead to any limit point on the equilibrium path. The design was verified in the context of the analytical, standard-based design formulas, which should themselves be conservative. Due to this, failure should not be reached within the range of the applied loading. These predictions were confirmed by the fact that all analyses utilizing that model reached convergence in all load steps, and the crack pattern of the critical segment corresponded to the one expected for restrained rectangular plates experiencing bending. The crack pattern from the last load step of the final analysis run is presented in Fig. 48. The outer layer of the plate exhibited cracking at the edges where it connects

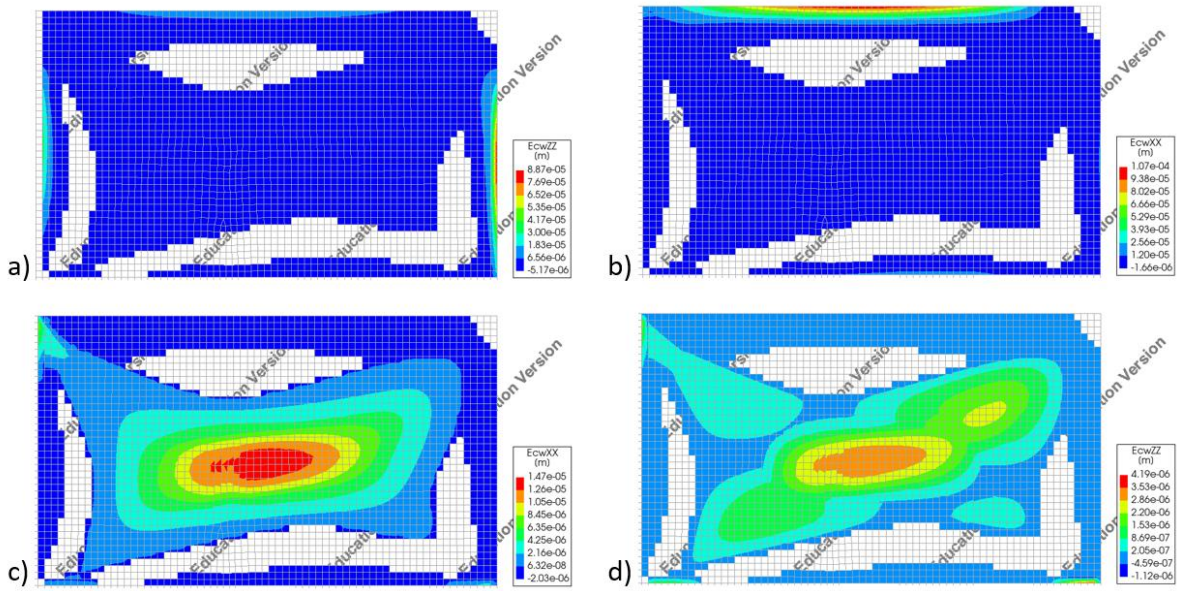

Fig. 48: Crack pattern in the critical plate

to the beam segments, while on the opposite side, the cracks appeared concentrated in the middle and along the 45° inclined lines from the corners of the plate. It was also visible that the cracks reached very small widths, with the largest ones at the edge of the plate being approximately 0.1 mm in width. Deflections in the "Y" direction (out of the plate's plane) reached a value of approximately 3 mm, while the size of the plate was in a range of 1.5 m x 3 m. These results, combined with the fact that during validation of the shell-based model in section 6.2.2.1 the behaviour of the model in terms of crack pattern and deflections resembled that of the real element, suggest that the capacity to resist the load was higher than the considered design load combination. The model is likely overtly stiff, since the rest of the gate was modelled in a physically linear way. However, all the information gathered, combined

with the internal forces' distribution, suggests that it provides a conservative estimation of those forces in the element. That assessment can therefore be used for the purposes of the analytical design process and will provide an improvement upon the original linear model-based estimation, since the real plate would have further force redistribution capacity.

Internal forces based on the nonlinear model

The model had been used to calculate the internal forces in the plates for the cross-sectional analysis. Once the design was verified in terms of the dimensions and the utilized reinforcement grid, the model was updated with the new parameters, and new forces were calculated. Fig. 49 below depicts the comparison between the final distributed moments calculated with the nonlinear model and their counterparts evaluated using the linear model.

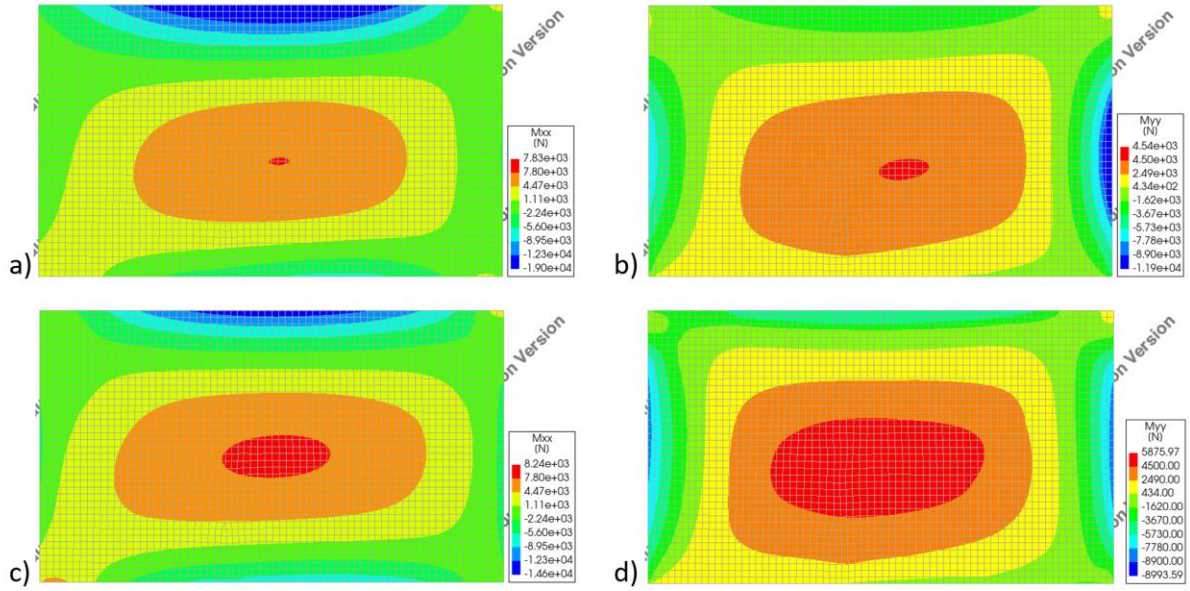

Fig. 49: Final distributed moment in the critical plate. a) mxx in the linear model. b) myy in the linear model. c) mxx in the NL model. d) myy in the NL model.

As predicted, due to the UHPFRC's significant potential for force redistribution, the maximal moments reached within the element were significantly lower (approx. 23%) when the shell-based nonlinear finite element model was applied.

6.3.3 Application of the NLFE approach – ULS bending verifications

Analytical methods for bending ULS verification of UHPFRC elements are usually based on sectional analysis. In that method, the cross-section of an element is divided into multiple layers. Assuming that the cross-section remains plane and using an experimentally defined stress-strain relation, the stress conditions in the cross-section are evaluated. Equilibrium conditions are verified in an iterative procedure where the curvature and position of the neutral axis are adjusted until a state of deformation is reached in which the strain in the reinforcing steel reaches ϵ_u. The analytical method utilized in the project was also based on this approach.

In the case of simplified methods, such as the one described in [7], there is a risk that they will not be sufficiently well calibrated with respect to the specific UHPFRC mix used. In the case of full sectional analysis, it is an iterative process that, anyways requires conducting experimental tests on the utilized mix to establish an accurate stress-strain relation. As such, verifying the ULS in bending for beams by directly utilizing the NLFE model is a viable alternative. It should provide more accurate results than the simplified methods. While its application is, to some extent, more demanding than

sectional analysis, it can be used to assess the structural capacity at a macro scale while evaluating load redistribution effects between different segments of the structure.

Scope of application of the model

Fully utilizing the potential of the NLFE model, as outlined above, was not possible within the scope of the project, as the modelling uncertainty of the shell-based model could not be assessed based on the available literature and experimental data. As such, the interaction between different parts of the structure could not be reliably assessed by the developed approach, as it is significantly affected by the plate segments. However, to complete the process of development, validation, and application of an NLFE-based solution strategy in the design procedure, this section describes the application of the plane stress element-based model in evaluating the bending ULS for the beam segments within the structure.

The model has been used to simulate a four-point bending test of UHPFRC beams with cross-sectional dimensions and longitudinal reinforcement corresponding to those of the respective beam segments present within the analysed sluice gates. The conditions of the setup ensured a bending failure mode of the considered beams and created a zone of approximately uniform bending moment within their central part, between the points where the load was applied. The load was systematically increased until the failure of each of the analysed beams. Based on the loads corresponding to failure, the moments present in the zone in the middle were calculated and assumed as the bending moment capacities of the specific beams.

Beam FE models

As described in Fig. 29, eight different beams/beam groups were identified within the project. Each of these had a separate FE model prepared. For the purpose of this section, one of the models is presented, and the approach followed is described using it as an example. The results for the other beams are presented only in aggregate in chapter 8.

The example model represents one of the internal beams of size $h = 250mm$, $b = 240mm$. This beam was described in Fig. 29 as “internal horizontal beam 3”. The plane stress approach presented in section 6.2.2.1 was applied. Eight-node quadrilateral isoparametric plane stress elements (CQ16M) were utilized. The UHPFRC material model used was the one developed for the specific mix in section 6.2.1.2, which, to reiterate, is:

Material model of the utilized UHPFRC	
Smeared cracking:	Total strain-based crack model
Crack orientation	Rotating
Tensile curve:	Exponential
Tensile strength	5.5 N/mm^2
Model-I tensile fracture energy	4.844 N/mm
Crack bandwith	According to Rots
Compressive curve:	Elastic
Young’s modulus:	64646 N/mm^2
Poisson’s ratio:	0.2

Table 6: Assumed non-linear material model

Utilizing the symmetry of the 4-point bending test, only half of the beam was modelled. Fig. 50 presents the geometry, loading, and boundary conditions of the FE model. Blue lines represent the reinforcing bars, while the green arrow symbolizes the load applied to the beam. The symmetry condition was included as a horizontal translational constraint at the centre of the beam throughout

its height. The beam support was modelled as a point translational constraint in the vertical direction. The loading took the form of a displacement applied at the top of the beam, 200 mm from its centre. The reinforcement was included in the form of embedded reinforcement bars. Both top and bottom

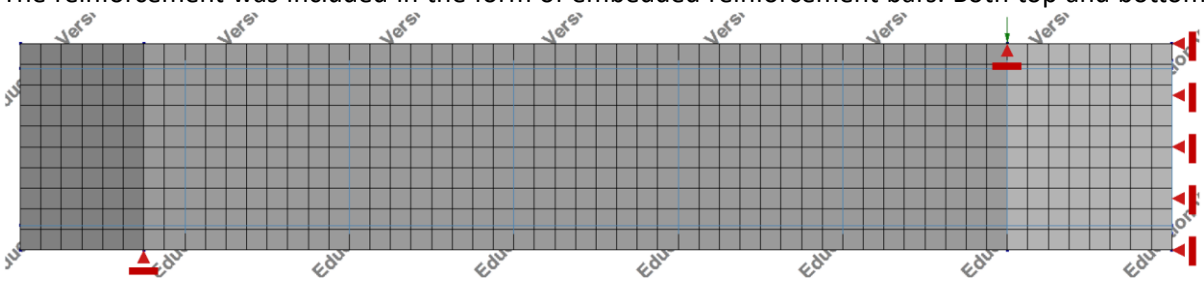

Fig. 50: Model geometry and mesh for bending ULS verifications for beams

longitudinal reinforcement bars were modelled. Shear reinforcement was also included to ensure that the possibility of a shear failure mode was excluded. Steel was modelled as an ideally plastic material (no hardening), with a yield strength of 500 N/mm² and a Young's modulus of 2.1×10^5 MPa. The nonlinear finite element procedure included only physical nonlinearities. The nonlinear analysis was based on the modified Newton-Raphson iterative method. Energy and out-of-balance force norms were applied, with convergence tolerances of 0.001 and 0.01, respectively.

Models for all the other beams were based on the same principles, the only differences between them being the cross-sectional dimensions of the specific beams and the utilized reinforcement. In the case of some of the beams, due to differences in their depth, their spans were also adjusted.

Evaluating bending moment capacity

For the example "internal horizontal beam 3", four 8 mm diameter bars were used as the main longitudinal reinforcement. After running the model, data on the displacement and the induced reaction force were utilized to create a load-deflection curve for the considered beam, presented in Fig. 51.

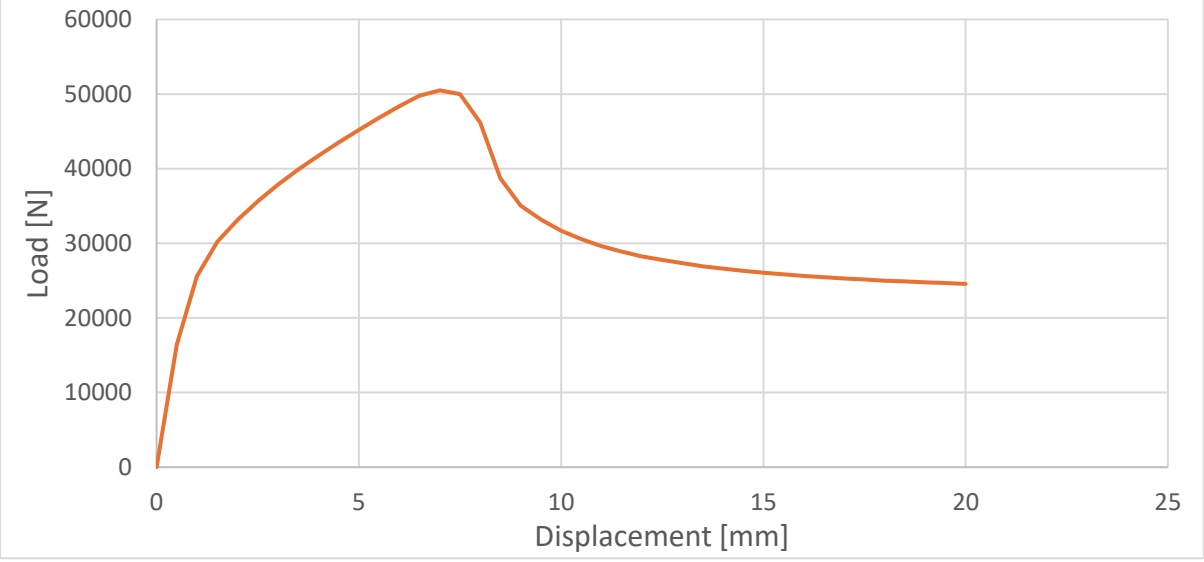

Fig. 51: Simulated load deflection curve for "internal horizontal beam 3" with four 8 mm bars

As expected, the load-deflection curve exhibited typical behaviour for UHPFRC (very similar to that presented in [42]), where, after a short elastic phase, the microcracking phase began, during which the steel fibres were still capable of resisting the load. The microcracks grew in width and

number as the load increased. In this phase, there was still a linear relation between the growth of load and deflection. At some point, the steel fibres in one of the microcracks started to be pulled out of the concrete matrix. The width of the crack began to increase rapidly. Since a very small amount of conventional reinforcement was used, the structure then lost most of its capacity to resist the load. The point of transition between these phases was assumed to be the failure point. As predicted, in all of the conducted analyses, the beams experienced a bending failure mode, with the main crack developing in the central region of the beam. Fig. 52 presents the location of the main crack in the case of the example beam.

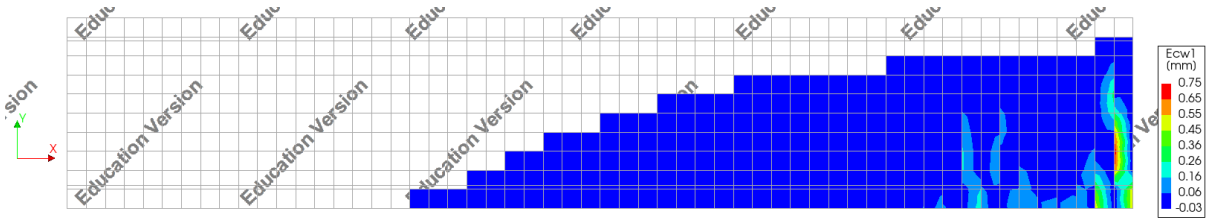

Fig. 52: Cracking pattern of the analysed beam

The maximal reaction force was assumed to be the beam's load capacity F_{cap}. Its value was taken and used to calculate the moment corresponding to it, present in the central part of the beam between the points of application of the load. The model's geometry, as outlined in Fig. 53, was used to calculate that moment.

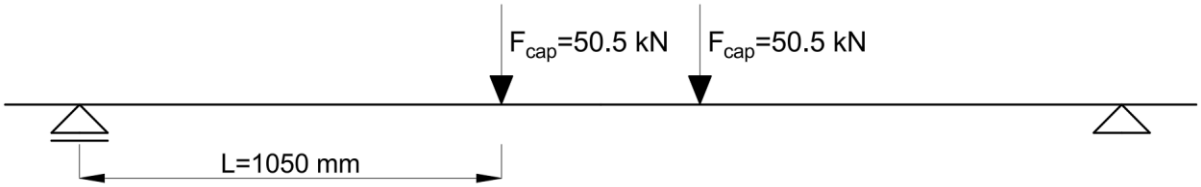

Fig. 53: Simplified model geometry

The value of the acquired moment was then divided by the global factor accounting for the NLFE solution strategy's modelling uncertainty, calculated in section 6.2.3.1 as $\gamma_R = 1.041$. This new value is then assumed to be the bending moment capacity, M_{cap}, of the analysed beam, which in the case of "internal horizontal beam 3" reinforced with four $8\,mm$ diameter bars was equal to $M_{cap} = 50.9\,kNm$.

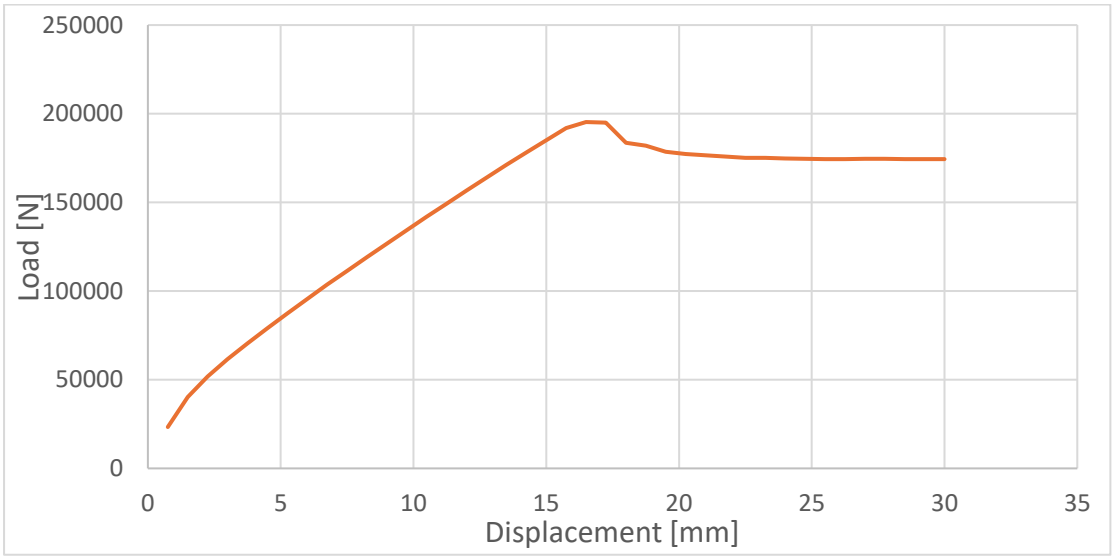

Fig. 54: Load deflection curve for "bottom beam" reinforced with 5, 20 mm bars

Most of the beams within the analysed sluice gates required very small amounts of longitudinal reinforcement under the considered design load conditions. They exhibited the same rapid decrease in load-resisting capacity after failure. The beam with the highest longitudinal reinforcement ratio was the “bottom beam,” which, under the most unfavourable loading combination, experienced a bending moment of $274\,kNm$. Fig. 54 presents its load-deflection diagram as a result of applying the NLFE solution strategy. In this case, it was determined that despite UHPFRC’s significant compressive strength, there was a possibility that concrete crushing could occur at the top part of the beam. Based on the load-deflection curve, a load step was identified at which failure occurred, which in this case was load step 24, as confirmed by the primary crack width growth between steps 23 and 24, depicted respectively in Fig. 55 and Fig. 56.

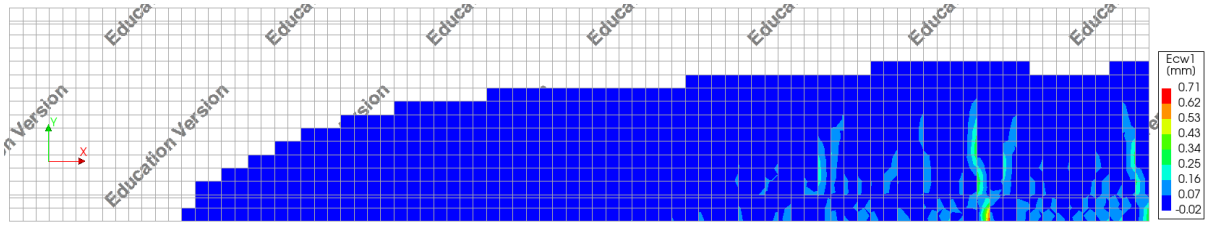

Fig. 55: "bottom beam" primary crack width right before failure

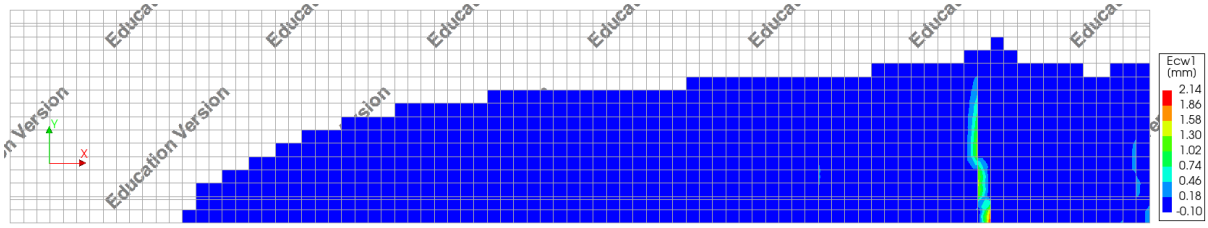

Fig. 56: "bottom beam" primary crack width just after failure

The principal stress data from the step 24 as presented in Fig. 57, were compared with the compressive strength of the utilized UHPFRC, $f_{cd} = 116.7 N/mm^2$. Except for a singular stress concentration point resulting from an idealized point load, the compressive stresses do not exceed a value of $112.2\ N/mm^2$. Therefore, since this beam required the highest longitudinal reinforcement ratio of all those present in the structure and its load-carrying capacity dropped the least after failure,

it was determined that none of the beams was at risk of brittle concrete crushing failure, and analogous checks were not performed for their cases.

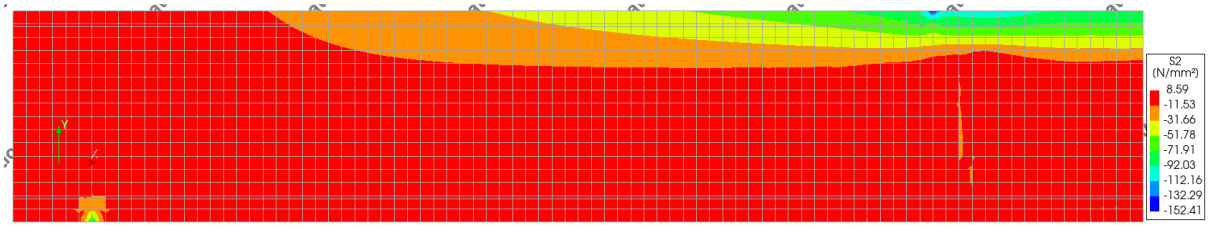

Fig. 57: 2nd primary stress data readout for the "bottom beam" in the 1st step after failure

6.3.3.1 Deformation SLS verifications

The SLSs are especially crucial in the case of this UHPFRC sluice gate structure, as the main advantage making UHPFRC an interesting alternative for the design of the gates is its durability. This durability is highly dependent on the proper management of the cracking process throughout the structure. A structure that cracks and deforms significantly more than the design analysis predicted could fail to fulfil its most crucial serviceability requirements, related to its water tightness. Additionally, excessive deformation could hinder the proper functioning of the gates.

In the original design, the deformation SLS was verified by simply using a linear finite element model and comparing the results with the allowable maximal deflection for the sluice gates. This approach is non-conservative when compared to the NLFEA-based approach. Regardless of the modelling uncertainty of the developed solution strategy, estimations based on it will be safer assessments of reality than those produced by an LFE model. It also needs to be pointed out that the developed shell element-based solution strategy presented results that corresponded very well to the experimental data available for similar UHPFRC plates. Due to the points outlined above, and additionally because of the importance of the serviceability requirements placed on the structure, the NLFEA-based approach is, on all fronts, a sounder design approach regarding deflection verifications.

The shell element-based solution strategy was applied to the model of the gate as developed in Chapter 4. The model was updated with geometrical parameters corresponding to values resulting from the new design process. Alongside the reinforcement net modelled throughout the plate segments with embedded reinforcement grids, the longitudinal reinforcement was also modelled in the beam segments using embedded bar reinforcement. The loading took the form of serviceability limit state load combinations as defined within Rijkswaterstaat (ROK 1.4, 2017) [36]. The gate model set up according to these rules could then undergo NLFEA, and the results could then be assumed as the predicted deflections of the gate structure.

7 New gate design

7.1 Overview

This chapter contains a description of the results of the analytical design procedure. The approach itself was based on the methodology described in Chapter 5. Chapter 7 does not contain the calculations and other deliberations that were part of the design process; it merely presents the final results. Information such as the structural calculations and design internal force diagrams is provided in the annexes to this report, specifically in Annex 6 and Annex 5, respectively. The new gate design, as established in this chapter, was then compared with the prior gate design in Chapter 8.

7.2 Geometry of the gate

The redesign process was based on "Design Alternative 1" from Chapter 4. As such, the cross-sectional parameters of the structural subsegments of the new gate are largely similar to those of "Design Alternative 1." Since the beam segments of the gate had been divided into groups for the purpose of the design, they are referred to in the same way within this chapter. These names are once again presented in Fig. 58.

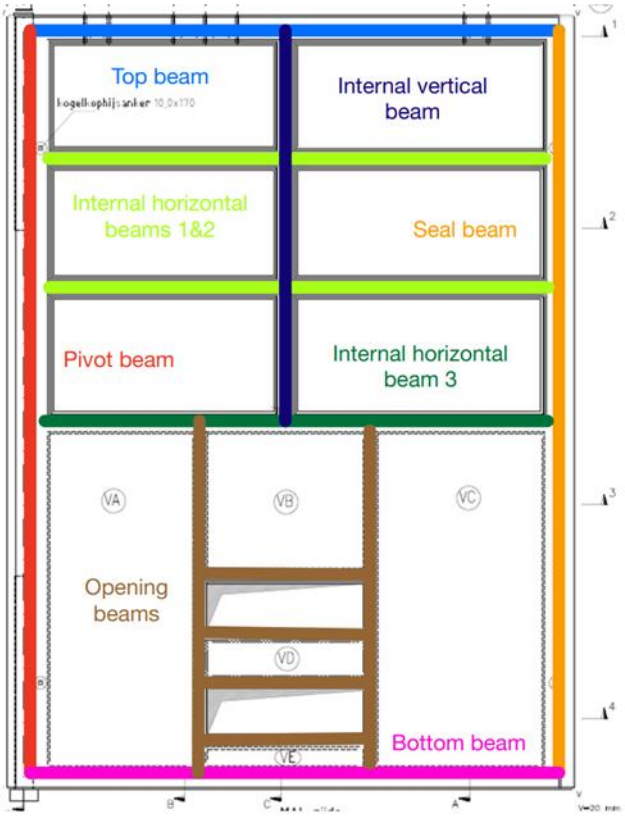

Fig. 58: Division of the gate structure into sub-elements considered separately in the design process

The plate segments maintained their original thickness of $60\ mm$, as it was generally the minimum possible due to requirements concerning the minimum concrete cover, and there was no need to increase their cross-sectional dimensions.

In the original design, all beam segments were characterized by a height of $h = 400\ mm$ and a width of b in most cases significantly smaller than h (in the case of the pivot beam, h and b cross-sectional dimensions were equal). During the design process, it was noticed that some of the beam segments experienced higher transverse forces in the "in the gate's plane" direction than in the "out of the gate's plane" direction, while simultaneously not experiencing particularly significant bending

moments about their major axes. It was decided that those beams should have their heights decreased and widths increased to reduce the amount of shear reinforcement necessary inside them. This group essentially included all the inner beam segments, as well as the "top beam." The other three "outer" beams (bottom, pivot, and seal) retained their original design cross-sectional dimensions. The changes included a new $h = 250\ mm$ and significantly increased widths for all the modified beams. The lengths and distances between all of them were kept unchanged. Fig. 59 presents the geometry of the new gate design after the inclusion of all of the described changes.

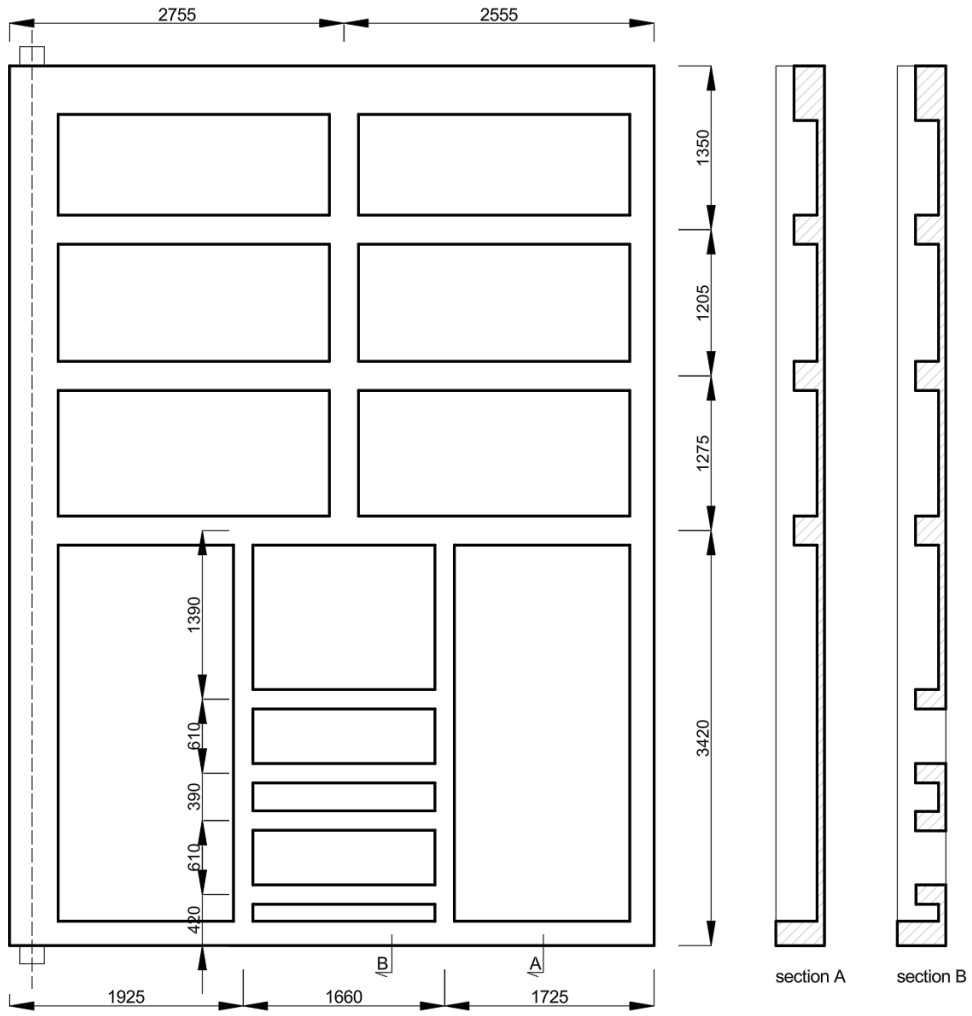

Fig. 59: Geometry of the new gate design

7.3 Internal forces in structural sub-segments

The linear finite element model, as described in Section 5.3.3.2, was utilized to calculate the internal forces in the sub-segments of the gate. Whenever the intermediate cross-sectional dimensions were changed, the model was updated with the new geometry. As the model utilized beam and shell elements, their outputs were directly used as the internal forces in the corresponding segments.

For each identified segment, an extreme force resulting from the applied design load combinations was utilized to evaluate the capacity. In some cases, as described in the following section, additional readings of the internal forces were also considered. Unfortunately, as the force/moment envelope functionality was not available in Diana FEA [38], the forces had to be defined by searching

for the extreme values resulting from the applied combinations. Annex 5 contains all the information on internal force values identified for the purpose of the design. Fig. 60 presents an example of the readout of that information in the form of results for the transverse force acting in the direction “in the gate’s plane” (this force reached extreme values in all segments in one specific load combination).

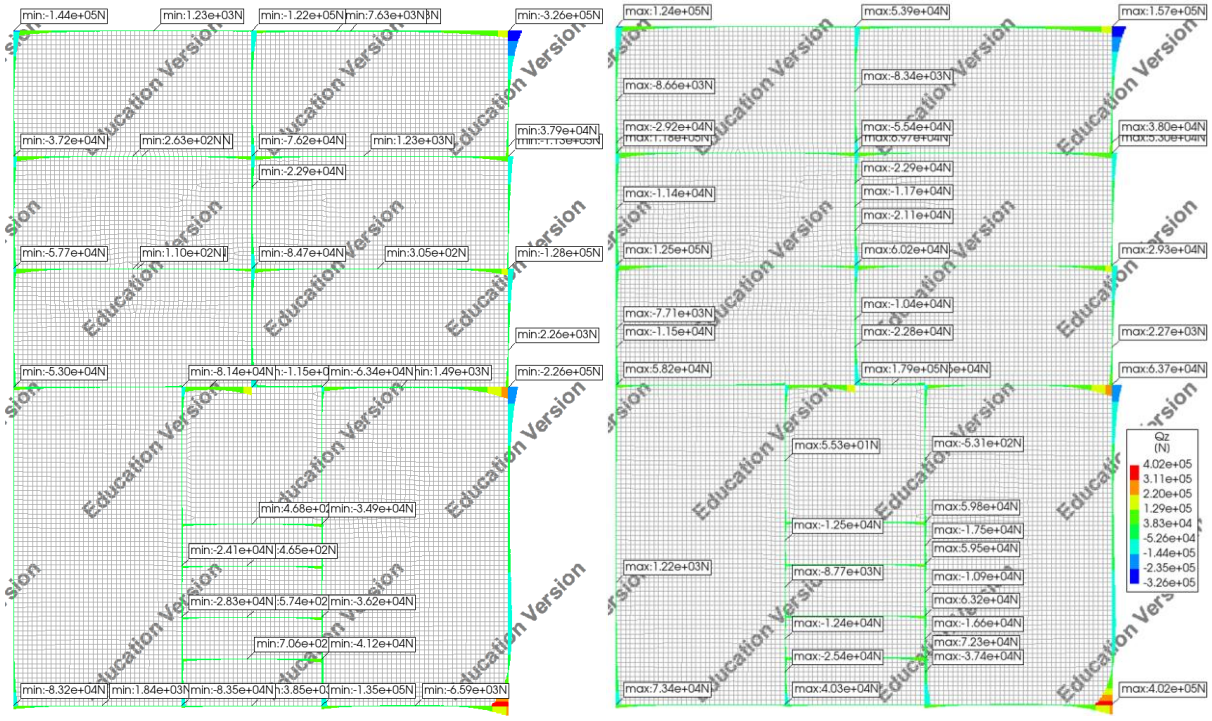

Fig. 60: Readout of the internal "in the gate's plane" transverse force values. Minimums on the left, maximums on the right.

7.4 Reinforcement design

7.4.1 General

The following subsections present the final reinforcement design of all the identified sub-elements of the structure. Each section describes the summary of evaluations concerning the specific element. This information includes data such as:

- Cross sectional dimensions,
- Internal forces used as the design forces,
- Calculated values of capacities important for the reinforcement design (bending moment resistance, shear resistance with no shear reinforcement, shear resistance for the extreme loading etc.),
- Utilization rate for the SLS verifications,
- Calculated and used amounts of reinforcement,
- lengths of beams, and specification in which parts the reinforcement is present.

In general, beam segments were reinforced with longitudinal reinforcement in all possible directions (positive/negative moments about both major and minor axes). The minimal amount of longitudinal reinforcement was four $8\ mm$ diameter bars, one in each corner of the steel stirrups. This reinforcement was included as all the beams required shear reinforcement in at least some part of their length. When needed—due to any of the considered ULSs or SLSs—the diameter or number of the bars was increased in the specific direction.

According to the calculations, no minimal shear reinforcement was required. Regions of the beams where the design shear force exceeded the design shear resistance of the UHPFRC, $V_{Rd,F}$, were reinforced with the shear reinforcement necessary for resisting the critical load experienced by the specific beam. Throughout the rest of a beam, some shear stirrups were still provided in order to facilitate the manufacturing of the reinforcement grid.

Due to serviceability/durability requirements, the concrete cover required throughout the structure was calculated as $15\ mm$. For the same reason, the maximum allowable crack width was restricted to $w_{max} = 0.1\ mm$.

7.4.2 Plate segments in x direction

The concrete cover was increased in case of the plate segments to $c_{cover} = 18\ mm$. With this value and a 3-layer reinforcement net of 8 mm bars, the total thickness of the plate segments was established as $h_{plate} = 60\ mm$. Based on the calculations, the required reinforcement was determined as $\phi = 8mm$, with $s = 100\ mm$ spacings between the bars in the "x" direction. The bars going in the x-direction were the two outer layers of the reinforcement bars in the gate's plates. The reinforcement net was assumed to be the same throughout all the plate segments in the gate, with the difference that the "x" and "z" directions switch at the height of the "internal horizontal beam 3." Below it, the "x" direction was the horizontal direction and "z" was the vertical direction (when the gate is positioned upright), while above, it's the opposite. Table 7 presents the summary of the results of the analytical design process for the plates in the "x" direction.

Summary of results for plate segments "x" direction				
Description	Parameter	Value	Unit	
Height	h_{plate}	60	mm	
Bar diameter	ϕ_{plate}	8	mm	
Bar spacing	$s_{\phi,plate,x}$	100	mm	
Reinforcement area	A_s	502.7	mm^2	
Distributed moment xx multiplied by 1m	$M_{x,Ed}$	14.7	kNm	
Distributed shear force xz	$v_{x,Ed}$	123.1	kN/m	
Impact load (40kN/200kN distributed in a square 0.1m x 0.1m/0.5m x 0.5m	-	-	-	
Description	Parameter	Value	Unit	Unity check
Bending ULS / bending moment resistance	$M_{x,Rd}$	15.4	kNm	0.95
Shear ULS / distributed shear resistance	$v_{x,Rd}$	127.9	kN/m	0.96
Impact load check / design shear resistance	$v_{Rd,imp}$	124	kN/m	0.81
Cracking SLS / Minimum reinforcement area	$A_{s,min}$	197.6	mm^2	ok
Cracking SLS / Design crack width	w_d	0.07	mm	≤0.1

Table 7: Summary of results for plate segments "x" direction

7.4.3 Plate segments in z direction

Based on the calculations, the required reinforcement was determined as $\phi = 8mm$, with $s = 150\ mm$ spacings between the bars in the "z" direction. The bars running in the "z" direction formed the inner layer of the reinforcement bars in the gate's plates. The reinforcement net was assumed to be the same throughout all the plate segments in the gate, with the difference that the "x" and "z" direction reinforcement switch at the height of the "internal horizontal beam 3." Below it, the "x" direction was the horizontal direction and "z" was the vertical direction (when the gate is positioned upright), while above, it is the opposite. Table 8 presents the summary of the results of the analytical design process for the plates in the "z" direction.

Summary of results for plate segments “z” direction				
Description	Parameter	Value	Unit	
Height	h_{plate}	60	mm	
Bar diameter	ϕ_{plate}	8	mm	
Bar spacing	$s_{\phi,plate,z}$	150	mm	
Reinforcement area	A_s	335.1	mm^2	
Distributed moment yy multiplied by 1m	$M_{y,Ed}$	9	kNm	
Distributed shear force yz	$v_{y,Ed}$	106.2	kN/m	
Impact load (40kN/200kN distributed in a square 0.1m x 0.1m/0.5m x 0.5m	-	-	-	
Description	Parameter	Value	Unit	Unity check
Bending ULS / bending moment resistance	$M_{y,Rd}$	11.9	kNm	0.76
Shear ULS / distributed shear resistance	$v_{y,Rd}$	125.4	kN/m	0.85
Impact load check / design shear resistance	$v_{Rd,imp}$	124	kN/m	0.81
Cracking SLS / Minimum reinforcement area	$A_{s,min}$	197.6	mm^2	ok
Cracking SLS / Design crack width	w_d	0.1	mm	≤0.1

Table 8: Summary of results for plate segments “z” direction

7.4.4 Beam segments

Based on the calculations, the longitudinal and shear reinforcement of the beams was calculated. Tables Table 9-Table 16 present the summary of those results for all the identified beam segments. Fig. 61 provides the explanation of the parameters included in the tables.

Shear reinforcement spacing y direction $s_{w,out}$, describes the spacing between the shear stirrups demanded by the presence of a design shear force acting in the direction out of the gate’s plane. Shear reinforcement spacing z direction $s_{w,in}$, describes the spacing between the shear stirrups demanded by the presence of a design shear force acting in the direction in the gate’s plane. $M_{z,+}$ considers moment that results in deflection of the beam out of the gates plane with tension present on the side of the beam opposite to the one common with the plate segment. $M_{z,-}$considers moment that results in deflection out of the gates plane with tension present on the side where the beam interests with the plate segment. M_{in} considers the moment that results in the beam deflection in the gate’s plane.

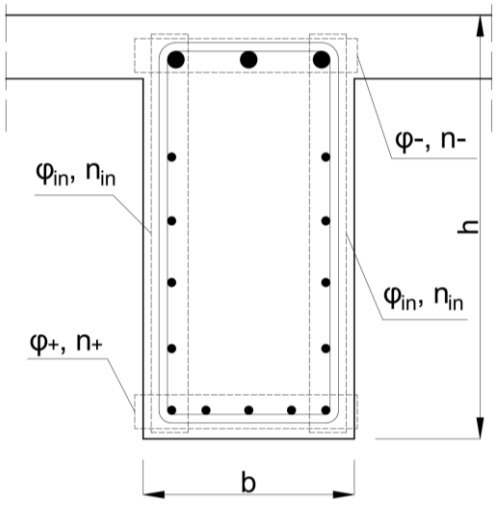

Fig. 61: Schematic representation of the beam cross -section with relevant parameters

If one of the bar groups, as presented in Fig. 61, has a different diameter than the group it shares a corner bar with, the corner bar was assumed to have the larger of the two diameters.

The descriptions provided regarding the parameters inside the table here apply to all the tables in this section.

In most cases, the bending capacity of the beams is heavily underutilized. This is caused by the increase in the reinforcement needed to meet the design crack width SLS requirements.

7.4.4.1 Internal horizontal beams 1 and 2

Summary of results for internal horizontal beams 1 and 2				
Description	Parameter	Value	Unit	
Height	h	250	mm	
Width	b	240	mm	
Bar diameter inner edge	ϕ_+	8	mm	
Number of bars inner edge	n_+	6	-	
Bar diameter outer edge	ϕ_-	8	mm	
Number of bars outer edge	n_-	2	-	
Bar diameter sides	ϕ_{in}	8	mm	
Number of bars sides	n_{in}	6	-	
Bar diameter shear reinforcement	ϕ_w	8	mm	
Shear reinforcement spacing y direction	$s_{w,out}$	Not req.	mm	
Shear reinforcement spacing z direction	$s_{w,in}$	80	mm	
Description	Parameter	Value	Unit	Unity check
Bending ULS / bending moment resistance, major axis, positive	$M_{z,+}$	60.8	kNm	0.71
Bending ULS / bending moment resistance, major axis, negative	$M_{z,-}$	42.4	kNm	0.54
Bending ULS / bending moment resistance, minor axis, extreme	M_{in}	58.2	kNm	0.7
Cracking SLS / Design crack width	w_d	0.1	mm	1
Shear ULS / Shear (out of gate plane) resistance of concrete	$V_{Rd,F,out}$	88.9	kN	-
Shear ULS / Shear (out of gate plane) resistance with reinforcement	$V_{Rd,out}$	88.9	kN	0.74
Shear ULS / Shear (in gate plane) resistance of concrete	$V_{Rd,F,in}$	53.2	kN	-
Shear ULS / Shear (in gate plane) resistance with reinforcement	$V_{Rd,in}$	157.9	kN	0.93
Torsion ULS / Torsion capacity (unity check according to 5.3.3.4.3)	-	-	-	0.2

Table 9: Summary of results for internal horizontal beams 1 and 2

7.4.4.2 Internal horizontal beam 3

Summary of results for internal horizontal beams 3				
Description	Parameter	Value	Unit	
Height	h	250	mm	
Width	b	240	mm	
Bar diameter inner edge	ϕ_+	10	mm	
Number of bars inner edge	n_+	7	-	
Bar diameter outer edge	ϕ_-	10	mm	
Number of bars outer edge	n_-	3	-	
Bar diameter sides	ϕ_{in}	10	mm	
Number of bars sides	n_{in}	7	-	
Bar diameter shear reinforcement	ϕ_w	10	mm	
Shear reinforcement spacing y direction	$s_{w,out}$	150	mm	
Shear reinforcement spacing z direction	$s_{w,in}$	60	mm	
Description	Parameter	Value	Unit	Unity check
Bending ULS / bending moment resistance, major axis, positive	$M_{z,+}$	82.2	kNm	0.57
Bending ULS / bending moment resistance, major axis, negative	$M_{z,-}$	54.0	kNm	0.96
Bending ULS / bending moment resistance, minor axis, extreme	M_{in}	78.7	kNm	0.89
Cracking SLS / Design crack width	w_d	0.8	mm	0.8
Shear ULS / Shear (out of gate plane) resistance of concrete	$V_{Rd,F,out}$	114.8	kN	-
Shear ULS / Shear (out of gate plane) resistance with reinforcement	$V_{Rd,out}$	173.0	kN	0.81
Shear ULS / Shear (in gate plane) resistance of concrete	$V_{Rd,F,in}$	65.8	kN	-
Shear ULS / Shear (in gate plane) resistance with reinforcement	$V_{Rd,in}$	281.0	kN	0.92
Torsion ULS / Torsion capacity (unity check according to 5.3.3.4.3)	-	-	-	0.2

Table 10: Summary of results for internal horizontal beams 3

7.4.4.3 Internal vertical beam

Summary of results for internal vertical beam				
Description	Parameter	Value	Unit	
Height	h	250	mm	
Width	b	240	mm	
Bar diameter inner edge	ϕ_+	8	mm	
Number of bars inner edge	n_+	6	-	
Bar diameter outer edge	ϕ_-	8	mm	
Number of bars outer edge	n_-	2	-	
Bar diameter sides	ϕ_{in}	8	mm	
Number of bars sides	n_{in}	6	-	
Bar diameter shear reinforcement	ϕ_w	8	mm	
Shear reinforcement spacing y direction	$s_{w,out}$	150	mm	
Shear reinforcement spacing z direction	$s_{w,in}$	100	mm	
Description	Parameter	Value	Unit	Unity check
Bending ULS / bending moment resistance, major axis, positive	$M_{z,+}$	60.8	kNm	0.41
Bending ULS / bending moment resistance, major axis, negative	$M_{z,-}$	33.7	kNm	0.45
Bending ULS / bending moment resistance, minor axis, extreme	M_{in}	58.2	kNm	0.53
Cracking SLS / Design crack width	w_d	0.1	mm	1
Shear ULS / Shear (out of gate plane) resistance of concrete	$V_{Rd,F,out}$	88.9	kN	-
Shear ULS / Shear (out of gate plane) resistance with reinforcement	$V_{Rd,out}$	147.3	kN	0.66
Shear ULS / Shear (in gate plane) resistance of concrete	$V_{Rd,F,in}$	53.2	kN	-
Shear ULS / Shear (in gate plane) resistance with reinforcement	$V_{Rd,in}$	137.0	kN	0.89
Torsion ULS / Torsion capacity (unity check according to 5.3.3.4.3)	-	-	-	0.2

Table 11: Summary of results for internal vertical beam

7.4.4.4 Beams around the openings

Summary of results for beams around the openings				
Description	Parameter	Value	Unit	
Height	h	250	mm	
Width	b	160	mm	
Bar diameter inner edge	ϕ_+	8	mm	
Number of bars inner edge	n_+	4	-	
Bar diameter outer edge	ϕ_-	8	mm	
Number of bars outer edge	n_-	2	-	
Bar diameter sides	ϕ_{in}	8	mm	
Number of bars sides	n_{in}	4	-	
Bar diameter shear reinforcement	ϕ_w	8	mm	
Shear reinforcement spacing y direction	$s_{w,out}$	150	mm	
Shear reinforcement spacing z direction	$s_{w,in}$	50	mm	
Description	Parameter	Value	Unit	Unity check
Bending ULS / bending moment resistance, major axis, positive	$M_{z,+}$	40.5	kNm	0.67
Bending ULS / bending moment resistance, major axis, negative	$M_{z,-}$	31.2	kNm	0.87
Bending ULS / bending moment resistance, minor axis, extreme	M_{in}	25.1	kNm	0.52
Cracking SLS / Design crack width	w_d	0.1	mm	1
Shear ULS / Shear (out of gate plane) resistance of concrete	$V_{Rd,F,out}$	73.9	kN	-
Shear ULS / Shear (out of gate plane) resistance with reinforcement	$V_{Rd,out}$	132.4	kN	0.7
Shear ULS / Shear (in gate plane) resistance of concrete	$V_{Rd,F,in}$	32.4	kN	-
Shear ULS / Shear (in gate plane) resistance with reinforcement	$V_{Rd,in}$	137.0	kN	0.99
Torsion ULS / Torsion capacity (unity check according to 5.3.3.4.3)	-	-	-	0.13

Table 12: Summary of results for beams around the openings

7.4.4.5 Top beam

Summary of results for top beam				
Description	Parameter	Value	Unit	
Height	h	250	mm	
Width	b	400	mm	
Bar diameter inner edge	ϕ_+	8	mm	
Number of bars inner edge	n_+	8	-	
Bar diameter outer edge	ϕ_-	8	mm	
Number of bars outer edge	n_-	6	-	
Bar diameter sides	ϕ_{in}	8	mm	
Number of bars sides	n_{in}	10	-	
Bar diameter shear reinforcement	ϕ_w	8	mm	
Shear reinforcement spacing y direction	$s_{w,out}$	Not req.	mm	
Shear reinforcement spacing z direction	$s_{w,in}$	150	mm	
Description	Parameter	Value	Unit	Unity check
Bending ULS / bending moment resistance, major axis, positive	$M_{z,+}$	101.3	kNm	0.34
Bending ULS / bending moment resistance, major axis, negative	$M_{z,-}$	82.3	kNm	1
Bending ULS / bending moment resistance, minor axis, extreme	M_{in}	165.5	kNm	0.48
Cracking SLS / Design crack width	w_d	0.1	mm	1
Shear ULS / Shear (out of gate plane) resistance of concrete	$V_{Rd,F,out}$	167.9	kN	-
Shear ULS / Shear (out of gate plane) resistance with reinforcement	$V_{Rd,out}$	167.9	kN	0.52
Shear ULS / Shear (in gate plane) resistance of concrete	$V_{Rd,F,in}$	76.4	kN	-
Shear ULS / Shear (in gate plane) resistance with reinforcement	$V_{Rd,in}$	174.3	kN	0.9
Torsion ULS / Torsion capacity (unity check according to 5.3.3.4.3)	-	-	-	0.14

Table 13: Summary of results for top beam

7.4.4.6 Seal beam

Summary of results for seal beam				
Description	Parameter	Value	Unit	
Height	h	400	mm	
Width	b	200	mm	
Bar diameter inner edge	ϕ_+	8	mm	
Number of bars inner edge	n_+	5	-	
Bar diameter outer edge	ϕ_-	8	mm	
Number of bars outer edge	n_-	2	-	
Bar diameter sides	ϕ_{in}	8	mm	
Number of bars sides	n_{in}	6	-	
Bar diameter shear reinforcement	ϕ_w	8	mm	
Shear reinforcement spacing y direction	$s_{w,out}$	150	mm	
Shear reinforcement spacing z direction	$s_{w,in}$	90	mm	
Description	Parameter	Value	Unit	Unity check
Bending ULS / bending moment resistance, major axis, positive	$M_{z,+}$	147.3	kNm	0.34
Bending ULS / bending moment resistance, major axis, negative	$M_{z,-}$	86.8	kNm	0.33
Bending ULS / bending moment resistance, minor axis, extreme	M_{in}	70.7	kNm	0.52
Cracking SLS / Design crack width	w_d	0.1	mm	1
Shear ULS / Shear (out of gate plane) resistance of concrete	$V_{Rd,F,out}$	94.7	kN	-
Shear ULS / Shear (out of gate plane) resistance with reinforcement	$V_{Rd,out}$	192.5	kN	0.96
Shear ULS / Shear (in gate plane) resistance of concrete	$V_{Rd,F,in}$	70.4	kN	-
Shear ULS / Shear (in gate plane) resistance with reinforcement	$V_{Rd,in}$	146.0	kN	0.99
Torsion ULS / Torsion capacity (unity check according to 5.3.3.4.3)	-	-	-	0.15

Table 14: Summary of results for seal beam

7.4.4.7 Pivot beam

Summary of results for pivot beam				
Description	Parameter	Value	Unit	
Height	h	400	mm	
Width	b	400	mm	
Bar diameter inner edge	ϕ_+	14	mm	
Number of bars inner edge	n_+	8	-	
Bar diameter outer edge	ϕ_-	14	mm	
Number of bars outer edge	n_-	2	-	
Bar diameter sides	ϕ_{in}	14	mm	
Number of bars sides	n_{in}	8	-	
Bar diameter shear reinforcement	ϕ_w	8	mm	
Shear reinforcement spacing y direction	$s_{w,out}$	200	mm	
Shear reinforcement spacing z direction	$s_{w,in}$	60	mm	
Description	Parameter	Value	Unit	Unity check
Bending ULS / bending moment resistance, major axis, positive	$M_{z,+}$	326.3	kNm	0.32
Bending ULS / bending moment resistance, major axis, negative	$M_{z,-}$	116.9	kNm	0.3
Bending ULS / bending moment resistance, minor axis, extreme	M_{in}	326.3	kNm	0.32
Cracking SLS / Design crack width	w_d	0.1	mm	1
Shear ULS / Shear (out of gate plane) resistance of concrete	$V_{Rd,F,out}$	306.0	kN	-
Shear ULS / Shear (out of gate plane) resistance with reinforcement	$V_{Rd,out}$	378.8	kN	0.99
Shear ULS / Shear (in gate plane) resistance of concrete	$V_{Rd,F,in}$	181.4	kN	-
Shear ULS / Shear (in gate plane) resistance with reinforcement	$V_{Rd,in}$	423.9	kN	0.95
Torsion ULS / Torsion capacity (unity check according to 5.3.3.4.3)	-	-	-	0.68

Table 15: Summary of results for pivot beam

7.4.4.8 Bottom beam

The bottom beam experiences the largest bending moments of all beam segments at its connection to the gate's lower pivot point. This design moment requires 5 reinforcing bars with $\phi = 20\,mm$. However, just 2 bars of $\phi = 20\,mm$ can carry the design moments in most of the beam. Therefore, only the part of the bottom beam between the "pivot beam" and the openings is reinforced with 5 bars, and the rest with only 2.

Summary of results for bottom beam				
Description	Parameter	Value	Unit	
Height	h	400	mm	
Width	b	200	mm	
Bar diameter inner edge	ϕ_+	8	mm	
Number of bars inner edge	n_+	6	-	
Bar diameter outer edge	ϕ_-	20	mm	
Number of bars outer edge	n_-	5	-	
Bar diameter sides	ϕ_{in}	8	mm	
Number of bars sides	n_{in}	7	-	
Bar diameter shear reinforcement	ϕ_w	8	mm	
Shear reinforcement spacing y direction	$s_{w,out}$	70	mm	
Shear reinforcement spacing z direction	$s_{w,in}$	50	mm	
Description	Parameter	Value	Unit	Unity check
Bending ULS / bending moment resistance, major axis, positive	$M_{z,+}$	117.4	kNm	0.47
Bending ULS / bending moment resistance, major axis, negative	$M_{z,-}$	289.6	kNm	0.95
Bending ULS / bending moment resistance, minor axis, extreme	M_{in}	70.7	kNm	0.68
Cracking SLS / Design crack width	w_d	0.9	mm	0.9
Shear ULS / Shear (out of gate plane) resistance of concrete	$V_{Rd,F,out}$	102.5	kN	-
Shear ULS / Shear (out of gate plane) resistance with reinforcement	$V_{Rd,out}$	312.2	kN	0.98
Shear ULS / Shear (in gate plane) resistance of concrete	$V_{Rd,F,in}$	108.9	kN	-
Shear ULS / Shear (in gate plane) resistance with reinforcement	$V_{Rd,in}$	245.0	kN	0.96
Torsion ULS / Torsion capacity (unity check according to 5.3.3.4.3)	-	-	-	0.26

Table 16: Summary of results for bottom beam

7.4.4.9 Complete shear reinforcement of the new gate design

Calculated shear reinforcement is present in sections of the corresponding beams where the design shear force for any of the included design load combinations exceeds the value defined by, respectively, $V_{Rd,F,out}$, or $V_{Rd,F,in}$ for that beam. Based on that rule, and the fact that according to the calculations there is no need for minimal shear reinforcement, all the areas requiring shear reinforcement were evaluated. In areas where the reinforcement was not necessary, there are still some stirrups present to facilitate the manufacturing of the reinforcement grid as a whole. Fig. 62 presents the total shear reinforcement of the new gate design, while Fig. 62 presents the shear reinforcement required by shear ULS conditions. In Fig. 63, the reinforcement required for proper shear capacity is marked with a thicker line, and the additional one with a thinner line.

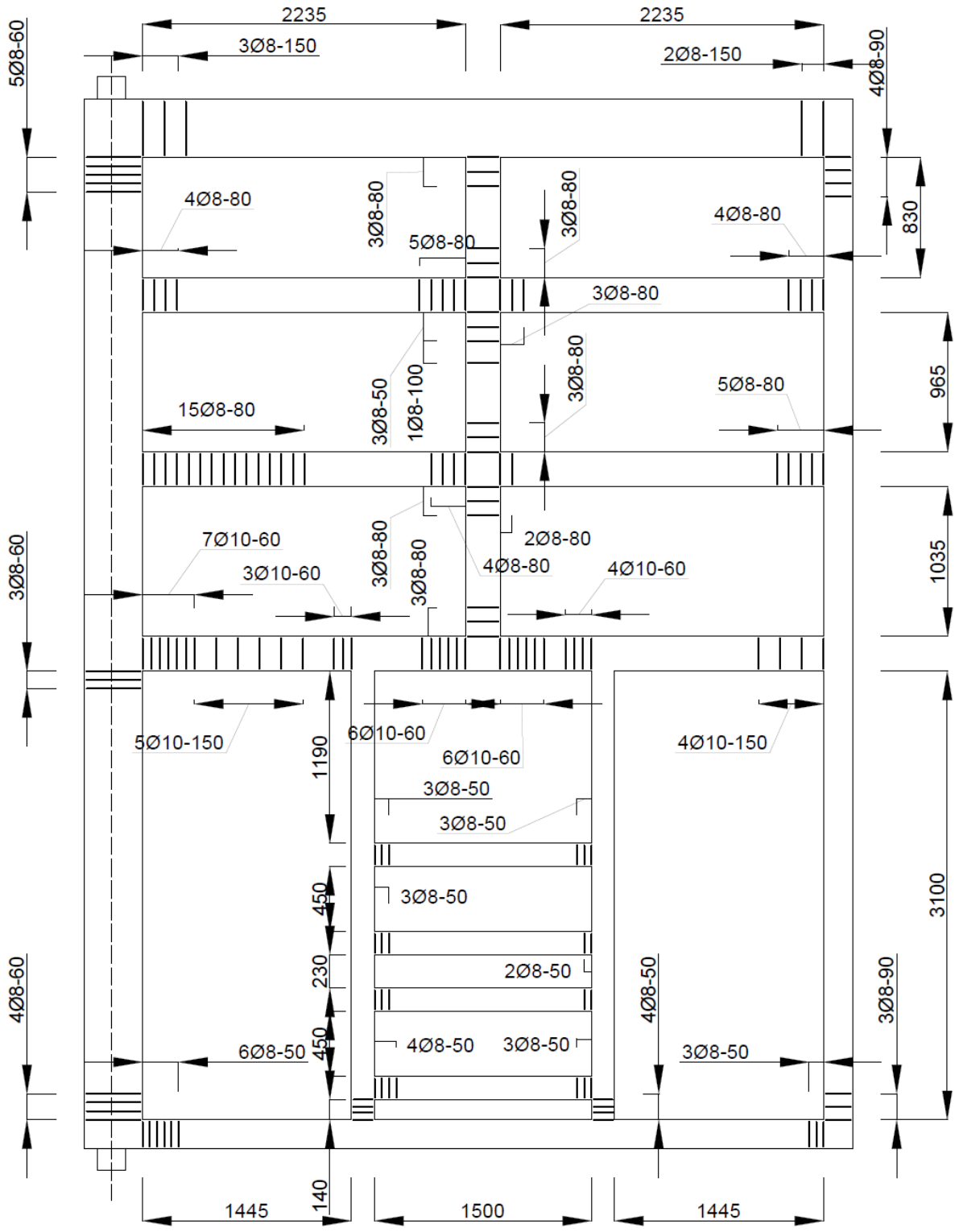

Fig. 62: Shear reinforcement of the new gate design required by shear ULS conditions. Dimensions in mm

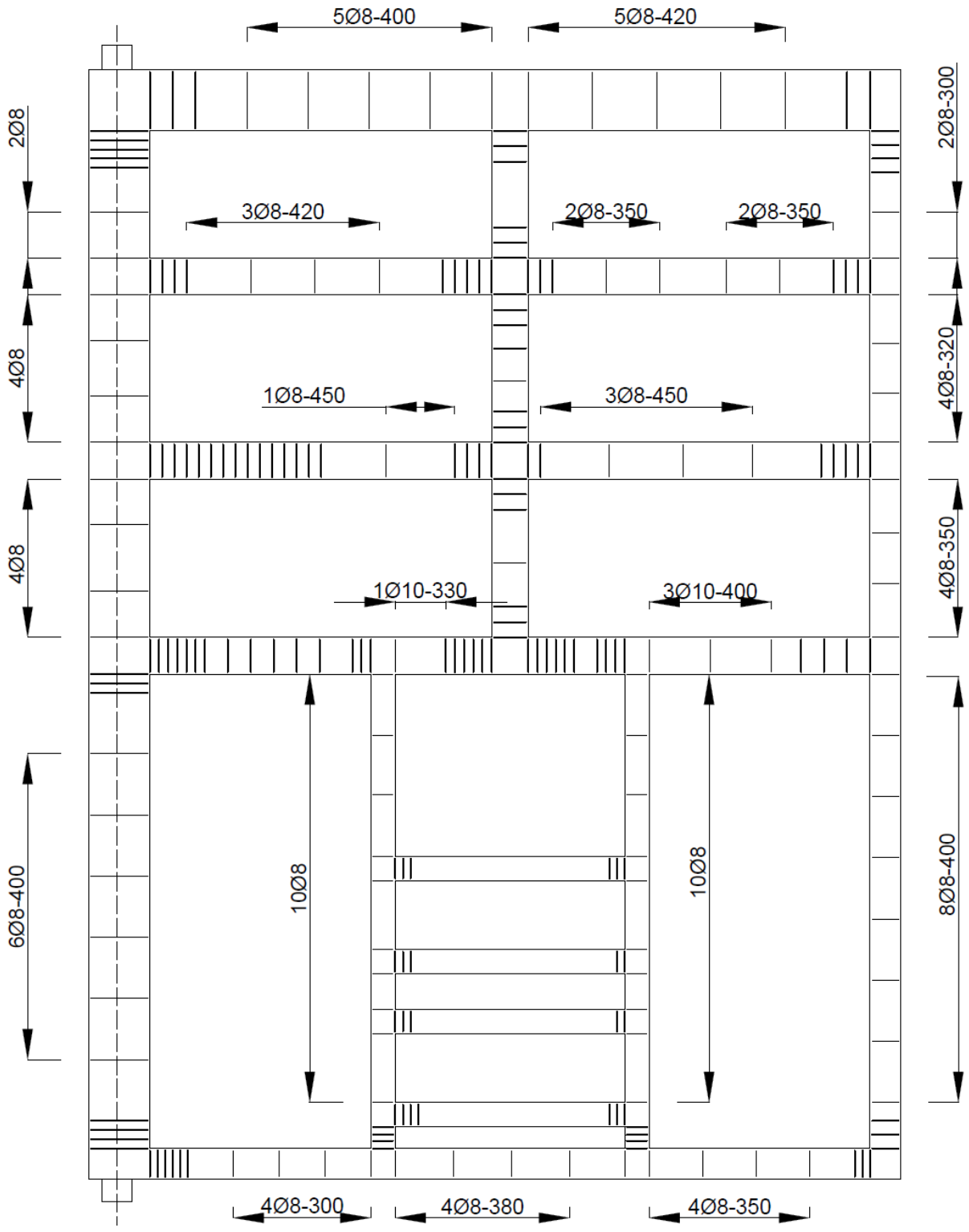

Fig. 63: Total shear reinforcement of the new gate design. Dimensions in mm

8 Comparison of the results

8.1 Overview

This chapter contains the comparison of the results acquired throughout the project. Two different comparisons were conducted. The first one had the goal of aiding in assessing the value of the devised NLFE material model and method of analysis. Bending moment capacities of beams, evaluated with the numerical method utilized in the project, were compared with the those acquired using the analytical method described in Section 5.3.3.4.1. The second comparison evaluated the prior design of the sluice gate against the new design.

8.2 Comparison of NLFE and analytical assessments of beam bending capacity

The goal of this comparison was to provide a means to assess whether the devised NLFE solution strategy approach, and on a deeper level the NLFE material model, were indeed accurate at predicting the bending capacity of beams.

To that aim, bending moment capacities of a set of beams were calculated using both the NLFE solution strategy proposed in Chapter 6 and the simplified analytical approach proposed by Fehling [7]. The analysed beams had the dimensions of beam segments present in the gate structure. Table 17 presents the comparison between those capacities for all the considered beams.

Beam number	Height [mm]	Width [mm]	Number of bars	Bar diameter [mm]	Reinforcement ratio	Bending moment capacity - NLFE approach [kNm]	Bending moment capacity - analytical [kNm]	Ratio M_{NLFE}/M_{anal}
1	250	240	2	8	0.0017	41.9	42.7	0.98
2	250	240	3	8	0.0025	46.5	47.1	0.99
3	250	240	4	8	0.0034	50.9	51.5	0.99
4	250	240	5	14	0.0128	103.2	99.2	1.04
5	250	160	2	8	0.0025	30.8	31.4	0.98
6	250	400	6	8	0.0030	80.9	81.9	0.99
7	400	200	2	8	0.0013	82.0	87.0	0.94
8	400	200	5	20	0.0196	300.2	287.5	1.04
9	400	400	2	8	0.0006	150.7	158.9	0.95

Table 17: Comparison between the bending moment capacities evaluated with the NLFE approach and the analytical approach

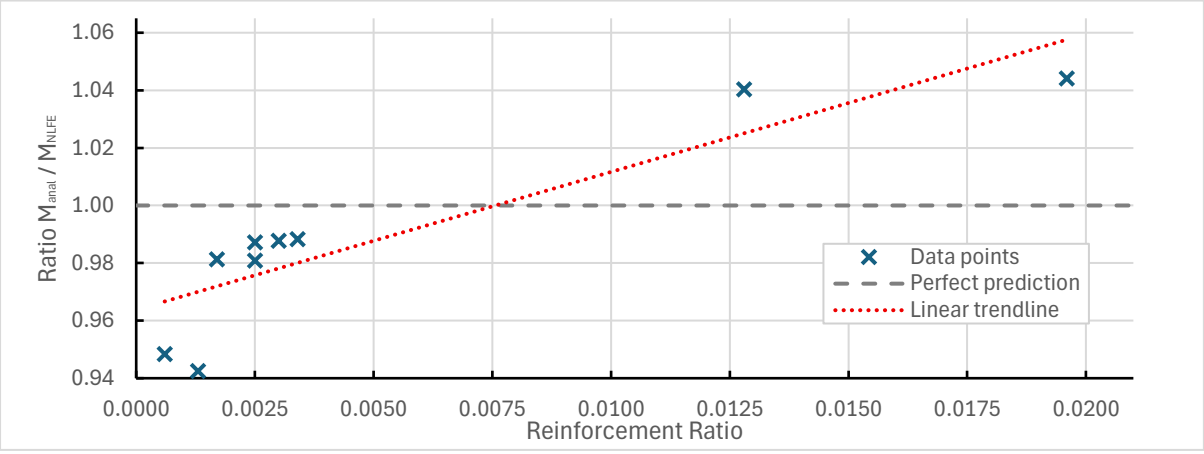

Fig. 64: Accuracy of numerical prediction of the analytical estimation vs reinforcement ratio of the analysed beam

The accuracy of the NLFE prediction of the analytical estimation of the bending moment capacity of a beam was clearly influenced by the longitudinal reinforcement ratio as depicted in Fig. 64. In the case of low reinforcement ratios, the numerical estimations were more conservative, while in the case of high reinforcement ratios they were less conservative. The relative difference between the estimations stayed within the range of -5.7%/+4.4%.

8.3 Comparison of prior and new gate designs

The original gate design was compared with the new one in terms of the amount of materials required to manufacture each variant. The goal of this section was to quantitatively compare the two designs. As such, although the project objectives included reviewing aspects such as manufacturing difficulties, these other issues were not considered in this chapter. Finding an approach that would allow for a quantitative evaluation of such aspects would be difficult; instead, they are considered qualitatively in Chapter 9 as part of the discussion. Only aspects such as the amount of UHPFRC and the amount of reinforcing steel used were compared in this section.

All the calculations conducted to evaluate the amount of materials required for each variant neglected detailing aspects such as smoothed-out corners for UHPFRC, etc. The absolute numbers in this section describe the amounts of materials needed for one piece of the gate (mitre sluice gates consist of two identical door pieces).

The new gate design required $5.53\ m^3$of UHPFRC, while the original required $6.46\ m^3$of the material. This constituted a 14.5% decrease in the volume of UHPFRC necessary to manufacture the gate. This reduction was caused by the removal of the second layer of plates in the bottom half of the gate and the decrease in the volume of the internal beam segments (beams at the edges of the gate maintained the same volume).

After the redesign, the reinforcement of the new gate's plate segments was significantly reduced. This was partially due to the removal of the second layer of plates from the bottom half of the structure, as well as the increase in spacing between the bars from $50\ mm$ to $100\ mm$ and $150\ mm$, respectively, for "x" and "z" directions. The new gate required $315\ kg$ of plate reinforcing bars, while the old one required $1028\ kg$. Which constituted a 69.3% reduction in required plate segment reinforcement.

The total amount of longitudinal beam segment reinforcement needed in the new gate design was $583\ kg$, while the original required $878\ kg$. The necessary longitudinal reinforcement was thus reduced by 33.6%.

The new gate design required $61\ kg$ of shear reinforcement (this includes just the reinforcement needed to provide sufficient shear capacity). The original design included $283\ kg$ of shear reinforcement in total. This constituted a 78.5% decrease.

Considering all of the above, the total amount of reinforcing steel needed for the new design was equal to $959\ kg$, while the prior gate design required $2189\ kg$ of reinforcing steel. In total, the amount of reinforcing steel necessary was reduced by 56.2%. Table 18 presents a summary of the data presented in this section.

Amount of the required:	Unit	New design	Original Design	Decrease
UHPFRC [m^3]	[m^3]	5.53	6.46	14.5%
plate segment reinforcement	[kg]	315	1028	69.3%
longitudinal beam segment reinforcement	[kg]	583	878	33.6%
shear reinforcement	[kg]	61	283	78.5%
total reinforcement	[kg]	959	2189	56.2%

Table 18: Comparison between the amount of reinforcing steel and UHPFRC needed for the original and new designs

9 Discussion, conclusions and recommendations

9.1 Discussion

During the graduation project, a redesign procedure of the UHPFRC sluice gate was conducted. Both numerical and analytical analysis approaches were utilised. The newly acquired design of the sluice gate requires significantly less reinforcement than the original. The reductions were achievable just with the application of the altered analytical design procedure. The main changes in the process included reassessment of parameters such as fibre efficiency or residual tensile strengths. Some previously utilised design verifications were also replaced with alternate methods suggested by MC2020 (2024) [5]. In the case of some of the segments of the structure, fibre orientation factors were also modified, as in the case of the orientation factor for the plate segments. Where based on [39], it was assumed to be equal to 1. Due to fibre length and the size of the clear height of the plates, it was assessed that the fibres will indeed be positioned in the plane of the plate. This modification, same as others, was completely justifiable in the case of the structure at hand, although it had not been considered previously. Reductions in reinforcement were significant, as outlined in Table 18. The validity of the changes applied was also confirmed by the numerical approach. The NLFE solution strategy led to results closely correlated with those of the bending moment capacity evaluated using the analytical method.

A significant part of the project was devoted to the NLFE approach. The exponential tensile curve as defined in DIANA FEA [38], proved to resemble the tensile behaviour of the analysed UHPFRC mix in an accurate way. Two NLFE solution strategies were investigated, a shell element-based one and a plane stress element-based one. Both approaches led to the same failure mechanisms as the real structural elements. Based on the available experimental data, the models were also validated to closely resemble the results acquired in the case of their real counterparts. The plane stress element solution strategy also had its modelling uncertainty evaluated utilising a set of benchmark experiments acquired from the literature [41], [42]. MC2020 (2024) [5] Global Factor approach was applied to quantify the modelling uncertainty. However, in the case of the shell element-based solution strategy, enough test data could not be acquired to verify its modelling uncertainty.

As the shell-based solution strategy's modelling uncertainty could not be verified, this approach ultimately could not be applied to verify various design capacities. However, it was utilised within the scope of the project to evaluate the potential for load redistribution within the gate's structure. Results confirmed UHPFRC's predicted capability for load redistribution as the stresses and strains spread much more uniformly within the critical plate, while reaching approximately 23% lower extreme values. Cracks and deflections exhibited predicted patterns and sizes.

The plane stress element-based solution strategy was used to evaluate the bending moment capacities of the reinforced UHPFRC beam segments. The load-deflection curves acquired utilising the models, closely resembled those present in literature for other UHPFRC mixes [42] and exhibited the same crack patterns. Bending moment capacities of analogous beams were evaluated using both the analytical method, as applied for the gate design, and the NLFE model. Results of the numerical analyses closely predicted the values of the capacities obtained through the analytical approach, with the numerical approach providing capacities smaller/larger by between -5.7% and +4.4%. The numerical model provided more conservative estimates for beams with no or very small reinforcement ratios, and slightly less conservative ones for those with high reinforcement ratios. Throughout the numerical analyses, within the range of reinforcement ratios used in the structure, there was no risk of concrete crushing occurring in the compression zone of the beams.

Regarding the analytical procedure, potential improvements that could have been introduced based on the performance for the bending ULS were hindered by the fact that the crack width SLS required significantly more reinforcement than was otherwise called upon. On one hand, this was a predictable result as the sluice gate is a watertight structure, with high requirements regarding its serviceability, of maximum crack width staying underneath $0.1\ mm$. On the other hand, some research [43], suggested that the formulas evaluating crack width could provide overtly conservative assumptions in the case of the UHPFRC beams. Such a possibility is further supported by findings [21], that the steel bars-concrete bond strength is underestimated by the formulas based on results for other types of concretes.

Several improvements were introduced in the new gate design. The height-to-width ratios of the internal beam segments were adjusted to better correspond to the internal forces present within the structure. The amount of required reinforcement has been significantly reduced. While this change was not extremely significant in absolute numbers, considering the total amount of reinforcement present in the gate structure, it proved influential in terms of the number of reinforcement pieces that needed to be screwed together to assemble the reinforcement grid for the structure. With this number being significantly lower, it will substantially reduce the workload required during the manufacturing of the structure. The EPS-filled segments at the bottom of the structure were removed (by eliminating one of the plate layers enclosing them). This was a significant improvement, as their presence had been particularly problematic during the early attempts to produce the gate. Their absence did not negatively affect the performance of the gate.

9.2 Conclusions

The analytical design process conducted based on the currently available methods and knowledge is a sufficient tool to design UHPFRC sluice gate structure, and it allows to do so with substantially decreased material volumes than evaluated before. The gate designed utilising that approach, based on its dimensions and amounts of materials used, and the superior durability of UHPFRC structures, should be a competitive alternative compared to the currently prevalent steel sluice gates. The proposed plate and beam segment-based gate structure provides a viable design approach for sluice gates characterised by a similar range of dimensions and loading conditions.

As proven by the comparison with the validated numerical counterparts, the results of the applied analytical process present a safe assessment of the gate's structural behaviour.

The reinforcement design is, however, decisively affected by the cracking SLS verifications. They demand significantly higher reinforcement ratios than the ULS requirements. Based on that and on the available literature, the conservativeness of the crack width SLS verifications for UHPFRC should be reevaluated.

The applied NLFE approach is accurate in predicting the structural capacity of the UHPFRC in bending. However, due to the decisiveness of the crack width SLS, there is no practical need for NLFE verifications of the bending ULS, even if it were to be more efficient than the analytical ones. Instead, the utilised NLFE approach, with modifications, such as inclusion of the reinforcement-steel bond strength, etc., could be used to reevaluate the verifications of the design crack width.

The exponential tensile curve, as provided in Diana FEA [44], is a suitable tool for the modelling of the tensile behaviour of UHPFRC. The devised (CQ40S) shell-element solution strategy requires more test data to properly estimate its modelling uncertainty. However, were it to be done, it could prove a very useful tool in modelling the whole gate structure, to comprehensively evaluate the load redistribution effects present in the case of UHPFRC, and fully utilise the benefits provided by the material. The (CQ16M) plane stress element-based solution strategy accurately predicts the behaviour

of the considered UHPFRC. The decision not to model nonlinear compressive behaviour of the material was correct, as due to the significant strength of the UHPFRC, within the relevant dimensions and reinforcement ratios, there was no risk of concrete crushing failure.

The new gate design represents a substantial improvement in comparison to the original one. The amount of concrete was slightly reduced. The required reinforcement was significantly reduced, decreasing both the material requirements and the workload needed to manufacture the gate. The removal of the EPS cores also provides an important simplification during the gate manufacturing process. None of the changes negatively affected the performance or serviceability of the structure.

The main limitations of the research were the necessity for an expanded benchmark pool of experiments considering UHPFRC plates. As well as the discrepancy between the utilisation rate of the crack width SLS and other verifications.

9.3 Recommendations

Based on the deliberations, some recommendations for future research can be proposed. They include both aspects that could further improve the proposed analytical design approach, as well as aspects that could serve to broaden the applicability of the outlined NLFE solution strategies.

- The approach to verifying crack width SLS for UHPFRC should be reevaluated. This can be done either by reviewing the standard proposed methods, especially regarding the suggested crack bond strength estimations for UHPFRC, or by utilizing an NLFE solution strategy, prepared and validated in a similar way to that presented in the project, to directly analyse the cracking in the concerned structure.
- More tests regarding UHPFRC plates could be conducted to acquire a set of benchmark experiments that would allow for assessing the modelling uncertainty of shell element-based solution strategies utilizing nonlinear UHPFRC material models. As UHPFRC has a significant load redistribution capacity, these solution strategies would prove useful in evaluating the structural behaviour of plate-based UHPFRC structures.
- It is recommended to research the possibility of adding a completely new type of crack bandwidth-based tensile curve suitable for various UHPFRCs to the FE software. While the predefined exponential tensile curve proved accurate at predicting the behaviour of the UHPFRC considered in the project, different UHPFRC mixes can vary significantly in their performance. This would, on one hand, allow approaches similar to that presented in the project to be applied to a wider range of UHPFRCs. On the other hand, as reasoned in the project, the values of material parameters acquired in tests had to be manipulated in the process of curve fitting to adjust the exponential curve and produce the correct response. Because of this, the Partial Factor Method could not be utilised for assessing the modelling uncertainty in the project. Developing a tensile curve type calibrated specifically for UHPFRC modelling would make it possible to use both the Global Factor and the Partial Factors methods for assessing the modelling uncertainty of the solution strategies utilising it.

10 References

[1] Groupe de travail BFUP. (2002). Interim Recommendations. Ultra High Performance Fibre-Reinforced Concretes. Association Francaise de Génie Civil.

[2] Groupe de travail BFUP. (2013). Ultra High Performance Fibre-Reinforced Concretes. Recommendations. Association Francaise de Génie Civil. https://www.researchgate.net/publication/290274871_Ultra_High_Performance_Concrete_New_AFGC_Recommendations

[3] Societé suisse des ingénieurs. (2016). SIA 2052:2016. Béton fibré ultra-performant (BFUP) - Matériaux, dimensionnement et exécution. SIA.

[4] L'Association française de normalisation. (2016). NF P18-710. Design of concrete structures - Specific rules for UHPFRC. AFNOR.

[5] The International Federation for Structural Concrete (fib). (2024). *fib Model Code for Concrete Structures 2020* (MC2020). https://www.fib-international.org/publications/model-codes/model-code-2020.html

[6] Resplendino, J., & Toulemonde, F. (2013). *Designing and Building with UHPFRC.* Wiley-ISTE.

[7] Fehling, E., Schmidt, M., Walraven, J., Leutbecher, T., & Fröhlich, S. (2014). Ultra-High Performance Concrete UHPC. Wilhelm Ernst & Sohn.

[8] Betoniek. (2017). Da's sterk! Betoniek Standaard, 1-12.

[9] Markovic, I. (2006). *High-performance hybrid-fibre concrete - Development and utilisation* [Doctoral thesis, Delft University of Technology]. https://repository.tudelft.nl/record/uuid:44ed51cd-fc27-4353-ab81-cf8348f52443

[10]Abrishambaf, A., Pimentel, M., & Nunes, S. (2017). Influence of fibre orientation on the tensile behaviour of ultra-high performance fibre reinforced cementitious composites. Cement and Concrete Research, 97, 28-40.

[11]Huang, H., Gao, X., & Teng, L. (2021). Fiber alignment and its effect on mechanical properties of UHPC: An overview. Construction and Building Materials, 296.

*[12]*Khorami, M. (2023). *Serviceability behaviour of reinforcement UHPFRC tensile elements* [Doctoral thesis, Universitat Politecnica de Valencia].

[13]Androuët, C., & Charron, J. P. (2021). Shrinkage Mitigation of an Ultra-High Performance Concrete Submitted to Various Mixing and Curing Conditions. Materials, 14. https://doi.org/10.3390/ma14143982.

[14]Wu, L., Farzadnia, N., Shi, C., Zhang, Z., & Wang, H. (2017). Autogenous shrinkage of high performance concrete: A review. Construction and Building Materials, 149, 62-75

[15]Mezquida-Alcaraz, E., Navarro-Gregori, J., Marti-Vargas, J., & Serna-Ros, P. (2021). Effects of tension stiffening and shrinkage on the flexural behavior of reinforced UHPFRC beams. Case Studies in Construction Materials, 15

[16]Liu, Y., Wang, L., Wei, Y., Sun, C., & Xu, Y. (2024). Current research status of UHPC creep properties and the corresponding applications – A review. Construction and Building Materials, 416.

[17]Ul-Islam, R., Khalil, J., & Hanif, A. (2025). Fatigue performance of ultra-high-performance concrete (UHPC): A critical review. Journal of Building Engineering, 101. https://doi.org/10.1016/j.jobe.2025.111881

[18]Millon, O., Riedel, W., Thoma, K., Fehling, E., & Nöldgen, M. (2009). Fiber-reinforced ultra-high performance concrete under tensile loads. DYMAT, 1, 671-677. https://doi.org/10.1051/dymat/2009095

[19]Jungwirth, J., & Muttoni, A. (2004). Structural behavior of tension members in UHPC. In Proceedings of the international symposium on ultra-high-performance concrete, Kassel, Germany, pp. 533–544.

[20]Yoo, D. Y., Shin, H. O., Yang, J. M., & Yoon, Y. S. (2014). Material and bond properties of ultra high performance fiber reinforced concrete with micro steel fibers. Composites Part B: Engineering, 58, 122-133. https://doi.org/10.1016/j.compositesb.2013.10.081

[21]Yoo D., & Yoon, Y. (2016). A Review on Structural Behavior, Design, and Application of Ultra-High-Performance Fiber-Reinforced Concrete. International Journal of Concrete Structures and Materials, 10(2), 125-142.

[22]Plos, M., Shu, J., Zandi, K., & Lundgren, K. (2017). A multi-level structural assessment strategy for reinforced concrete bridge deck slabs. *Structure and Infrastructure Engineering*, *13*(2), 223–241. https://doi.org/10.1080/15732479.2016.1162177

[23]Max A.N. Hendriks and Marco A. Roosen (editors), "Guidelines for Nonlinear Finite Element Analysis of Concrete Structures", Rijkswaterstaat Centre for Infrastructure, Report RTD:1016-1:2019, 2019.

[24]Royal Netherlands Standardization Institute (NEN). (2007). Beproevingsmethode voor staalvezelbeton - Meten van de buig-treksterkte (proportionaliteitsgrens (LOP), reststerkte) (NEN-EN 14651+A1). https://www.nen.nl/nen-en-14651-2005-a1-2007-en-120650

[25]Lee, S., Kim, H., & Joh, C. (2017). Inverse Analysis of UHPFRC Beams with a Notch to Evaluate Tensile Behavior. Advances in Materials Science and Engineering, 2017. https://doi.org/10.1155/2017/6543175

[26]Fairbairn, E., Toledo Filho, R., Battista, R., Rosa, J., Formagini, S., BrandÃo, J. (2006). EXPERIMENTAL AND NUMERICAL ANALYSIS OF UHPFRC PLATES AND SHELLS. In: KONSTA-GDOUTOS, M.S. (eds) Measuring, Monitoring and Modeling Concrete Properties. Springer, Dordrecht. https://doi.org/10.1007/978-1-4020-5104-3_6

[27]van der Aa, P.J., van den Bos, A.A. (2021). Material Characterisation for Nonlinear Finite Element Analysis (NLFEA). In: Serna, P., Llano-Torre, A., Martí-Vargas, J.R., Navarro-Gregori, J. (eds) Fibre Reinforced Concrete: Improvements and Innovations. BEFIB 2020. RILEM Bookseries, vol 30. Springer, Cham. https://doi.org/10.1007/978-3-030-58482-5_46

[28]Engen, M., Hendriks, MAN., Overli, JA., & Aldstedt, E. (2014). Large scale non-linear finite element analyses of reinforced concrete structures. In J. Bastien, N. Rouleau, M. Fiset, & M. Thomassin (Eds.), Proceedings of the 10th fib international PhD symposium in civil engineering (pp. 541-552). CRIB.

[29]Engen, M., Hendriks, M.A.N., Monti, G., Allaix, D.L. (2021). Treatment of modelling uncertainty of NLFEA in fib Model Code 2020. Structural Concrete; 22: 3202–3212. https://doi.org/10.1002/suco.202100420

[30]Royal Netherlands Standardization Institute (NEN). (2011). Eurocode: Basis of structural design (NEN-EN 1990+A1+A1/C2). https://connect.nen.nl/Standard/Detail/161789?compId=10037&collectionId=0

[31]Royal Netherlands Standardization Institute (NEN). (2019). *Eurocode 1: Actions on structures - Part 1-1: General actions - Densities, self-weight, imposed loads for buildings* (NEN-EN 1991-1-1). https://www.nen.nl/en/nen-en-1991-1-1-c1-c11-2019-nl-207218

[32]Royal Netherlands Standardization Institute (NEN). (2011). *Eurocode 1: Actions on structures - Part 1-4: General actions - Wind actions* (NEN-EN 1991-1-4+A1+C2). https://connect.nen.nl/Standard/Detail/161137?compId=10037&collectionId=0

[33]Royal Netherlands Standardization Institute (NEN). (2011). *Eurocode 2: Design of concrete structures - Part 1-1: General rules and rules for buildings* (NEN-EN 1992-1-1:2005+C2:2011). https://connect.nen.nl/Standard/Detail/159356?compId=10037&collectionId=0

[34]Royal Netherlands Standardization Institute (NEN). (2005). *Structural bearings - Part 3: Elastomeric bearings* (NEN-EN 1337-3). https://connect.nen.nl/Standard/Detail/93144?compId=10037&collectionId=0

[35]The International Federation for Structural Concrete (fib). (2010). *fib Model Code for Concrete Structures 2010* (MC2010). https://www.fib-international.org/publications/model-codes.html

[36]Rijkswaterstaat, Ministerie van Infrastructuur en Milieu (2017). *ROK 1.4* (RTD 1001:2017). https://www.rijkswaterstaat.nl/zakelijk/werken-aan-infrastructuur/bouwrichtlijnen-infrastructuur/kunstwerken

[37]Rijkswaterstaat, Ministerie van Infrastructuur en Milieu (2011). *Richtlijnen Vaarwegen 2011* (*Richtlijnen Vaarwegen 2011*). https://www.rijkswaterstaat.nl/zakelijk/werken-aan-infrastructuur/bouwrichtlijnen-infrastructuur/vaarwegen

[38]TNO. (2023). *DIANA FEA* [Computer software]. DIANA FEA BV.

*[39]*SFRC Consortium (2014). *DESIGN GUIDELINE FOR STRUCTURAL APPLICATIONS OF STEEL FIBRE REINFORCED CONCRETE.* SFRC Consortium. https://www.dti.dk/_/media/63902_Guideline%20for%20Design%20of%20steel%20fibre%20reinforced%20SCC_2014-01-05.pdf

[40]Falbr, J., Hunger, M., & Spiesz, P. (2016). Rekenregels UHSB beproefd. *Betoniek, 2016/2*.

[41]Yoo, D., & Yoon, Y. (2015). Structural performance of ultra-high-performance concrete beams with different steel fibers. *Engineering Structures, 102, 409–423.*

[42]Yang, H., Joh, C., & Kim, B. (2010). Structural behavior of ultra high performance concrete beams subjected to bending. *Engineering Structures, 32, 3478–3487.*

[43]Xu H., & Deng Z. (2014). Cracking moment and crack width of ultra-high performance concrete beams. Journal of Harbin Institute of Technology, 46(4), 87-92.

[44]DIANA FEA BV. (2025). DIANA User's Manual (Release 10.10). https://manuals.dianafea.com/d1010/?lang=en

[45]Microsoft Corporation. (2021). Microsoft Excel (Version 2504) [Computer software]. Microsoft Corporation.

[46]PTC Inc. (2021). *Mathcad Prime* (Version 7.0.0.0) [Computer software]. PTC Inc. https://www.ptc.com/en/products/mathcad

[47]Spyder Development Team. (2023). Spyder: Scientific Python Development Environment (Version 5.4.5) [Computer software]. https://www.spyder-ide.org/